Capacity of Deep Water Flexible Risers

by

Mats Jørgen Thorsen

Master thesis

Marine Structural Engineering

NTNU – Trondheim
Norwegian University of
Science and Technology

Department of Marine Technology
Faculty of Engineering Science and Technology
Norwegian University of Science and Technology

June, 2011

Summary

A flexible riser operating in deep water will experience large environmental forces. Due to the length of the riser, dynamic tension from drag forces will be substantial. The tensile force is transferred directly into the end fitting, and fatigue damage may be critical at this point. In addition, the large hydrostatic pressure at the ocean floor may induce compressive stresses in the tensile armor, something this component is not designed for. In connection with these challenges, this thesis deals with two different phenomenons relevant for deep water risers:

- Local stresses in tensile armor wires at the end fitting due to contraint effects.
- Radial and lateral buckling of tensile armor wires.

The first part of this report, section 2 and 3, is the result of a literature study regarding flexible pipe technology, failure modes and design criteria with special focus on those relevant for deep water applications. In section 4, theory important to the thesis work is presented. This includes analytical methods for stress analysis of flexible pipes, theory of thin curved beams, basic theory of restrained warping and finite element methods.

In the last part of section 4, a new curved beam element for the nonlinear finite element program Aflex is presented. A central part of the thesis work has been to implement this new element into the original Aflex code. The element has rotational degrees of freedom about the bi-normal direction in addition to the degrees of freedom included in the original Aflex code. Hence, the element is capable of investigating both radial and lateral buckling modes. The element has also been implemented in a special version of the Bflex2010 computer program.

Section 5 is dedicated to analyses of stresses in tensile armor wires at the end fitting. The load case considered is axial straining of the pipe, which leads to a small change in lay angle. As the wires are restrained at the end fitting, a change in lay angle will not be allowed, and this constraint will induce local stresses. First, analytical calculations neglecting friction between the armor wire and supporting layer are performed for different wire dimensions. Next, the new curved beam element is used for numerical analyses of the same cases, and the transverse bending stress at the end fixation is studied for varying friction coefficients. Both analytical and numerical results show that the relative magnitude of the local transverse bending stress increases as the axial straining of the pipe increase. As an example, the bending stress is found to exceed 16 % of the nominal axial stress when the axial stress is 400 MPa, for a flexible pipe including two tensile armor layers and a friction coefficient of 0.15.

Section 6 deals with different buckling modes for tensile armor wires. Three different modes are presented, namely radial failure due to anti buckling tape rupture, radial elastic buckling and lateral buckling. Analytical formulas for predicting the capacity with respect to all three modes are established, and governing physical effects are discussed. Numerical analyses with the new curved beam element are performed, and the results are compared to the analytical solutions. It is found that the first radial failure mode is determined primarily by the strength of the anti buckling tape, while the elasticity of the tape is critical to the second radial mode. Comparison between the analytical solutions and finite element results indicate that the radial failure modes are accurately predicted by both methods.

The lateral buckling capacity is more difficult to predict, as the behaviour is dominated by friction forces, and the stick-slip transition. However, analytical and numerical results

all indicate a strong dependence upon friction coefficient and pipe curvature. The finite element model reports the lowest capacity, and these results are also believed to be the most accurate due to the more realistic modelling of friction.

A smaller investigation of the lateral buckling capacity under cyclic curvature is done with the FE model, and it is found that buckling of tensile armor wires may occur after a number of curvature cycles even if the combination of stress and curvature is significantly lower than critical in static curvature conditions. The results from these analyses are unfortunately somewhat unclear, as they were found to be slightly influenced by the numerical parameters defining the friction springs. Nevertheless it is concluded that lateral buckling may occur as a result of gradual transverse slip under cyclic curvature conditions, and that this may happen for curvatures in the vicinity of 0.1 m^{-1} combined with a compressive stress in the armor wire equal to 300 MPa, given a friction coefficient of 0.15.

Preface

This report is the result of my master thesis work in marine structural engineering at the Departement of Marine Technology, NTNU.

An important part of the work has been to familiarize with the computer program Aflex. Because I was to modify the program and implement a new beam element, I had to get a complete overview of the details in the code. This was challenging, as the program is based on the theory of curved beams, which I was unfamiliar with at the start. I have learned a lot through this work, especially about how nonlinear finite element programs work in practice.

I am also pleased in that I have been given the opportunity to do both analytical and numerical work in this thesis. This combination is a great way of increasing your knowledge, because you get an understanding of the physics through deriving analytical formulas, while you get a more "practical" understanding of things through numerical analyses.

I owe my supervisor, Prof. Svein Sævik great thanks for many reasons. He has been very helpful with my questions regarding Aflex (which he is the creator of), and he has personally implemented the new Aflex element into a special version of Bflex2010, which has been beneficial to me. His advices have been appreciated, and our discussions have been both rewarding and encouraging.

I assume that those reading this report are familiar with mathematics and structural mechanics.

Trondheim, June 2011

.....
Mats Jørgen Thorsen

Scope of work

The flexible riser is a vital part of a floating production system. For deep water risers, radial and lateral buckling phenomena in the tensile armour may govern the design. Further due to the length of the catenary, significant dynamic tension may occur due to the tangential drag force. Since the dynamic tension is transformed directly into the end fitting, fatigue due to constraint effects may take place. This thesis focus on establishing a simplified FEM based model that is capable of investigating both failure modes. Together with the supervisor, it has been decided that the thesis work is to be carried out as follows:

1. Literature study including flexible pipe technology, failure modes and design criteria specially focusing on external pressure buckling, analytical methods for stress analysis of flexible pipes, the theory of thin curved beams and relevant non-linear finite element methods as those used in the softwares Aflex and Bflex.

2. Establish analytical formulas for the local bending and end section warping stresses at the end fitting (neglect transverse friction) when considering the changes in lay angle from dynamic axi-symmetric loads.

3. Establish analytical formulas for transverse and radial buckling of tensile armours considering the anti-buckling tape strength and the natural transverse buckling mode when considering imperfections from bending loads and friction resistance.

4. Familiarize with the computer code Aflex and implement a new curved beam element that include 2 additional DOFs describing bi-normal rotation. As input, a full version of the Aflex symbolic code will be provided by the supervisor.

5. Model a single armour layer and simulate axial tensile armour straining of the pipe by a combination of X1 and X2 prescribed displacements of the tendon. Study the transverse bending stress at the end fixation for variable friction coefficients. Compare the results against the analytical values.

6. Use the same Aflex model and apply compressive loads by a combination of prescribed displacements and external pressure radial load. Find out under which circumstances the tendon buckle radially or transversally. Again, compare with the analytical prediction.

7. Conclusions and recommendations for further work.

Nomenclature

General rules

- Vectors, tensors and matrices are written with bold letters, e.g. $\mathbf{K}$, $\mathbf{u}$.
- The transpose of a matrix is denoted by superscript T.
- Derivatives are denoted in either of the following ways:
  $F_{,1} \equiv \frac{dF}{dX^1} \equiv F'$
- Einstein's summation convention is adopted whenever index form is used, i.e:
  $Z^I_{,1}\mathbf{E_I} = Z^1_{,1}\mathbf{E_1} + Z^2_{,1}\mathbf{E_2} + Z^3_{,1}\mathbf{E_3}$
- The scalar product of two second order tensors is denoted by a double dot:
  $\mathbf{a} : \mathbf{b} = a^{ij}b_{ij}$
- The cross product between two vectors are denoted by a cross $\times$.

Roman letters

Unfortunately, some letters have been used for more than one single purpose. The meaning of different symbols are usually explained in the text whenver they are introduced, so misunderstandings should be avoided.

a	Width of tensile armor wire
A	Cross sectional area
b	Thickness of tensile armor wire (except in section 4.2.4, where it is the width)
C_σ	Youngs modulus, modulus of elasticity
C_τ	Shear modulus
E	Youngs modulus, modulus of elasticity
$\mathbf{E^I}$	Base vectors in the Z^I-system
E^*_{KL}	Component KL of the Green strain tensor in local curvilinear coordinates
$\mathbf{E}, E_{IJ}$	Tensor and component form of the Green strain tensor in local Cartesian coordinates
EI	Bending stiffness
G	Determinant of metric tensor (in section 4.3 only)
G	Shear modulus (except in section 4.3)
$\mathbf{G^I}$	Base vectors along local armor wire curvilinear axes
$\mathbf{I^I}$	Unit tanget, unit normal and unit binormal vectors
I_t	Cross section torsion constant
I_p	Polar moment of inertia
I_2	Second moment of area about the X^2 axis
I_3	Second moment of area about the X^3 axis
$\mathbf{k}, \mathbf{K}$	Element and system stiffness matrix respectively
l, L	Length
m	Distributed moment
M	Moment
M_f	Friction moment
M_t	Torsion moment
n	Number of armor wires
$\mathbf{N}$	matrix of interpolation polynomials
p	Pressure
q	Distributed force
Q	Force
$\mathbf{r}$	Position vector in deformed configuration (in section 4.3)
$\mathbf{r}$	Global degrees of freedom
$\mathbf{R}$	Initial position vector (in section 4.3)
$\mathbf{R}$	External nodal point loading
R	Radius
S	Surface
$\mathbf{S}$	Generalized nodal point forces
t	Thickness
$\mathbf{t}$	Surface traction
T_e	Effective axial force
T_w	True axial force in pipe wall

$\mathbf{u^0}, u_i^0$	Displacement vector of wire center line and its component in direction i
$\mathbf{u}, u_i$	Displacement vector and its component in direction i
$\mathbf{v}$	Element degrees of freedom
V	Volume
W_i, W_e	Internal and external work
X^I	Local curvilinear coordinates for armor wire
Z^I	Cartesian coordinates with origo in center of pipe

Greek letters

The letter σ is used for a number of stress components. Only the most important are listed below, as the different stress components are explained as they appear in the text. In any case, the particular type of stress is indicated by subscripts.

α	Lay angle of armor layer relative to the longitudinal axis of the pipe
β	Twist
γ	Change in lay angle due to axial straining when no end restraints are present
Γ	Warping stiffness
δ	Indicates "virtual"
ϵ, ϵ_{ij}	Tensor and component form of strain tensor (in section 4.3)
ϵ	Axial strain along strained helix (in section 5)
ϵ_a	Axial strain in tensile armor wire
ϵ_p	Axial strain in pipe
η	Actual change in lay angle
θ	Polar coordinate angle defining helix position
θ_i	Armor cross section rotation around local axis i
κ	Principal curvature of armor wire (except in section 4.2.4 where it is the pipe curvature)
κ_1	Total geometric torsion of armor wire
κ_2	Total transverse curvature of armor wire
κ_3	Total normal curvature of armor wire
κ_t	Surface curvature along the transverse direction
μ	Friction coefficient
ξ	Non dimensional arc length coordinate
ρ	Radius of curvature of pipe
$\boldsymbol{\sigma}, \sigma_{ij}$	Stress tensor and its component in ij-direction
σ_a	Axial stress
σ_b	Bending stress
σ_w	Warping stress
τ	Geometric torsion/twist
φ	Warping function
ω	Angle between surface normal and curve normal
ω_1	Geometric torsion/twist deformation
ω_2	Transverse curvature deformation
ω_3	Normal curvature deformation

Contents

List of Figures

List of Tables

1 Introduction

The use of flexible risers in floating production systems has increased rapidly since the 1990s [7]. As time passes, the number of available oil and gas reservoirs in shallow waters decreases, and the offshore industry is forced to move into deeper waters. This introduces challenges with respect to the extreme tensile loads that may occur due to drag forces and riser weight. Risers operating in deep water may also experience compressive axial force induced by the large hydrostatic pressure at the ocean floor.

1.1 Motivation

To ensure safe operation of flexible risers in deep water applications, there is a need for analytical and numerical models capable of providing accurate predictions of the capacity with respect to certain failure modes. Tensile loads are transferred directly into the end fitting, and this may be a critical point with respect to fatigue. It is therefore necessary to have insight in the different stress components at this point, and the magnitude of local stresses due to end restraints.

The stress distribution inside an end fitting has previously been investigated by Shen et al. [8]. They developed a finite element model of a tensile armor wire and the surrounding end fitting structure, however the model did not take the actual 3D helical shape of the armor wire into account. This model is therefore unable to predict bending stresses due to bending around the strong axis of the armor wires.

Another failure mode relevant for deep water flexible risers is buckling of tensile armor wires. The external pressure will induce a compressive axial force, which may result in compressive axial stresses in the armor wires. The armor wires are not designed to withstand this type of loading, and instabilities in the radial or lateral direction may take place. This may result in severe structural damage, loss in capacity against other types of loading and leakage.

There is a small number of papers concerning buckling of tensile armor wires in the open literature. Becarte and Coutarel describes both bird caging (radial failure) and lateral buckling [4]. Test procedures for lateral buckling is described, and a computer model is mentioned, but no details with respect to methods or results are given. Tan et al. also described the behaviour of tensile armor wires under compression [9]. A strain energy approach for modelling the buckling and post-buckling behaviour of the wires is outlined, but no usable expressions or results are actually presented. However, some test results are presented which state that lateral buckling of the wires under cyclic bending was observed under wet annulus conditions.

This indicates that there is a need for better understanding of the behaviour of tensile armor wires under compressive axial load. Also, test results show that if not properly taken into account, this failure mode is not unlikely to occur in the future, as the limits for depth capabilities are being pushed.

1.2 Main contributions

This thesis focuses on establishing a finite element model of a tensile armor wire, including contact interaction with surrounding layers. The model is capable of describing both local bending stresses at end restraints, and the different wire buckling modes. Numerical investigations of the local stress at the end restraint is performed for different wire dimensions and friction coefficients. The capacity with respect to different buckling modes

is also assessed, and it is observed how the capacity changes when key parameters are varied.

The investigation is however not limited to numerical analyses. Attempts to find analytical solutions to the different problems have also been made. These solutions are often simplified and based on assumptions, but the understanding attained from deriving analytical expressions is often bigger than what is obtained from interpreting numerical results.

Hopefully, the combination of analytical and numerical analyses will provide both useful information and understanding.

1.3 Organization of the thesis

The outline of the report is as follows:

Section 2 gives a short review of the flexible pipe technology.

Section 3 focuses on known failure modes and design criteria.

In **Section 4**, theory and methods important to the work done in this thesis are presented. Most of the material is taken from other sources, except section 4.6, which presents a new curved beam element developed as a part of this thesis work.

Section 5 deals with local stresses at end fittings. First, an analytical solution is presented which aims at determining which physical effects that are important, and which are not. Expressions for both warping and bending stresses are given. Next, a finite element model using the new curved beam element is established, and a number of analyses of the local bending stress at the end restraint is performed. The importance of friction is investigated.

In **Section 6**, analytical formulas for the armor wire buckling capacity with respect to radial and lateral failure is presented. The developed finite element model is used to analyse the same cases. This model is also used to investigate the armor behaviour under the combined action of compression and cyclic bending.

Section 7 summarizes the main findings and gives recommendations for further work.

2 Flexible pipe technology

2.1 Introduction

The aim of this chapter is to give a short overview of the flexible pipe technology. There are many applications for such pipes, however the common factor is the need for the ability to undertake large flexural deformations while being subjected to high pressure and tensile forces. A typical example is a marine riser transporting hydrocarbons from a subsea well up to a floating production platform. In such a situation, the flexible pipe is preferrable over a rigid steel riser because it will not require a heave compensation and tensioner system at the top. Another favourable property of such pipes is that transportation and installation is easier, as it is possible to prefabricate long lengths and store it on reels.

2.2 Flexible pipes and applications in the offshore industry

The following section is based on information found in [10]. The main application of flexible pipes are as riser lines connecting subsea installations and production units at the sea surface. Such a riser may have many functions, where the most important are:

- Transportation of well products such as oil, gas and condensate
- Well control lines
- Injection of water and gas
- Export of processed product

The detailed requirements for the riser such as size, pressure rating and internal coating depends on the transport function. When it comes to maintaining structural integrity, the main requirements will depend on:

- Water depth
- Motion characteristics of the surface vessel
- Current and wave loads
- Fluid characteristics (important for the choice of materials)

When designing a riser system, one must take the above mentioned parameters into account, and ensure that the system of risers is arranged in such a way that the loading is kept at a safe level when it comes to tension, curvature, torsion, compression and contact with other structures. Assessment of the fatigue resistance is also important in dynamic applications.

An important issue when designing such a riser system is to determine the type of riser configuration. Some examples of used configurations are presented in figure 1. Selecting a suitable set up for a particular floating production system is based on experience and engineering judgement, and a basic knowledge of the dynamic behaviour of the system is essential.

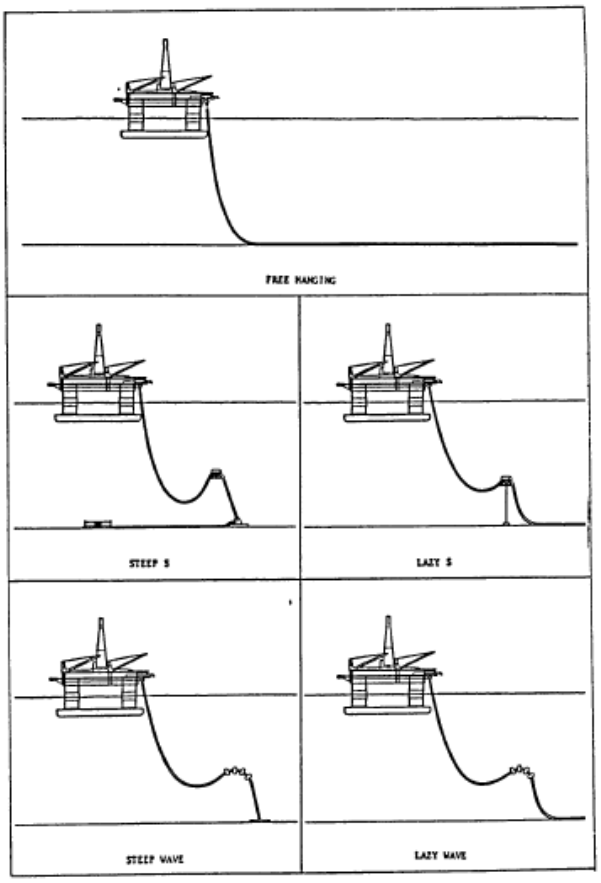

Figure 1: Some possible riser configurations [1]

Flexible pipes may also be used as flowlines connecting subsea wells, wellhead platforms, templates or loading terminals and processing platforms. In these types of applications, the pipe is not expected to be subjected to dynamic loading in the operational phase. The flexibility requirements are mainly related to transport and installation of the pipe.

Other applications are as loading hoses between shuttle tankers and a storage tanker/loading buoy and as jumper lines connecting a fixed platform to a floating support vessel.

2.3 Structure of flexible pipes

This section is also largely based on [10] as well as [11]. In order to safely transport hydrocarbons from the seabed up to the surface, a pipe which combines both strength and flexibility is required. The strength requirements are mainly due to high internal fluid pressure as well as external hydrostatic pressure at large depths and also due to tensile forces. Ensuring sufficient strength is essential in order to prevent loss of containment. The need for flexibility is due to the large motions which a floating production platform will experience. These motions would inevitably result in yielding and structural failure of the pipe if it was rigid.

The key to the flexiblility is the composite structure of the pipe cross section. A flexible pipe consists of multiple cylindrical layers, and the basic components are:

- Armor layers (pressure and tensile) which usually are made up of steel wires helically wounded around the pipe axis. These layers are carrying most of the loading.

- Polymer layers. The main function of these layers are to provide containment of the transported fluids, or preventing seawater from coming in contact with the armor layers.

There are two different types of flexible pipe constructions. These are bonded and nonbonded structures. In a nonbonded structure the armor layers will be able to slide relative to the surrounding layers, while in a bonded construction the different layers are bonded together through a vulcanization proceess. The focus of this report will be on the nonbonded type.

Nonbonded pipes can further be divided into two groups, namely rough bore and smooth bore structures. In a rough bore pipe there is a steel carcass supporting the inner liner. This is to prevent collapse of the liner, which may happen if a sudden pressure drop in the transported fluid occurs. A smooth bore pipe is very similar to the rough bore except that the carcass is omitted. This means that such a pipe can only be used when there is no gas diffusion through the internal thermoplastic layer. An example of a typical flexible pipe cross section is shown in fig 2.

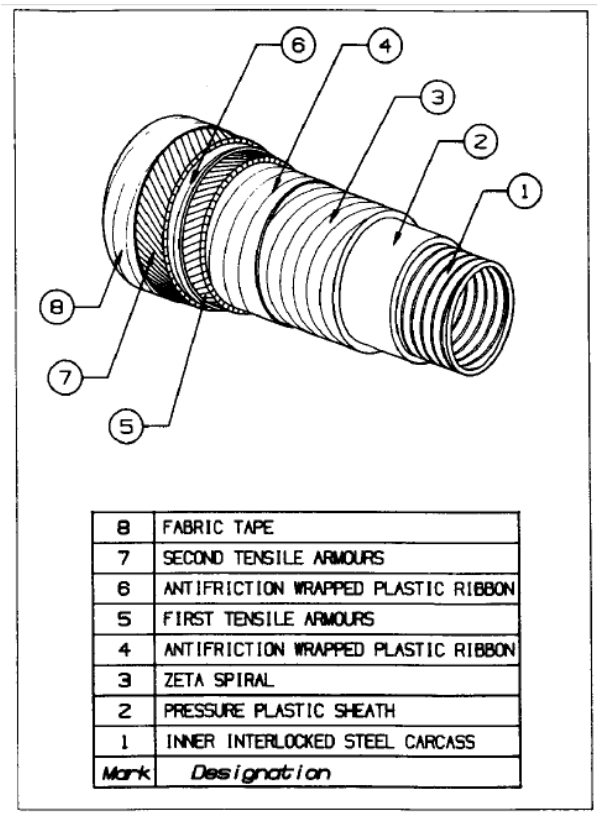

Figure 2: A typical flexible pipe cross section [2]

The different layers and their functions are as follows:

- The inner steel carcass supports the inner liner and prevents it from collapsing inwards. The carcass is built up of profiled steel strips, and is *not* fluid tight. This means that the carcass will only be experiencing external compression forces due to contact with the inner liner.

- The inner liner, or internal thermoplastic sheath, contains the transported fluids.

- The pressure armor provides strength with respect to both internal and external pressure. It is usually made up of a Z-shaped wire or two sets of C-profiles.
- Intermediate thermoplastic sheaths are used to reduce friction and wear between armor layers.
- The helically wound tensile armor layers provide axial and torsional capacity. They are usually made of flat steel wires with a lay angle of around 35 °. The most common type is the double crosswound tensile armor, having two layers with opposite winding direction. To reduce friction and wear, a thermoplastic anti wear layer is inserted between the tensile armor layers.
- The external thermoplastic layer keeps the seawater on the outside, and prevents corrosion and abrasion of the armor beneath. It also holds the tensile armor in place.

In addition to the layers mentioned above, a so called anti buckling tape layer may be included. This is essentially a high strength tape wrapped around the tensile armor layers. The function of the tape is to provide extra support for the armor in the radial direction. This extra support is necessary for the tensile armor to resist axial compression. The anti buckling tape is particularly important for deep water applications, and is critical to the capacity of the pipe if the annulus is flooded (meaning there is no hydrostatic pressure difference over the external sheath). Further discussions of the importance of the anti buckling tape strength is presented in section 6, which deals with buckling of tensile armor wires.

2.4 Flexible pipe behaviour

When a flexible pipe is subjected to axisymmetric loads, the response will be linear as long as the loading is within the linear range of the material [3]. The bending behaviour is however quite different. For small bending moments, the bending stiffness is relatively large, but at a certain value called the *friction moment*, the stiffness will drop significantly. This is the slip point, and it is from this point that the pipe really starts to be flexible.

The physical explanation behind this is that the friction forces between the layers are able to hold the tensile armor wires in place as long as the bending moment is small. When the bending moments exceeds the friction moment M_f, the wires starts to slip, and the stiffness drops significantly. It is noted that M_f will be a function of the contact pressure between the layers, meaning that it will depend on the internal and external pressure as well as the tensile force in the pipe.

For bending moments below M_f the assumption that plane sections remain plane holds true, and the bending stiffness can be assessed in the same way as for a composite beam. In the slip phase the main contribution to the bending stiffness comes from the circular plastic sheaths, however local straining (bending and torsion) of the armor wires will also contribute to the stiffness.

As discussed in [12], not all the armor wires in a layer will start to slip at the same time. If the pipe curvature is increased, the wires at the neutral axis will start to slip first, and the wires at the extreme fiber position will be the last to slip. Hence, there is a gradual transition from full stick to full slip. When all the wires in a layer has begun sliding, the bending stiffness of the layer has reached zero.

When full slip in all tensile armor layers is reached, the bending stiffness of the pipe remains constant until the critical curvature is exceeded. This is the point where the pipe is bent so much that the gaps between the armor wires are closed, and the wires come into contact with each other. A further increase of curvature would lead to very high stresses in the armor wires, and therefore the critical curvature should not be exceeded under normal operation. The bending behaviour of a nonbonded flexible pipe is illustrated in figure 3 below.

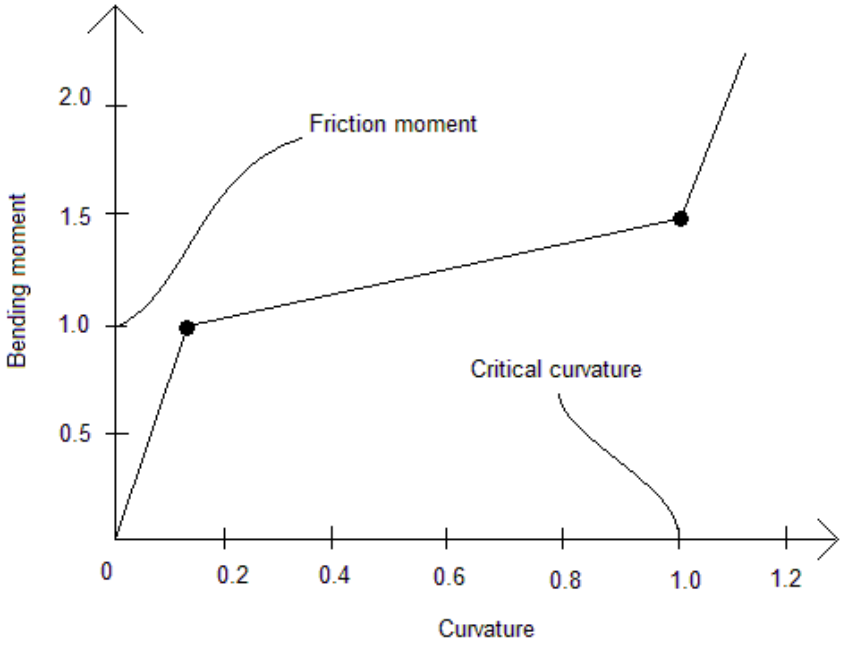

Figure 3: Bending behaviour of a nonbonded flexible pipe [3].

2.5 End termination

The most critical part of a flexible pipe construction is the point where the pipe is terminated to a rigid structure [10]. A typical way of doing this is to lead the pipe through a bending stiffener before the pipe is terminated at the end fitting. The bending stiffener ensures a gradual increase of bending stiffness towards the end of the pipe and most importantly keeps the pipe curvature below a critical value [3]. At the end of the pipe an end fitting is mounted in order to [11]:

- terminate the different layers of the flexible pipe in such a way that axial loads and bending moments may be transferred to an end connector.
- secure a pressure-tight connection between the pipe and the connector.

Inside the end fitting the armoring wires are locked relative to each other and the sealing layers. This means that close to the termination, in a zone corresponding to a couple of tensile armor pitch lengths, the flexibility of the pipe is reduced. Also, the pipe cannot be expected to have the same curvature capacity in this zone as in the rest of the pipe [10]. The local stresses that may arise in the tensile armor wires due to the anchoring of the tendons at the end fitting are investigated in section 5.

3 Failure modes and design criteria

3.1 Introduction

Knowledge of flexible pipe performance and possible failure modes is essential in order to do a successful design. There are numerous known failure modes, and checklists for design against them are found in API Recommended Practice 17B [11]. A flexible pipe should be designed to satisfy its functional requirements under the actual loading conditions. Load types that must be considered are functional, environmental and accidental loads during both installation and service conditions [11].

As the water depth at which flexible risers are being used increases, failure modes which are unlikely in less deep water may become more important. This section summarizes failure modes and design criteria with special focus on those relevant for deep water applications.

3.2 Failure modes

Failure is often defined as an event where a system ceases to fulfill its purpose. As the purpose of a flexible pipe is to transport fluids from one place to another, failure is an event which prevents this from happening. In general, this would be one of the two following events [10]:

- Leakage
- Reduction of internal cross section

Due to the complexity of the flexible pipe structure it is likely that such a failure will happen as a result of several less severe events. To avoid this, the design should take all possible partial failure modes into account. Table 1 shows a checklist of failure modes which should be taken into account during design. The table is taken from API Recommended Practice 17B [11].

Table 1: Failure modes for unbonded flexible pipes

Pipe failure mode	**Potential failure mechanisms**
Collapse	1) Collapse of carcass and/or pressure armor due to excess external pressure or tension. 2)Collapse of carcass and/or pressure armor due to installation loads or ovalization due to installation loads. 3)Collapse of internal pressure sheath in smooth-bore pipe.
Burst	1) Rupture of pressure armors because of excess internal pressure. 2) Rupture of tensile armors due to excess internal pressure.
Tensile failure	1) Rupture of tensile armors due to excess tension. 2) Collapse of carcass and/or pressure armors and/or internal pressure sheath due to excess tension. 3) Snagging by fishing trawl board or anchor, causing overbending or tensile failure.
Compressive failure	1) Bird-caging of tensile-armor wires. 2) Compression leading to upheaval buckling and excess bending.
Overbending	1) Collapse of carcass and/or pressure armor or internal pressure sheath. 2) Rupture of internal pressure sheath. 3) Unlocking of interlocked pressure or tensile-armor layer. 4) Crack in outer sheath.
Torsional failure	1) Failure of tensile armor wires. 2) Collapse of carcass and/or internal pressure sheath. 3) Bird-caging of tensile armor wires.
Fatigue failure	1) Tensile armor wire fatigue. 2) Pressure armor wire fatigue.
Erosion	Of internal carcass.
Corrosion	1) Of internal carcass. 2) Of pressure- or tensile armor exposed to seawater. 3) Of pressure- or tensile armor exposed to diffused product.

Of the failure modes listed in table 1, those related to collapse, tensile failure and compressive failure may be more pronounced for deep water applications because of large external pressure and tension. Fatigue failure may also be relevant, as high dynamic stresses are likely be present due to the large length which the environmental forces act along.

Failure due to the external hydrostatic pressure may happen either by collapse of the pressure armor/carcass or by so called bird-caging of the tensile armor. The pressure armor and carcass are designed to take this kind of loading, so failure of these components should be avoided by proper design. The bird-caging failure is different, because it occurs as a result of the tensile armor carrying loads which it is not designed for. Tensile armors are not designed to withstand compression, and may fail by radial expansion or lateral buckling.

The name bird-caging comes from the shape, which is seen in figure 4. The picture shows dissection of a bird-cage produced in a pressure tank test.

Figure 4: Bird-cage failure of flexible pipe [4].

Lateral buckling of the armor wires have also been reproduced in pressure tank tests, and a picture of this is shown in figure 5.

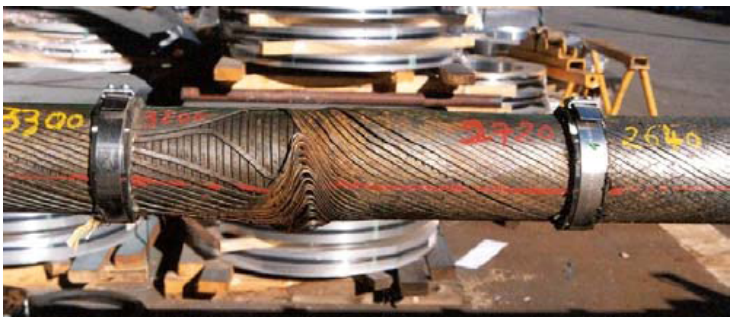

Figure 5: Lateral buckling of tensile armor causing severe dislocation [4].

Both pictures are taken from [4], which deals with instability issues of tensile armor wires. The conclusion of this paper is that the current methods used to predict these failure modes are inherently conservative, and that more accurate models may help increase the water depth capability of flexible risers.

Both radial and lateral failure modes for the tensile armor when subjected to compression from external pressure are investigated in section 6.

3.3 Design criteria

In order to prevent failure, a multiple of design criteria are to be satisfied. A design criteria is usually stated in the form of an utilization factor, which is the ratio between the structural capacity and the applied load. Because there are many uncertainties involved, for instance in the yield stress of the material, residual stresses and applied loading, the allowable utilization factor given in rules are much lower than 1.

Relevant design criteria for unbonded flexible pipes are explained in API RP 17B [11], and are described in terms of:

- strain
- creep
- stress
- hydrostatic collapse
- mechanical collapse
- torsion
- crushing collapse and ovalization (during installation)
- compression
- service life factors

Strain is a critical parameter for both the internal and external polymer layers. The strain must not exceed the allowable strain, which is specified either in rules or by the manufacturer.

Creep is relevant for the inner pressure sheath as this layer will creep into gaps in the pressure armor under normal service conditions. This must be taken into account when the wall thickness is to be determined.

Allowable stress is used as a design criteria for steel materials. Presence of residual stresses must be taken into account.

Hydrostatic collapse is equivalent to buckling of the internal carcass due to the external pressure. It should be verified that the collapse-to-design ratio is in the acceptable range for the case of both a breached and intact outer sheath.

Mechanical collapse of the internal carcass as a result of excessive tension should also be checked. The contribution from the surrounding steel layers may be taken into account.

When it comes to torsion, there are two different collapse scenarions depending on which direction the pipe torsion is applied. If the outer tensile armor is turned inward, it will press towards the internal armor layer, and tensile forces will develop. The stress in the wires should not exceed the allowable stress. If torsion is applied in the opposite direction, a gap will develop between the tensile armor layers, and the damaging torsion may be taken as the torsion required to create a gap equal to half the thickness of a tensile armor wire.

The installation phase also needs attention. The pipe may be subjected to significant loads when tightened to a tensioner or under reeling/unreeling, and it should be controlled that collapse or significant ovalization is avoided.

Compression may as previously mentioned cause bird-caging of the tensile armor layers. This means that the tensile armor wires moves outward in the radial direction, resulting in a bird cage shape. The allowable compression may be taken as the compression causing a gap between the underlying layers and the tensile armor wire equal to half the thickness of the wire. Buckling of the tensile armor wires should also be checked.

The main service life factors are fatigue and degradation of the material. There are several fatigue mechanisms, and careful evaluation of these should be performed. Corrosion and wear/fretting between wires should be taken into account.

4 Theory and methods

4.1 Introduction

In this section, theory and methods which are important for the work performed in this thesis is described. It is however not the intention to explain *all* the theory which is used. Much of the work is based on well known methods from structural mechanics and mathematics, and describing every aspect of this would be of little interest. Instead it is focused on topics which are not that well known (at least not to the author), and which are especially important in solving the problems of this thesis.

4.2 Analytical methods for stress analysis

When a nonbonded flexible pipe is subjected to axisymmetric loads (tension, pressure and torsion), the behaviour will be linear and the stiffness will be of the same order as for a steel pipe [13]. The loads do not change the cylindrical shape, and due to the symmetry of these problems, simple design formulas are obtained by introducing some basic assumptions. The bending behaviour is however more complicated, and analytical solutions for stress and strain in the helical tensile armor are based upon an assumed path and constant pipe curvature. This section contains a brief review of some relevant equations, and the assumptions behind them. The formulas for stress due to tension, pressure and torsion are found in [10], while the section covering bending is based on [5].

4.2.1 Tension

Tensile loads are mainly taken up by the tensile armor. The resistance of the plastic layers are negligible, and because of the very large lay angle of the pressure armor, its contribution will also be small.

Equilibrium in the longitudinal direction of a pipe subjected to an effective axial force T_e gives the following equation:

$$\sum_{i=1}^{N} n_i \sigma_i A_i \cos\alpha_i = T_w = T_e + \pi R_{int}^2 p_{int} - \pi R_{ext}^2 p_{ext} \tag{1}$$

where N is the number of layers contributing to the axial resistance, n_i is the number of wires in layer i, σ_i is the axial stress in the wire, A_i is the wire cross sectional area and α_i is the lay angle of the layer. It is observed that the internal and external pressure gives rise to axial end cap forces.

When the helical armor layers are exposed to tension they will tend to contract, however the underlying layers will prevent this. The resulting contact pressure can be approximated by:

$$p_T = \frac{T_w \tan^2\alpha}{2\pi R^2} \tag{2}$$

where R is the mean radius of the tensile armor layers.

4.2.2 Pressure

When subjected to pressure forces, it is mainly the armor layers that will carry the load. A good approximation is to say that the plastic sheaths simply transmit the pressure,

meaning that these layers do not give any contribution to the strength. The carcass does not carry any internal pressure, so it is the pressure and tensile armor alone that takes the internal pressure load. Equilibrium between internal and external pressure and internal forces in the radial direction gives this equation:

$$\sum_{i=1}^{N} \frac{n_i \sigma_i A_i \sin\alpha_i \tan\alpha_i}{2\pi R_i} = p_{int} R_{int} - p_{ext} R_{ext} \tag{3}$$

where N is the number of layers providing resistance to pressure, n_i is the number of wires, σ_i is the axial stress in each wire, A_i is the cross sectional area of a single wire, α_i is the lay angle and R_i is the radius of layer i.

The buckling strength is important with respect to collapse due to external pressure. The buckling pressure of the carcass or pressure armor layer may be determined from:

$$p_{cr} = \frac{3EI_{eq}}{R^3} \tag{4}$$

where R is the mean radius of the layer and EI_{eq} is the equivalent bending stiffness.

4.2.3 Torsion

If the torsional resistance of the plastic layers is neglected, the torsional moment M_t must be balanced by the stresses in the helically wound armor layers. It is found from this equilibrium consideration that:

$$\sum_{i=1}^{N} R_i n_i \sigma_i A_i \sin\alpha_i = M_t \tag{5}$$

It is mainly the tensile armors that provides the torsional resistance. This gives the following approximation for the stress in the tensile armor wires:

$$\sigma_t = \frac{M_t}{nRA_i \sin\alpha} \tag{6}$$

where n is the total number of tensile armor wires and R is the mean radius of the tensile armor layers.

4.2.4 Bending

As previously mentioned, the bending behaviour of a flexible pipe is more complicated than for the axisymmetric load cases. This is mainly related to the helical reinforcing layers which tend to slip relative to the surrounding layers when subjected to a bending moment larger that M_f (see section 2).

The challenge is to find the stresses in the tendons during the slip phase, and in order to do this analytically, a constant curvature is assumed along the pipe, and also which path the tendons follow as they slip. In previous work, both the geodesic and the loxodromic curve has been used to describe the path of the tendons, thus giving different results for the tendon stress.

The main properties of the two assumed curves are:

- Loxodromic curve:

  - Tendon slides in the longitudinal direction, inducing friction stress
  - No transverse sliding
  - Normal curvature (weak axis), transverse curvature (strong axis) and torsion

- Geodesic curve:
  - Sliding in both longitudinal and transverse direction
  - Normal curvature is larger than for the loxodromic curve
  - No transverse curvature
  - More torsion than for the loxodromic

Experiments have shown that the loxodromic curve gives the best fit with respect to dynamic stresses for realistic friction coefficients. [5].

Stress components of armors

The relevant stress components of armors are:

- σ_{xx-fx}: The axial stress which is constant over the wire cross section, and a result of the axial force due to pressure, tension, torsion moment and friction.
- σ_{xx-my}: The normal curvature stress which is a result of bending about the weak axis. Has its maximum at the outer and inner surface of the armor wire.
- σ_{xx-mz}: The transverse curvature stress which is a result of bending about the strong axis. Has its maximum at the sides of the armor wire.
- σ_{yz}: The torsion shear stress.

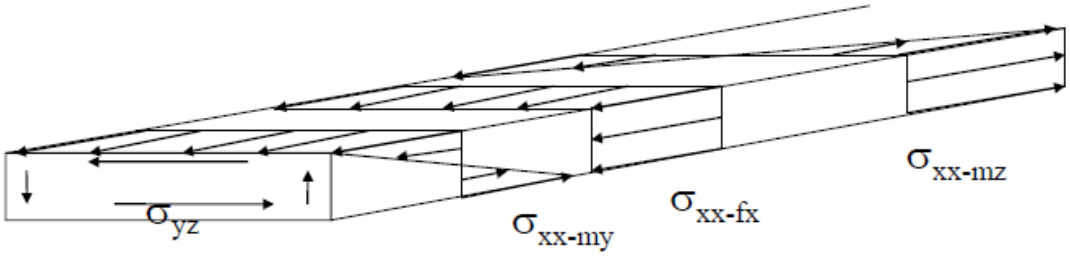

Figure 6: Relevant stress components in armors [5].

Stresses when assuming geodesic curve

If the armor wires follow the geodesic curve, the change in stresses as a result of a change in pipe curvature $\Delta\kappa$ may be expressed by the following formulas. The necessary parameters are defined in figure 7. In this figure, the coordinate system is positioned in the center of the pipe, and X indicates the longitudinal direction.

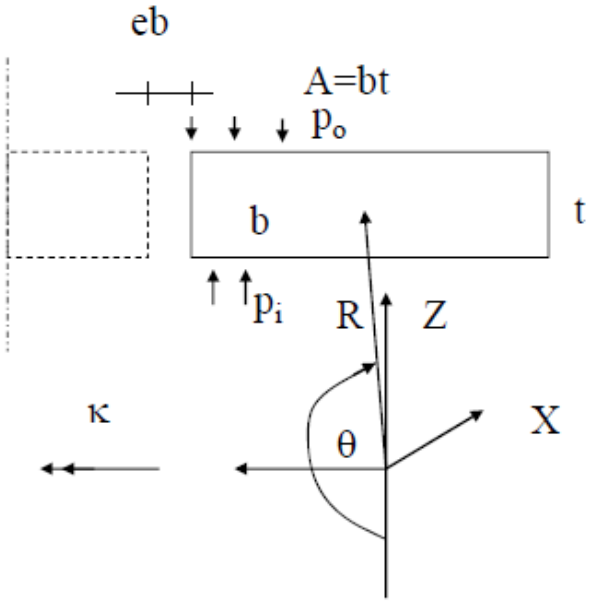

Figure 7: Parameters for calculation of stresses in armor wires [5].

Dynamic bending stress due to normal curvature:

$$\Delta\sigma_{xx-my} = \frac{3}{2}\cos^2\alpha\Delta\kappa tE\cos\theta \tag{7}$$

Dynamic bending stress due to transverse curvature:

$$\Delta\sigma_{xx-mz} = 0 \tag{8}$$

Dynamic axial stress (μ is the friction coefficient):

$$\Delta\sigma_{xx-fx} = min(ER\cos^2\alpha\Delta\kappa\cos\theta, 2\left[\frac{\pi R}{2\sin\alpha A}(p_o + p_i)b(1+e)\mu\cos\theta\right]) \tag{9}$$

Dynamic stress due to torsion:

$$\Delta\sigma_{yz} = \sin\alpha\cos\alpha(\frac{1}{\sin^2\alpha} - 3)\Delta\kappa\cos\theta \tag{10}$$

Stresses when assuming loxodromic curve

If instead the loxodromic curve is used to describe the path of the armor wires, the expressions for the different stress components will be as shown below.

Dynamic bending stress due to normal curvature:

$$\Delta\sigma_{xx-my} = \frac{1}{2}\cos^4\alpha\Delta\kappa tE\cos\theta \tag{11}$$

Dynamic bending stress due to transverse curvature:

$$\Delta\sigma_{xx-mz} = \frac{1}{2}\cos\alpha(1+\sin^2\alpha)\Delta\kappa bE\sin\theta \tag{12}$$

Dynamic axial stress (the same expression as for the geodesic):

$$\Delta\sigma_{xx-fx} = min(ER\cos^2\alpha\Delta\kappa\cos\theta, 2\left[\frac{\pi R}{2\sin\alpha A}(p_o+p_i)b(1+e)\mu\cos\theta\right]) \tag{13}$$

Dynamic stress due to torsion:

$$\Delta\sigma_{yz} = \sin\alpha\cos^3\alpha\Delta\kappa\cos\theta \tag{14}$$

4.3 Theory of thin curved beams

In order to correctly describe the behaviour of the tensile armor wires one needs a model that is based on the actual geometry, with the inherent twist and curvature. Because of the shape of the wire there will be a coupling between lateral and axial forces as well as bending and torsional moments which makes the analysis more complicated than for straight beams. This section is based on chapter 2 in [3], and gives a review of the theory of thin curved beams sliding on a circular cylindric surface.

4.3.1 Definitions

Assume that there is a fixed Cartesian coordinate system at the center of the pipe with axes Z^I and unit vectors $\mathbf{E_I}$. The underlying layers provide support such that the tendons slide on a cylindrical surface represented by a radius R. The center line of a tendon describes a curve in space which is characterized by its curvature components. Details about curves in space and curvature may be found in mathematical textbooks, e.g. [14].

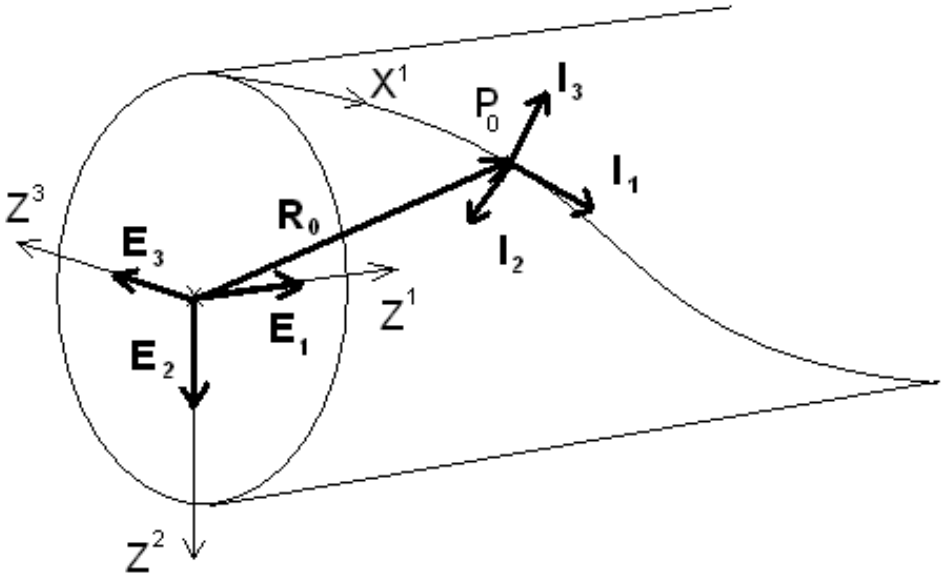

Figure 8: $\mathbf{E_I}$ and $\mathbf{I_I}$ coordinate systems.

Assume that the vector $\mathbf{R_0}$ describes any point P_0 on the center line of a tendon and let X^1 be the arc length coordinate along the tendon. At the point P_0 there is a local orthonormal coordinate system with base vectors $\mathbf{I_I}$. The concept is illustrated in figure 8. The base vectors $\mathbf{I_I}$ are known from differential geometry as the unit tangent, unit normal and unit binormal vectors and are determined as:

$$\mathbf{I_1} = \mathbf{R_{0,1}} = Z^I_{,1}\mathbf{E_I} \tag{15}$$

$$\mathbf{I_2} = \frac{1}{\kappa}\mathbf{R_{0,11}} = \frac{1}{\kappa}Z^I_{,11}\mathbf{E_I} \tag{16}$$

$$\mathbf{I_3} = \mathbf{I_1} \times \mathbf{I_2} \tag{17}$$

The base vectors will rotate as we go along the arc length coordinate X_1, and the rotation over a small distance dX^1 is given by the Seret-Frenet equation:

$$\begin{bmatrix} \frac{d\mathbf{I_1}}{dX^1} \\ \frac{d\mathbf{I_2}}{dX^1} \\ \frac{d\mathbf{I_3}}{dX^1} \end{bmatrix} = \begin{bmatrix} 0 & \kappa & 0 \\ -\kappa & 0 & \tau \\ 0 & -\tau & 0 \end{bmatrix} \begin{bmatrix} \mathbf{I_1} \\ \mathbf{I_2} \\ \mathbf{I_3} \end{bmatrix} \tag{18}$$

For a circular helix with lay angle α, the torsion τ and the principal curvature κ are:

$$\tau = \frac{\sin\alpha\cos\alpha}{R} \tag{19}$$

$$\kappa = \frac{\sin^2\alpha}{R} \tag{20}$$

The $\mathbf{I_I}$ base vectors defines the tendon center line only, and does not hold any information about the orientation of the tendons cross section. To describe the orientation of the cross section, another coordinate system is introduced with base vectors $\mathbf{G_I}$ and axes X^I. The orientation is such that $\mathbf{G_1}$ is parallel to $\mathbf{I_1}$ while $\mathbf{G_2}$ is always directed along

the inwards surface normal. The last vector, $\mathbf{G_3}$, is defined by being orthogonal to both $\mathbf{G_1}$ and $\mathbf{G_2}$. The relative angle between the $\mathbf{G_I}$ and $\mathbf{I_I}$ system is denoted ω as shown in figure 9.

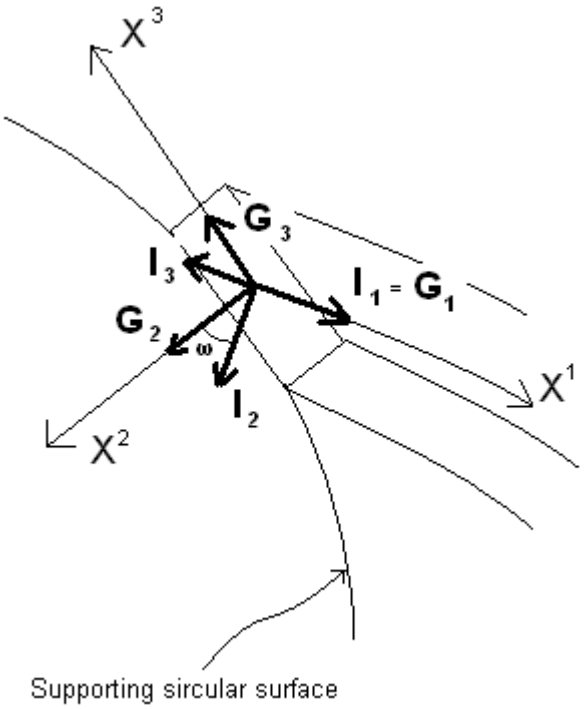

Figure 9: $\mathbf{G_I}$ and $\mathbf{I_I}$ coordinate systems.

The rotation of the $\mathbf{G_I}$ system may be expressed in a similar way as for the $\mathbf{I_I}$ base vectors, however this time through the *generalized* Seret-Frenet equation:

$$\begin{bmatrix} \frac{d\mathbf{G_1}}{dX^1} \\ \frac{d\mathbf{G_2}}{dX^1} \\ \frac{d\mathbf{G_3}}{dX^1} \end{bmatrix} = \begin{bmatrix} 0 & \kappa_3 & -\kappa_2 \\ -\kappa_3 & 0 & \kappa_1 \\ \kappa_2 & -\kappa_1 & 0 \end{bmatrix} \begin{bmatrix} \mathbf{G_1} \\ \mathbf{G_2} \\ \mathbf{G_3} \end{bmatrix} \tag{21}$$

Here, κ_2 and κ_3 is the components of the principal curvature, κ, in the X^1X^3 and X^1X^2 planes respectively. Thus κ_2 is called the transverse curvature and κ_3 is called the normal curvature. κ_1 is the total torsion of the center line. The curvature components relate to the principal curvature and geometric torsion through these formulas:

$$\kappa_1 = \tau + \frac{d\omega}{dX^1} \tag{22}$$

$$\kappa_2 = \kappa \sin\omega \tag{23}$$

$$\kappa_3 = \kappa \cos\omega \tag{24}$$

4.3.2 Equilibrium equations

Consider a small element of a curved beam with a local coordinate system with base vectors $\mathbf{G_I}$ as decribed in the previous subsection (see figure 10). The forces acting on the element are the stress resultants Q_I (forces) and M_I (moments), and also the distributed external loading q_I and m_I. At the far end of the element, both the magnitude *and* the direction of the forces has changed, and the change of direction is described by the Seret-Frenet formula.

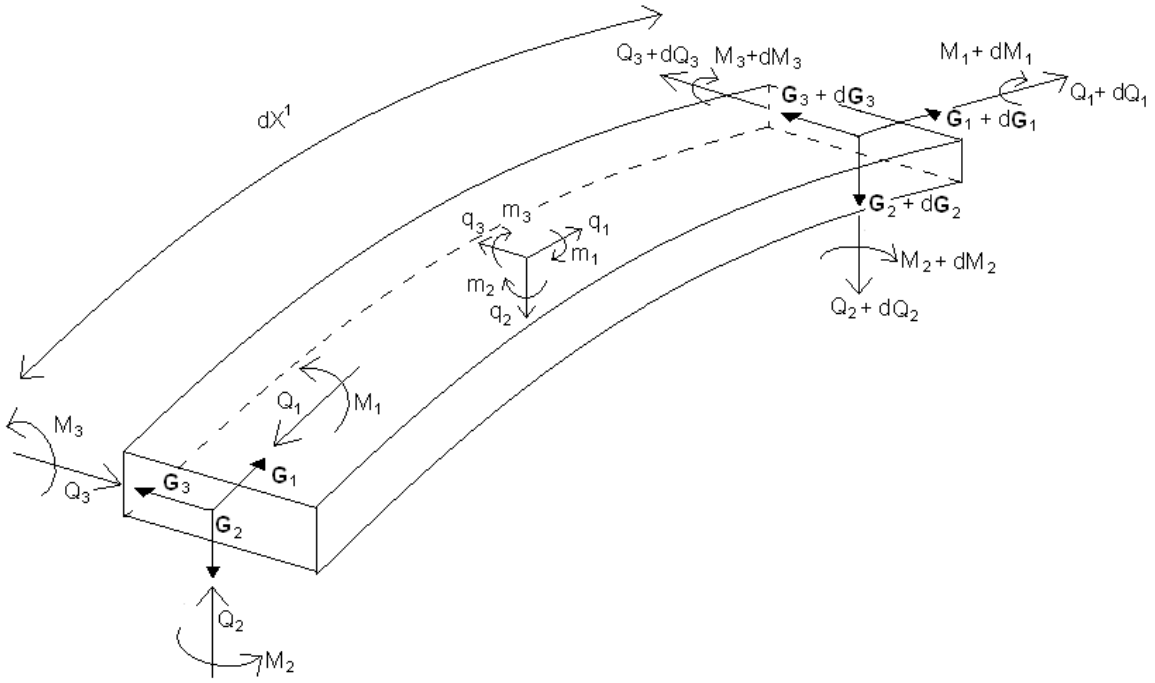

Figure 10: A small curved beam element subjected to stress resultants and external load.

Equilibrium equations are found by demanding zero net force and moment on vector form. The force equilibrium equation is:

$$\begin{aligned} Q_1\frac{d\mathbf{G_1}}{dX^1} + Q_2\frac{d\mathbf{G_2}}{dX^1} + Q_3\frac{d\mathbf{G_3}}{dX^1} + q_1\mathbf{G_1} + q_2\mathbf{G_2} + q_3\mathbf{G_3} \\ + \frac{dQ_1}{dX^1}\mathbf{G_1} + \frac{dQ_2}{dX^1}\mathbf{G_2} + \frac{dQ_3}{dX^1}\mathbf{G_3} = 0 \end{aligned} \tag{25}$$

and the moment equilibrium equation is:

$$\begin{aligned} M_1\frac{d\mathbf{G_1}}{dX^1} + M_2\frac{d\mathbf{G_2}}{dX^1} + M_3\frac{d\mathbf{G_3}}{dX^1} + m_1\mathbf{G_1} + m_2\mathbf{G_2} + m_3\mathbf{G_3} \\ + Q_2\mathbf{G_3} - Q_3\mathbf{G_2} + \frac{dM_1}{dX^1}\mathbf{G_1} + \frac{dM_2}{dX^1}\mathbf{G_2} + \frac{dM_3}{dX^1}\mathbf{G_3} = 0 \end{aligned} \tag{26}$$

As the two above equations are on vector form, they may be split into their three $\mathbf{G_I}$ components such that each vector equation yields three new equations. If one substitutes for the $\frac{d\mathbf{G_I}}{dX^1}$-terms using equation (21) and separates the different vector components, six coupled equilibrium equations are found:

$$\frac{dQ_1}{dX^1} - \kappa_3 Q_2 + \kappa_2 Q_3 + q_1 = 0 \tag{27}$$

$$\frac{dQ_2}{dX^1} - \kappa_3 Q_1 + \kappa_1 Q_3 + q_2 = 0 \tag{28}$$

$$\frac{dQ_3}{dX^1} - \kappa_2 Q_1 + \kappa_1 Q_2 + q_3 = 0 \tag{29}$$

$$\frac{dM_1}{dX^1} - \kappa_3 M_2 + \kappa_2 M_3 + m_1 = 0 \tag{30}$$

$$\frac{dM_2}{dX^1} + \kappa_3 M_1 - \kappa_1 M_3 - Q_3 + m_2 = 0 \tag{31}$$

$$\frac{dM_3}{dX^1} - \kappa_2 M_1 + \kappa_1 M_2 + Q_2 + m_3 = 0 \tag{32}$$

4.3.3 Deformation and strain

In an undeformed configuration, the position vector of a material particle at a specific point P in the cross section of the beam is:

$$\mathbf{R} = \mathbf{R}_0 + X^2\mathbf{G_2} + X^3\mathbf{G_3} \tag{33}$$

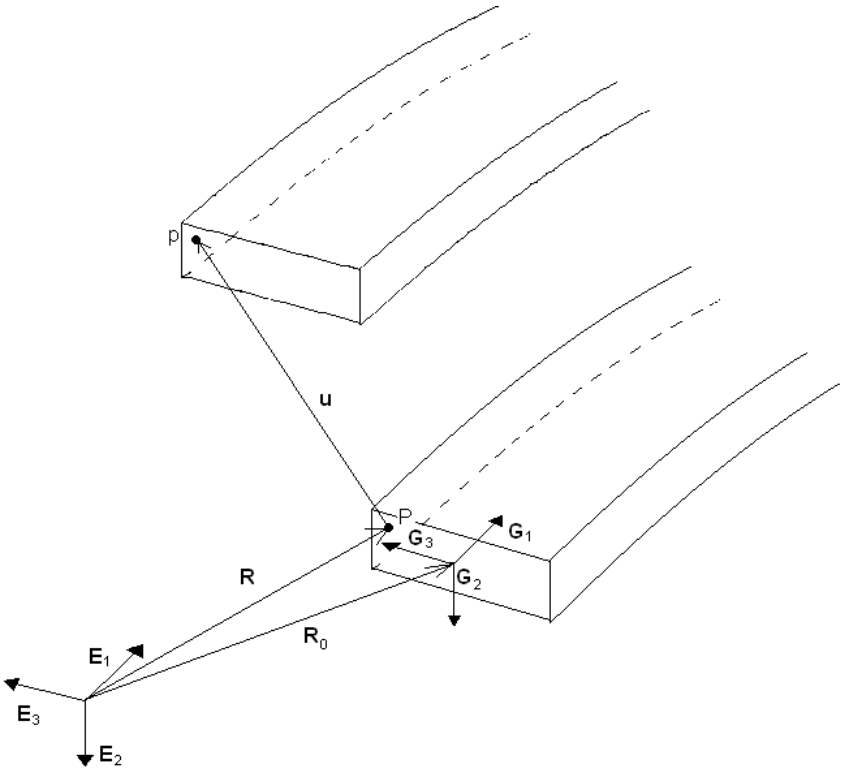

Figure 11: Curved beam element before and after deformation.

Assume now that the beam deforms, see figure 11. The material particle has now moved from P to p. The displacement **u** of the point P is:

$$\mathbf{u} = u_1\mathbf{G_1} + u_2\mathbf{G_2} + u_3\mathbf{G_3} \tag{34}$$

where each component is:

$$u_1 = u_1^0(X^1) + X^3\theta_2(X^1) - X^2\theta_3(X^1) + \beta(X^1)\varphi(X^2, X^3) \tag{35}$$

$$u_2 = u_2^0(X^1) - X^3\theta_1(X^1) \tag{36}$$

$$u_3 = u_3^0(X^1) - X^2\theta_1(X^1) \tag{37}$$

In the above equations, u_i^0 is the displacement of the center line of the beam in direction i, while θ_i is the rotation of the cross-section about axis i. β is the twist of the cross-section, which according to Saint-Venant's torsion theory for a straight beam loaded by a constant torque would be equal to $\theta_{1,1}$. All the variables are assumed to be dependent on the arc length coordinate X^1 only, except φ which is the warping function and varies over the cross section. More details about warping is given in section 4.4.

The Green strain tensor will be used as measure of strain in this case. Let E^*_{KL} be the Green strain tensor in the *local curvilinear* coordinate system. This is given on component form as:

$$E^*_{KL} = \frac{1}{2}\left(\frac{\partial \mathbf{r}}{\partial X^K}\frac{\partial \mathbf{r}}{\partial X^L} - \frac{\partial \mathbf{R}}{\partial X^K}\frac{\partial \mathbf{R}}{\partial X^L}\right) \tag{38}$$

By introducing $\mathbf{r} = \mathbf{R} + \mathbf{u}$ with the expressions for $\mathbf{R}$ and $\mathbf{u}$ given above and by using the Seret-Frenet equation to handle the derivatives of the $\mathbf{G_I}$ terms, the components of E^*_{KL} is found. This strain measure is however given in the *curvilinear* coordinate system X^I, while the material law which is to be used is given in Cartesian coordinates. Therefore the strain tensor E^*_{KL} must be transformed from curvilinear to Cartesian coordinates. In order to do this, a Cartesian coordinate system with axes Y^I is positioned so that it coincides with the curvilinear G^I system. The transformation can now be done using the following equation:

$$E_{IJ} = \frac{\partial X^K}{\partial Y^I}\frac{\partial X^L}{\partial Y^J}E^*_{KL} \tag{39}$$

By carrying out the calculations and neglecting insignificant second order terms, the Green strain tensor components in the Cartesian coordinate system is found to be:

$$GE_{11} = \sqrt{G}(\epsilon_1 + X^3\omega_2 - X^2\omega_3 + \varphi\beta_{,1} + \kappa_1\beta[X^3\varphi_{,2} - X^2\varphi_{,3}]) + \frac{1}{2}\epsilon_1^2 + \frac{1}{2}\epsilon_2^2 + \frac{1}{2}\epsilon_3^2 \tag{40}$$

$$2\sqrt{G}E_{12} = \epsilon_2 - \theta_3 - X^3\omega_1 + \beta[\sqrt{G}\varphi_{,2} + \kappa_3\varphi] \tag{41}$$

$$2\sqrt{G}E_{13} = \epsilon_3 + \theta_2 - X^2\omega_1 + \beta[\sqrt{G}\varphi_{,3} + \kappa_2\varphi] \tag{42}$$

where:

$$\epsilon_1 = u_{1,1}^0 - \kappa_3 u_2^0 + \kappa_2 u_3^0 \tag{43}$$

$$\epsilon_2 = u^0_{2,1} + \kappa_3 u^0_1 - \kappa_1 u^0_3 \tag{44}$$

$$\epsilon_3 = u^0_{3,1} - \kappa_2 u^0_1 + \kappa_1 u^0_2 \tag{45}$$

$$\omega_1 = \theta_{1,1} - \kappa_3 \theta_2 + \kappa_2 \theta_3 \tag{46}$$

$$\omega_2 = \theta_{2,1} + \kappa_3 \theta_1 - \kappa_1 \theta_3 \tag{47}$$

$$\omega_3 = \theta_{3,1} - \kappa_2 \theta_1 + \kappa_1 \theta_2 \tag{48}$$

and G is the determinant of the metric tensor:

$$G = (1 + X^3\kappa_2 - X^2\kappa_3)^2 \tag{49}$$

4.3.4 The principle of virtual displacements

The principle of virtual displacements states that [15]:

> "the total virtual work performed by a system in equilibrium while undergoing a set of virtual compatible displacements, is zero."

In other words, the work done by the *real* internal stresses $\boldsymbol{\sigma}$ when a structure is subjected to the *virtual* strains $\delta\epsilon$ must be equal to the work done by the *real* external surface tractions $\mathbf{t}$ over the *virtual* displacements $\delta\mathbf{u}$. A necessary presumption is, as suggested earlier, that the virtual strains and displacements are compatible and that the internal stresses are in equilibrum with the external tractions (volume forces are disregarded here). If the difference between one equilibrium state and the next is small, the second order terms in the Green strain tensor may be neglected. Therefore the strain measure ϵ is introduced where $\epsilon = \mathbf{E}$ when the second order terms are neglected. In mathematical terms the principle of virtual displacements is:

$$\int_V \boldsymbol{\sigma} : \delta\epsilon \; dV - \int_S \mathbf{t} \cdot \delta\mathbf{u} \; dS = 0 \tag{50}$$

Here, $dV = \sqrt{G}\; dX^1 dX^2 dX^3$, but in the present application $\sqrt{G} \approx 1$ will be used as this only introduces a very small error. When it comes to the stresses, a linear elastic material behaviour is assumed, meaning that the stress components are found directly from Hooke's law:

$$\sigma_{11} = C_\sigma \epsilon_{11} \tag{51}$$

$$\sigma_{12} = 2C_\tau \epsilon_{12} \tag{52}$$

$$\sigma_{13} = 2C_\tau \epsilon_{13} \tag{53}$$

In deriving the expression for the internal work, i.e. the first term of equation (50), it will further be assumed that the cross section considered is double symmetric. This means that:

$$\varphi(X^2, X^3) = -\varphi(-X^2, X^3) = -\varphi(X^2, -X^3) \tag{54}$$

By introducing the strain expressions from equations (40)-(42) and the material law from equations (51)-(53) into the first term of equation (50), the internal virtual work is found to be:

$$W_i = \int_0^l Q_1 \delta\epsilon_1 dX^1 + C_\sigma D\kappa_1 \int_0^l \epsilon_1 \delta\omega_1 dX^1 - C_\sigma \Gamma \int_0^l \omega_{1,11} \delta\omega_1 dX^1 + \int_0^l Q_2 \delta(\epsilon_2 - \theta_3) dX^1 + \int_0^l Q_3 \delta(\epsilon_3 + \theta_2) dX^1 + \int_0^l M_1 \delta\omega_1 dX^1 + \int_0^l M_2 \delta\omega_2 dX^1 + \int_0^l M_3 \delta\omega_3 dX^1 \tag{55}$$

Here, ϵ_i and ω_i represents the actual strains the structure, corresponding to the real stresses, while $\delta\epsilon_i$ and $\delta\omega_i$ represents the virtual strains. The stress resultants Q_i and M_i are defined as:

$$Q_1 = C_\sigma A\epsilon_1 + C_\sigma D\kappa_1\beta \tag{56}$$

$$Q_2 = C_\tau A(\epsilon_2 - \theta_3) \tag{57}$$

$$Q_3 = C_\tau A(\epsilon_3 + \theta_2) \tag{58}$$

$$M_1 = C_\tau I_t \beta + C_\tau I_p(\omega_1 - \beta) \tag{59}$$

$$M_2 = C_\sigma I_2 \omega_2 \tag{60}$$

$$M_3 = C_\sigma I_3 \omega_3 \tag{61}$$

In the above equations, A is the cross section area, I_2 and I_3 are the second moment of area about axis 2 and 3 respectively, I_t is the cross section torsion constant and I_p is the polar moment of inertia of the cross section. D and Γ are defined as:

$$D = I_2 + I_3 - \int_S \varphi_{,2} X^3 - \varphi_{,3} X^2 + X^2 X^2 + X^3 X^3 dS \tag{62}$$

$$\Gamma = \int_S \varphi^2 dS \tag{63}$$

The idea of deriving equation (55) is that it may be used to calculate the internal forces in an element when the strain state is known. The internal forces are equivalent to the internal load vector which is needed in the structural analysis. This will be explained further in section 4.5.1.

Before moving on, some observations on the stress resultants given above may be done. Recalling that a basic assumption in the traditional Euler-Bernoulli beam theory is that shear deformations may be neglected, it seems reasonable to assume the same in this case. Looking at the expressions for Q_2 and Q_3, this assumption leads to the following results:

$$\theta_2 = -\epsilon_3 \tag{64}$$

$$\theta_3 = \epsilon_2 \tag{65}$$

This means that the rotation about the X^2 and X^3 axes are uniquely defined by the displacement of the center line of the beam. It is also seen that if β equals ω_1, a familiar relation between the twist and torque for cylindrical shafts with constant twist and no restrained warping appears from equation (59). Directed by this observation, it is in the following assumed that:

$$\beta = \omega_1 \tag{66}$$

One last, but important observation, is that the quantites ω_1, ω_2 and ω_3 must be equal to the curvature change around axis 1,2 and 3 respectively. This is due to the manner of which the torque and bending moments are defined. It is therefore possible to define the curvature increments as:

$$\Delta\kappa_i = \Delta\omega_i \tag{67}$$

This result may be used to update the geometry in a stepwise solution method.

4.3.5 The principle of virtual displacements on incremental form

In large deformation problems of structural mechanics it is common to perform the analysis by increasing the external loading incremetally. In order to obtain the necessary stiffness relationship for such an analysis, the principle of virtual displacements on incremental form may be utilized. Imagine that an element goes from the current configuration, C^n, to the next, C^{n+1}. Let the physical stresses in the C^n configuration be denoted $\boldsymbol{\sigma} = \mathbf{C} : \epsilon$ and the surface tractions $\mathbf{t}$. As the structure moves to the next configuration, the quantities change to:

$$\boldsymbol{\sigma}_{n+1} = \mathbf{C} : (\epsilon + \Delta\mathbf{E}) \tag{68}$$

$$\mathbf{t}_{n+1} = \mathbf{t} + \Delta\mathbf{t} \tag{69}$$

Now take the principle of virtual displacements at the C^{n+1} configuration, and assume a virtual displacement $\delta\mathbf{u}$ and a corresponding virtual strain field $\delta(\epsilon + \Delta\mathbf{E})$:

$$\int_V \mathbf{C} : (\epsilon + \Delta\mathbf{E}) : \delta(\epsilon + \Delta\mathbf{E})\ dV - \int_S (\mathbf{t} + \Delta\mathbf{t}) \cdot \delta\mathbf{u}\ dS = 0 \tag{70}$$

Subtracting equation (50) and neglecting second order terms in Δ while assuming that the difference between two neighbouring equilibrium states is small yields:

$$\int_V \mathbf{C} : \Delta\epsilon : \delta\epsilon\ dV + \int_V \boldsymbol{\sigma} : \delta\Delta\mathbf{E}\ dV - \int_S \Delta\mathbf{t} \cdot \delta\mathbf{u}\ dS = 0 \tag{71}$$

The above equation may be used to find the stiffness matrix of a curved beam element. The first term represents the material stiffness, while the second term is the geometric, or initial stress stiffness. By inserting the strain expressions from equations (40)-(42) as well as the material law, the two internal work terms are expressed as:

$$W_i^M = C_\sigma A \int_0^l \Delta\epsilon_1 \delta\epsilon_1 dX^1 + C_\sigma D\kappa_1 \int_0^l (\Delta\kappa_1 \delta\epsilon_1 + \Delta\epsilon_1 \delta\omega_1) dX^1 - C_\sigma \Gamma \int_0^l \Delta\kappa_{1,11} \delta\omega_1 dX^1$$
$$+ (C_\tau I_t + C_\sigma \kappa_1^2 K_1 - C_\tau D + C_\tau \Gamma \kappa^2 + C_\tau K_2) \int_0^l \Delta\kappa_1 \delta\omega_1 dX^1$$
$$+ C_\sigma I_2 \int_0^l \Delta\kappa_2 \delta\omega_2 dX^1 + C_\sigma I_3 \int_0^l \Delta\kappa_3 \delta\omega_3 dX^1 \tag{72}$$

$$W_i^G = Q_1 \int_0^l (\Delta\epsilon_1 \delta\epsilon_1 + \Delta\epsilon_2 \delta\epsilon_2 + \Delta\epsilon_3 \delta\epsilon_3) dX^1 \tag{73}$$

where:

$$K_1 = \int_S (X^3 \varphi_{,2} - X^2 \varphi_{,3})^2 dS \tag{74}$$

$$K_2 = \int_S \varphi_{,2}^2 + \varphi_{,3}^2 dS \tag{75}$$

The warping function φ is given in the next section.

4.4 Torsion with restrained warping

In section 5 the local bending and end section *warping* stresses at the end fitting will be investigated. Here, an attempt will be made to explain the fundamentals of restrained warping and also how the arising stresses can be found. Warping is a phenomenon related to torsion of prismatic bars which can easily be visualized. Figure 12 is taken from [6] and shows an experiment where a rectangular bar is subjected to torsion.

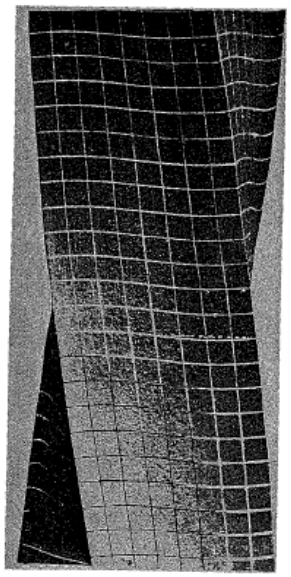

Figure 12: Prismatic bar subjected to torsion [6].

It is seen that the cross sections do not remain plane and that rectangular elements distort. This is what is referred to as *warping*. The twisting of the bar leads to displacements in the longitudinal direction, and for a straight bar the magnitude of this displacement is given by the angle of twist per unit length τ and the warping function $\varphi(X^2, X^3)$ [16]:

$$u_1 = \tau\varphi(X^2, X^3) \tag{76}$$

The warping function must of course satisfy the equilibrium equations of the cross section as well as the boundary conditions, which are zero net force at the cross section surface. In [6] it is shown that the equilibrium equations lead to the following requirement to the warping function, which is known as Laplace's equation:

$$\varphi_{,22} + \varphi_{,33} = 0 \tag{77}$$

Analytical expressions for the warping function may be found for some cross section geometries by solving this equation while fulfilling the boundary conditions. The warping function for a rectangular cross section of width a and thickness b is found in [16]:

$$\varphi(X^2, X^3) = -X^2X^3 + b^2(\frac{2}{\pi})^3 \sum_{n=0}^{\infty} \frac{(-1)^n}{(2n+1)^3} \frac{\sinh(\frac{2n+1}{b}\pi X^3)}{\cosh(\frac{2n+1}{2b}\pi a)} \sin(\frac{2n+1}{b}\pi X^2) \tag{78}$$

The warping function has been visualized in the computer program Matlab and is shown in figure 13 below. It is seen that the function value is zero at both axes where $X^2 = 0$ and $X^3 = 0$, i.e. the neutral axes of the cross section. It has its maximum/minimum values on the edges at some point close to the corners of the cross section.

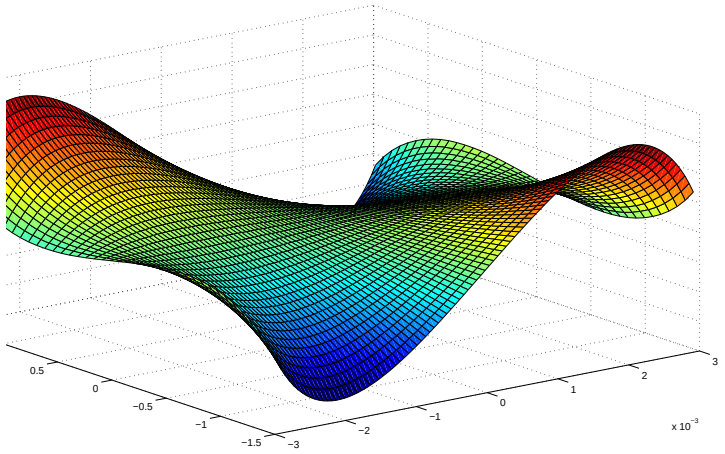

Figure 13: Visualization of the warping function of a rectangular cross section.

Now take a look back at figure 12 and imagine what the bar would look like if one of the end surfaces was fully fixed, for example attached to a rigid wall. Obviously, displacements in the longitudinal direction would have to change, because the material would now be fixed at the end. The rectangular elements would have to remain straight at the fixed end, and the warping would be *restrained*. The axial stresses that develop due to restrained warping are described in [17], and are given by:

$$\sigma_{11} = C_\sigma \epsilon_1 = C_\sigma u_{1,1} = C_\sigma \varphi(X^2, X^3)\tau_{,1} \tag{79}$$

This result indicates that there will only be axial warping stresses present whenever the twist per unit length changes along the structural member. As the warping stress distribution over the cross section is in fact determined by the warping function φ, one knows by looking at figure 13 at which points in the cross section the stresses are largest. As mentioned earlier, φ is largest on the edges and close to the corner of the cross section. This is interesting, as the *bending* stresses present in tensile armor wires will be largest at the corners, meaning that the corners of the cross section are the critical points with respect to stress. As the warping stress adds up to the total stress, the magnitude of stress at the corners will become even larger. Hence, the warping stress may give a contribution to fatigue which should be taken into account. This will be looked into in section 5.

One may intuitively understand that the bar has a stronger ability to withstand twisting when the warping is restrained, which means that a larger torque is needed in order to twist the bar a given angle. The torsional moment due to restrained warping is [17]:

$$M_w = -C_\sigma \tau_{,11} \int_S \varphi^2 dS = -C_\sigma \Gamma \tau_{,11} \tag{80}$$

The total torsional moment in the cross section of a straight beam is the sum of the warping moment M_w and the well known Saint-Venant torsional moment, $M_t = GI_t\tau$:

$$M_1 = M_t + M_w = GI_t\tau - C_\sigma \Gamma \tau_{,11} \tag{81}$$

4.5 Finite element methods

The finite element method has been important in the work with this thesis, as one of the main goals has been to familiarize with the computer code Aflex and also to implement a new curved beam element into the program. Therefore it seems natural to give a short review of the method in general.

The finite element method is a numerical procedure which is usually applied in solving structural problems which are too complex to solve analytically. The method is used in for example the design of buildings, ships, airframes and spacecraft [18]. The main issue in structural analyis is to determine the displacement field for a structure under a given load, and the classical approach to this will normally involve solving the differential equations of equilibrium. This will be virtually impossible if the geometry and boundary conditions are complicated. In the finite element method, a direct solving of the differential equations is avoided. Instead of having the entire displacement field as unknown, the problem is reduced to finding the displacements in each *node*.

The basic concept of the method is to *discretize* the structure into a finite number of elements. Each element has a certain number of nodes, and the displacment field within the element is assumed to be uniquely defined by the nodal displacements. This means that the finite element method is an approximate method, and the accuracy depends on the assumed displacement pattern within the elements. The assumed displacement pattern is usually linear, quadratic or qubic, depending on how many degrees of freedom/nodes each element is given. Increased accuracy is obtained by using higher order interpolation for the assumed displacement pattern at the cost of increased computational time.

For each element in the structure, a stiffness relationship is obtained using the principle of virtual displacments together with the assumed displacement pattern. This results in

a *weak formulation* of the problem, or an integrated equilibrium equation. This means that the individual element is in overall equilibrium, but every point of the element is not necessarily in equilibrium. The procedure results in an element stiffness relationship of the following form [18]:

$$\mathbf{S} = \mathbf{kv} + \mathbf{S^0} \tag{82}$$

Here, $\mathbf{S}$ is the generalized nodal point forces, $\mathbf{k}$ is the element stiffness matrix, $\mathbf{v}$ is a vector containing the nodal point displacements and $\mathbf{S^0}$ is equivalent nodal point forces due to distributed loading. Normally, numerical integration is applied in order to find the element stiffness matrix, which introduces another approximation to the method.

The contributions from all elements in a structure may be added into a single equation called the system stiffness relationship. This follows from the fact that every nodal point in the structure must be in equilibrium. The system stiffness relationship is then [18]:

$$\mathbf{R} = \mathbf{Kr} + \mathbf{R^0} \tag{83}$$

where $\mathbf{R}$ is a vector containing all external nodal point loads, and $\mathbf{r}$ represents the unknown global degrees of freedom. The system stiffness matrix is found by directly adding the contributions from each element, or more formally by:

$$\mathbf{K} = \Sigma_j \mathbf{a}_j^T \mathbf{k}_j \mathbf{a}_j \tag{84}$$

The $\mathbf{R^0}$-vector is found similarly:

$$\mathbf{R^0} = \Sigma_j \mathbf{a}_j^T \mathbf{S^0}_j \tag{85}$$

Here, the $\mathbf{a}$-matrix gives the relationship between the element degrees of freedom and the global degrees of freedom:

$$\mathbf{v}_j = \mathbf{a}_j \mathbf{r} \tag{86}$$

When the system stiffness relationship is established, it may be solved for the unknown global nodal point displacements, $\mathbf{r}$, after boundary conditions are introduced. To solve the equation, one must in principle invert the system stiffness matrix (which may be very large), and it is important to handle this in an efficient way. There are a variety of possible solution algorithms, but these will not be discussed here. When the global displacements are found, these may be used to calculate stresses in the structure by use of the material law.

When it comes to flexible riser calculations, a *nonlinear* finite element method is needed. In a nonlinear analysis, the nodal displacements are no longer a linear function of the external load. Sources of nonlinearities in structural analysis are in general [18]:

- Geometric nonlinearities
- Material nonlinearities
- Boundary conditions/contact

Geometric nonlinearities appears when one takes the effect of the changing geometry of the structure into account. This is often referred to as large displacement analyses. As

loading is applied, the structure deforms, and this will change the stiffness matrix of the elements and possibly also the load vector.

Material nonlinearities are a result of a nonlinear relationship betweeen strains and stresses. For steel structures, the relationship is usually linear up to a certain limit which is the yield strength of the material. When this limit is passed, the material law changes, and this must be taken into account when the element stiffness matrices are calculated.

For flexible risers, it is important to account for the nonlinearities that arise due to changing contact conditions. The different layers may slide relative to each other under friction, and this is a nonlinear process. At one step in the analysis the layers stick to each other, but when shear forces overcome the maximum static friction force, components begin to slide.

To solve the nonlinear equations, an incremental procedure is used, typically using equilibrium iterations for each load increment. The problem may be formulated in terms of a total and an incremental equilibrium equation [18]:

$$\Sigma_j \mathbf{a}_j^T \mathbf{S}_j = \mathbf{R} \tag{87}$$

$$\mathbf{K}_I(\mathbf{r}) d\mathbf{r} = d\mathbf{R} \tag{88}$$

For each increment the loading is increased an amount d$\mathbf{R}$. Equation (88) is used to predict the change in the displacement vector for a given increase in exteral load. Then equation (87), which is the total equilibrium equation, may be used to correct the answer by evaluating the difference between internal and external load. Then a new prediction/iteration is performed. This is repeated until the difference between the external and internal load is acceptable. The method with stepwise increments and equilibrium iterations is known as the *Newton-Raphson* method.

A more detailed explaination of how the finite element method works is given in the next section, which is devoted to the computer code Aflex.

4.5.1 Aflex

Aflex is a nonlinear finite element code developed as a tool for stress analysis of flexible pipes exposed to bending gradients close to terminations [19]. The program models a single tensile armor wire using curved beam elements based on the theory described in [3] and section 4.3 in this thesis. The behaviour of the armor wire is simulated for a given pipe curvature distribution. The program was developed as a part of Svein Sævik's dr. ing. research work at the Division of Marine Structures, NTH, and a summary of the program will be given here.

Kinematic restraint

The armor wire model is based on an assumption on the rotation of the cross section around the longitudinal axis. If the deformation of the supporting surface is small, the rotation θ_1 is determined by displacements along the X^1 and X^3 axes and the curvature of the supporting surface measured in the two orthogonal directions. Mathematically, this means that the cross section rotation about the longitudinal axis is determined as:

$$\theta_1 = -\kappa_t u_3^0 + \kappa_1 u_1^0 \tag{89}$$

Where κ_t is the curvature along the transverse direction, found as:

$$\kappa_t = \cos^2 \alpha \ \kappa_r + \sin^2 \alpha \ \kappa_c \tag{90}$$

where κ_r and κ_c are the principal curvatures in the circumferential and longitudinal directions of the surface respectively.

Curved beam element

The central part of the Aflex computer program is the finite element representing the armor wire. When the kinematic restraint on θ_1 is introduced, together with $\theta_2 = -\epsilon_3$ and $\theta_3 = \epsilon_2$ (this was discussed in section 4.3), the result is that the Green strain tensor components given in equations (40) - (42) are determined by the displacements of the beam center line alone. This means that the strain field within each element is uniquely defined by the three unknown displacement variables u_1^0, u_2^0 and u_3^0.

This means that the finite element can be based on an assumed displacement field for the center line displacements:

$$\mathbf{u^0} = \mathbf{Nv} \tag{91}$$

where $\mathbf{N}$ is a matrix containing interpolation functions and $\mathbf{v}$ is the element degrees of freedom. The Aflex element has 10 degrees of freedom, where 8 are external and 2 are internal and are eliminated by static condensation. The element with all its degrees of freedom is shown in figure 14 below:

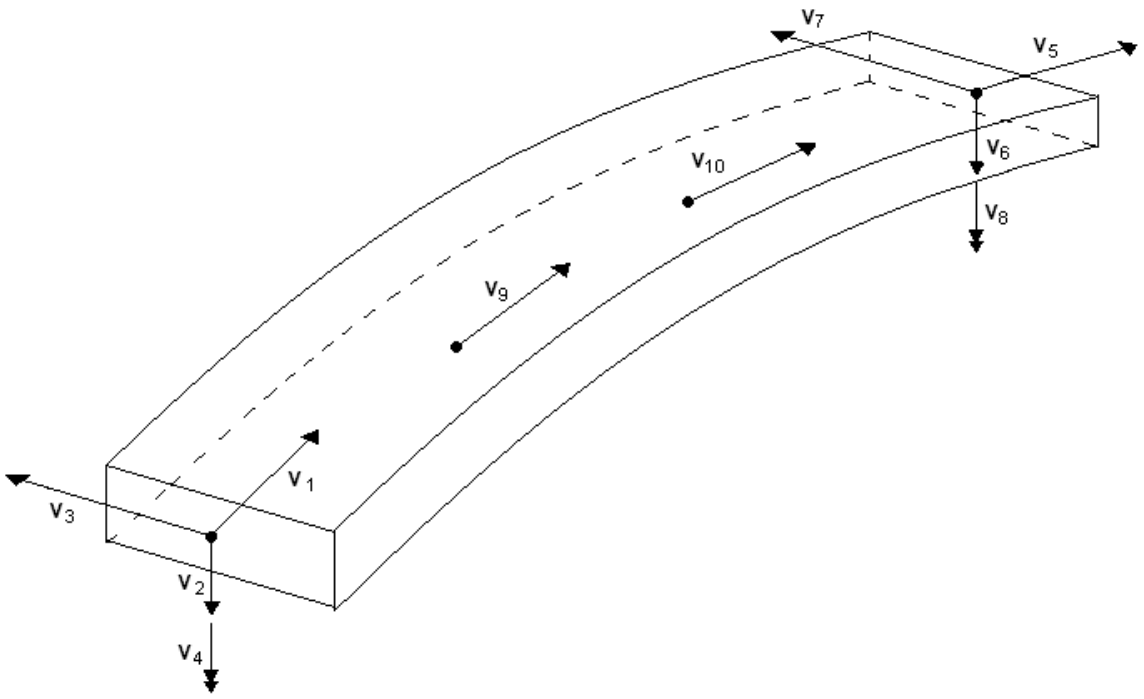

Figure 14: Aflex curved beam element.

The degrees of freedom implies that the assumed displacement pattern is cubic in u_1^0 and u_3^0, and linear in u_2^0. The matrix of interpolation functions is:

$$\mathbf{N}^T = \begin{bmatrix} 1-\frac{11}{2}\xi+9\xi^2-\frac{9}{2}\xi^3 & 0 & 0 \\ 0 & 1-\xi & 0 \\ 0 & 0 & 1-3\xi^2+2\xi^3 \\ 0 & 0 & -l\xi(\xi-1)^2 \\ \xi-\frac{9}{2}\xi^2+\frac{9}{2}\xi^3 & 0 & 0 \\ 0 & \xi & 0 \\ 0 & 0 & 3\xi^2-2\xi^3 \\ 0 & 0 & -l\xi^2(\xi-1) \\ 9\xi-\frac{45}{2}\xi^2+\frac{27}{2}\xi^3 & 0 & 0 \\ -\frac{9}{2}\xi+18\xi^2-\frac{27}{2}\xi^3 & 0 & 0 \end{bmatrix} \tag{92}$$

where ξ is the non-dimensional arc length coordinate and l is the element length. Using the relationship given in equation (91), all the strains may be expressed as a function of the nodal degrees of freedom. Inserting this into the virtual work expressions in equations (72) and (73) gives the material and geometric stiffness matrices.

Element load vector

A characteristic feature of the Aflex formulation is that the nodal degrees of freedom are the displacements *relative* to the supporting surface. This means that as the pipe is bent to a specific curvature, the wire elements will be subjected to strain and internal forces even if the degrees of freedom remain zero. The strain components for a fixed element are calculated based on the *loxodromic* curve, which is the curve a helix will follow if it is fixed to a curved cylinder. Proof of these expressions are given in [3], and the results are:

$$E_{11}^{*0} = -\frac{R}{\rho}\cos^2\alpha\cos\theta + \frac{1}{2}(\frac{R}{\rho})^2\cos^2\alpha\cos^2\theta \tag{93}$$

$$\Delta\kappa_1 = \frac{\sin\alpha\cos\alpha}{\rho}\cos^2\alpha\cos\theta \tag{94}$$

$$\Delta\kappa_2 = -\frac{\cos\alpha}{\rho}(1+\sin^2\alpha)\sin\theta \tag{95}$$

$$\Delta\kappa_3 = -\frac{\cos^2\alpha}{\rho}\cos^2\alpha\cos\theta \tag{96}$$

Here, E_{11}^{*0} is the longitudinal component of the green strain tensor, while the curvatures are as defined in section 4.3. ρ is the global pipe curvature, while θ is the polar coordinate angle defining the position of the helix.

By prescribing the changes in strain and curvatures using the above equations and the internal virtual work expression from equation (55), an internal element load vector is obtained. This is equivalent to the $\mathbf{S^0}$-vector in equation (82). In this way, the curvature load is treated as an initial strain problem.

Friction and contact

Interaction between the armor wire elements and the surrounding layers is simulated by hyperelastic or elastoplastic springs. The elastoplastic springs corresponds to a Coloumb friction model, and are used for nonbonded pipes. The springs characteristics in the X^1 and X^3 direction are coupled to the X^2 direction such that the stiffness is reduced when

the total friction force exceeds the friction coefficient times the normal contact force. This simulates sliding under friction.

Program execution

A summary of how the program executes is given below:

1. Read input file. Calculate cross section parameters and initial values for the curvature components.
2. Loop through all the load increments:
   (a) Prescribe the changes in strain and curvature components using equations (93)-(96). Then an iteration procedure is initiated in order to ensure equilibrium at the current load step:
      i. Calculate element stiffness matrix and element load vector for all elements. Internal degrees of freedom are removed by static condensation and element contributions are added to the global stiffness matrix and load vector.
      ii. Spring stiffnesses are added to the global stiffness matrix.
      iii. The incremental stiffness relation is solved for the incremental nodal displacements.
      iv. The kinematics are updated in terms of axial strain and curvature components.
      v. The contact springs are updated and the spring forces added to the internal load vector.
      vi. If the normalized Euclidean displacement norm and the unbalanced force norm are larger than the tolerance limit, repeat the iteration procedure.
   (b) End of iteration procedure, go to next load increment.
3. When all the load increments are completed, results are printed to the result file in terms of displacements and stresses.

4.5.2 Bflex

Bflex is a tailor made computer program for stress analysis of tensile armors in flexible pipes, which originally was developed by SINTEF Civil and Environmental Engineering. The details about how it works is found in [20]. The program establishes and solves finite element equations based on the principle of virtual displacements as well as kinematic compatibility, material law and displacement interpolation. Nonlinear behaviour is taken into account.

In [3] it was found that the transverse slip of the tensile armor wires may be neglected for realistic friction coefficients. This assumption is utilized in Bflex, and therefore the tendons only have longitudinal degrees of freedom. This reduces the number of degrees of freedom, and also contributes to the numerical stability. It is also assumed that the supporting cross-section maintains its shape sufficiently, so that local bending and torsion effects may be calculated analytically.

Stresses from internal pressure and external tension are found using a multilayer pipe element, and are assumed uncoupled with the stresses arising from pipe bending. When it comes to the bending response, there are three alternative formulations. The first one

(ITCODE0) is a sandwitch beam formulation. Here, each tendon is modelled using a finite elements with contact interaction with the pipe core. Displacements relative to the supporting surfaces introduce friction forces. The second formulation (ITCODE21) is a moment based model. Analytical expressions are used to calculate the bending moment contribution from the armor layers when the tendons start to slip, and when there is full slip. In ITCODE21, the moment-curvature relationship is based on the inner armor layer only, because this is the layer of concern for fatigue calculations. The last bending formulation (ITCODE31) is essentially the same as ITCODE21, but here the actual moment-curvature relationship for each armor layer is used.

Bflex also contains modules for postprocessing which are called Pflex, Boundary and Lifetime. Pflex performs pressure armor bending stress analysis based on results from Bflex bending analysis, while Boundary performs transverse cross section stress analysis using a boundary element method. Lifetime performs fatigue analysis.

4.6 A new curved beam element for Aflex

A central part of this thesis work has been to implement a new curved beam element into the Aflex computer program. The background for this is the study of radial buckling phenomena. In the original Aflex version, the curved beam element only has translational degrees of freedom in the radial direction. In order to describe non-uniform radial displacements of the tensile armor wire, rotational degrees of freedom around the weak axis of the wire is needed. Therefore, the Aflex code has been modified such that the element has the necessary rotational degrees of freedom.

4.6.1 Theoretical background

It is expected that radial buckling of tensile armor wires will be associated with a non-uniform radial displacement field. Thus an interpolation polynomial of a degree higher than one is needed in the radial direction. It is common for slender beam elements to have both rotational and translational degrees of freedom at each end, and use these as the basis for the displacement field. One rotation and one translation at each end gives a total of 4 parameters to determine the displacement field, meaning that the displacement polynomials will be cubic. The interpolation polynomials introduced for the new element are shown in figure 15.

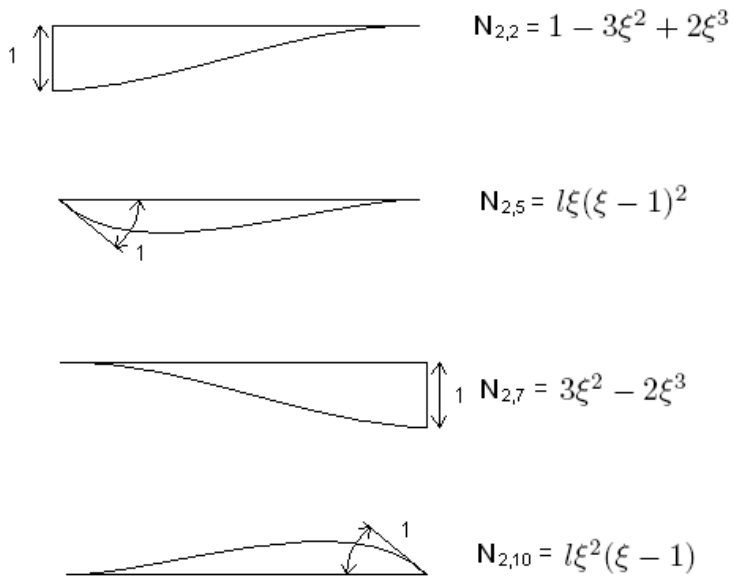

Figure 15: Interpolation polynomials introduced in the radial direction.

These are the same type of polynomials that are already used in the *transverse* direction. All other degrees of freedom and polynomials are kept the same, thus the matrix of interpolation polynomials in the new Aflex version is:

$$\mathbf{N}^T = \begin{bmatrix} 1-\frac{11}{2}\xi+9\xi^2-\frac{9}{2}\xi^3 & 0 & 0 \\ 0 & 1-3\xi^2+2\xi^3 & 0 \\ 0 & 0 & 1-3\xi^2+2\xi^3 \\ 0 & 0 & -l\xi(\xi-1)^2 \\ 0 & l\xi(\xi-1)^2 & 0 \\ \xi-\frac{9}{2}\xi^2+\frac{9}{2}\xi^3 & 0 & 0 \\ 0 & 3\xi^2-2\xi^3 & 0 \\ 0 & 0 & 3\xi^2-2\xi^3 \\ 0 & 0 & -l\xi^2(\xi-1) \\ 0 & l\xi^2(\xi-1) & 0 \\ 9\xi-\frac{45}{2}\xi^2+\frac{27}{2}\xi^3 & 0 & 0 \\ -\frac{9}{2}\xi+18\xi^2-\frac{27}{2}\xi^3 & 0 & 0 \end{bmatrix} \tag{97}$$

The new curved beam element with all the degrees of freedom is shown in figure 16. The total number of degrees of freedom are now 12, with 2 internal and 10 external, 5 at each end.

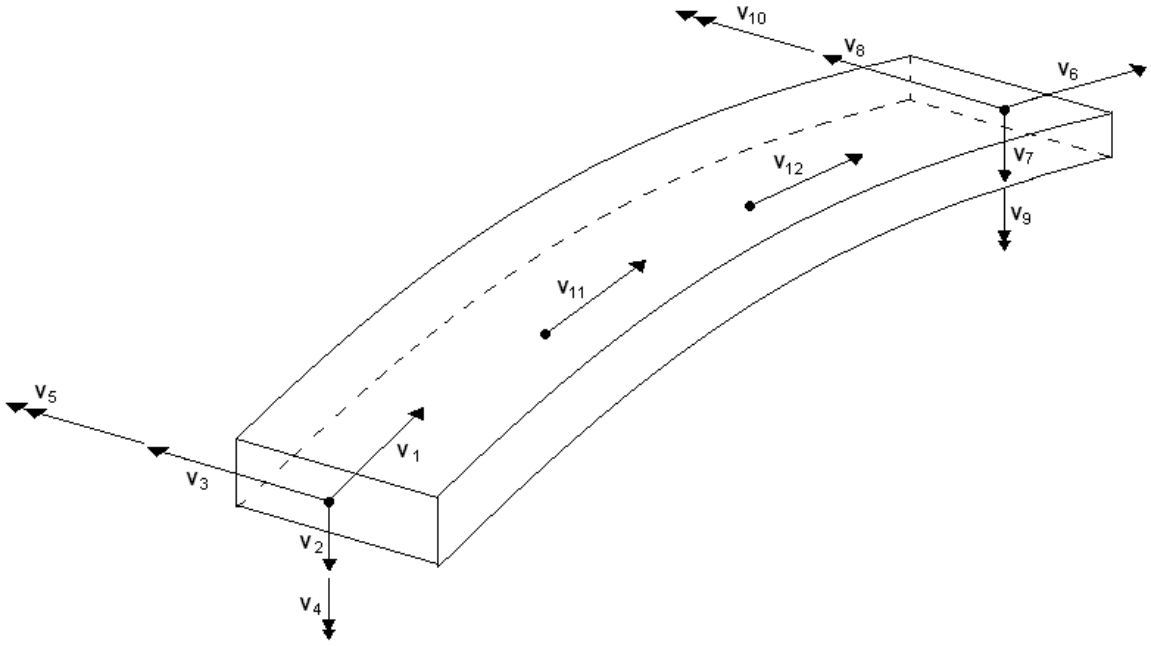

Figure 16: The new Aflex element.

4.6.2 Computer implementation

The original Alfex source code has been modified in order to implement the new curved beam element. A number of subroutines had to be changed, and a complete list of all changes are given in the appendix. In short, the changes are related to the increased number of degrees of freedom both globally and on element level. The number of degrees of freedom per global node has been changed from 4 to 5, and the dimension of the element stiffness matrices are changed from 10 x 10 to 12 x 12.

The biggest changes are in the subroutines creating the element stiffness matrices and load vectors, as it is these routines that uses the interpolation polynomials. The new interpolation polynomials are also included in the subroutine that updates the strain and curvature state of the element.

After the Aflex code was updated and tested, the source code was used to implement the new curved beam element into the Bflex2010 system under the name hshear353. This work was performed by the supervisor, Prof. Svein Sævik. This made it possible to utilize the available visualization and post processing tools, Xpost and Bflex2010Post. Bflex2010 also has a more advanced equation solver, with automatic load increment updating, and possibilites for dynamic analysis. This has been very beneficial in the buckling analyses performed in section 6.

5 Local stresses at end fittings

5.1 Introduction

As previously pointed out, a critical point in a flexible riser is the end fitting, where the pipe structure is terminated. In deep water applications, the tensile force being transferred at this point may become very large, however, the force magnitude depends strongly upon the specific riser configuration (see e.g. [21]). In order to have a safe design, it is important to have an understanding of the different stress components at this point. The complex anchoring of the structure inside the end fitting can however make it difficult to give accurate predictions of the magnitude of stresses. Sources of stress concentrations may be numerous and dependent on how the specific construction is made. The investigation of the stresses at the end fitting will in this case be based on a simple model of a single tensile armor wire, and no specific data for the end fitting itself is used. One can argue that the analysis is somewhat crude, but it may never the less provide important information and understanding.

The investigation performed here is directed at local stresses arising from one single phenomena: When a flexible pipe is axially stretched, the lay angle of the armor wires must change slightly. However, close to the point where the wires are terminated, this change in lay angle may not be allowed. In order to be conservative, it is in the succeeding analyses assumed that the wires are fully fixed at the termination, and this constraint will give rise to local stresses. Longitudinal stresses due to bending and warping will add to the total axial stress and this may possibly constitute a danger when it comes to fatigue of the pipe.

Two different types of analyses will be done. First a simplified analytical method where friction between the wires and the underlying layer is neglected. It is hard to say how good the results from this analysis will be before comparing to the more detailed FEM anlyses, but it is however a very good way to gain knowledge about the problem and also separate the important physical effects from the less important. Next, the finite element code Aflex with the new curved beam element is used. Here, friction forces between the wire and the supporing layer is included, and the importance of the friction coefficient is investigated.

5.2 Analytical investigation of end fitting stresses

5.2.1 Definitions and assumtions

It is assumed that the tensile armor wires are of a rectangular cross section and rests on a circular surface of radius R. The pressure armor is assumed to be stiff enough in order to neglect radial displacements. All displacements and strains are assumed to be sufficiently small to neglect second order terms. In the unloaded configuration the angle between the tensile armor wires and the longitudinal axis of the pipe (the lay angle) is α_0. Now consider a pipe section of length L_p subjected to a global pipe strain ϵ_p as shown in figure 17.

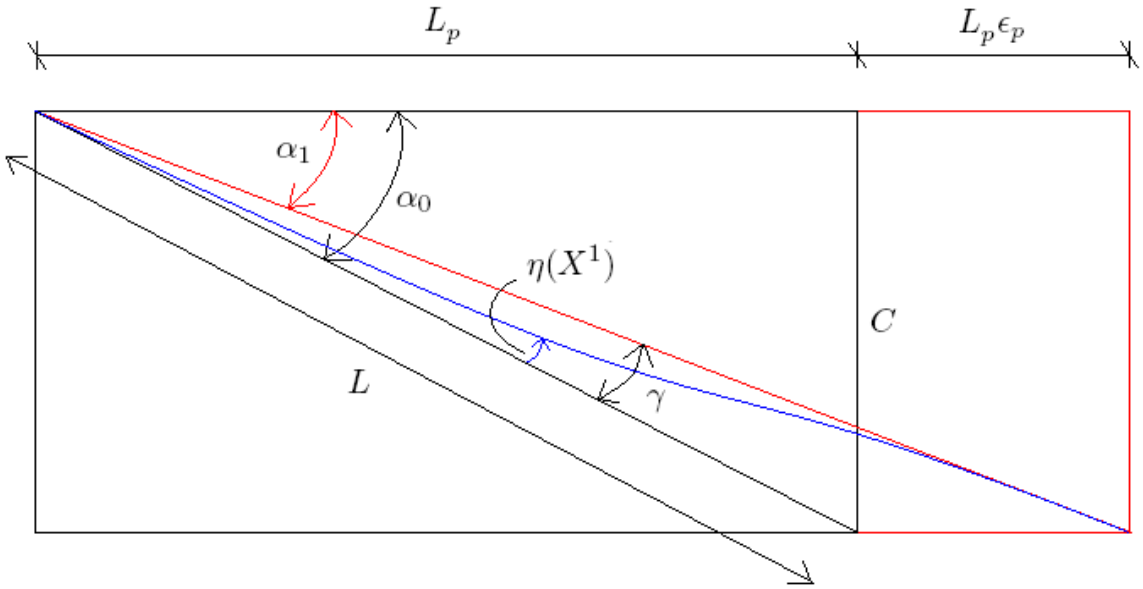

Figure 17: Definitions used when assessing the wire behaviour close to the end fitting.

As the pipe is axially strained, the curve which the tendon follows must change. If no end restraints are present, the change in lay angle would be the same at all points along the wire, and the wire would assume a path like the red one in the above figure. The new lay angle is denoted α_1 and from geometry the difference between α_0 and α_1 is:

$$\gamma = \alpha_0 - \alpha_1 = \alpha_0 - \tan^{-1}\left(\frac{C}{L_p(1+\epsilon_p)}\right) = \alpha_0 - \tan^{-1}\left(\frac{\tan\alpha_0}{1+\epsilon_p}\right) \tag{98}$$

Let the axial strain along the curve defined by α_1 be denoted ϵ. By neglecting second order terms, ϵ is found using the Pythagorean theorem:

$$\begin{aligned} L^2(1+\epsilon)^2 &= C^2 + L_p^2(1+\epsilon_p)^2 \\ &\Updownarrow \\ L^2 + 2L^2\epsilon &= C^2 + L_p^2 + 2L_p^2\epsilon_p \\ \Rightarrow \epsilon &= \frac{L_p^2}{L^2}\epsilon_p = \cos^2(\alpha_0)\cdot\epsilon_p \end{aligned} \tag{99}$$

As mentioned earlier, this displacement pattern (α_1) and strain (ϵ) is only possible when no end restraints are present. The wire is in fact fixed at the end fitting, meaning that the lay angle must remain at α_0 at the end fitting and gradually increase towards α_1 as one moves away from the end. This is illustrated in figure 17 with a blue line. The challenge is to find out just how this change in lay angle is. Therefore the *actual* change in lay angle is introduced as the variable $\eta(X^1)$, meaning that the new lay angle at any point along the wire is given as $\alpha_0 - \eta(X^1)$.

5.2.2 Curvature and strain

The undeformed tensile armor wire has the shape of a cylindrical helix, and as stated in section 4, the curvature and twist components are given as

$$\kappa_2 = 0 \tag{100}$$

$$\kappa_3 = \frac{\sin^2 \alpha_0}{R} \tag{101}$$

$$\tau = \frac{\cos \alpha_0 \sin \alpha_0}{R} \tag{102}$$

where, again, κ_2 is the transverse curvature, κ_3 the normal curvature and τ the twist, or geometrical torsion. Now imagine that the helical angle changes slightly due to axial straining of the pipe. The shape of the wire is still a helix, but the angle is now changed to $\alpha_0 - \eta$, where η is a very small angle. Inserting this in the curvature expressions while using double angle identities and neglecting second order terms in η gives:

$$\begin{aligned}
\kappa_3 &= \frac{\sin^2(\alpha_0 - \eta)}{R} = \frac{1}{R}[\sin\alpha_0 \cos\eta - \cos\alpha_0 \sin\eta]^2 \\
&= \frac{1}{R}[\sin^2\alpha_0 \cos^2\eta - 2\sin\alpha_0 \cos\eta \cos\alpha_0 \sin\eta + \cos^2\eta \sin^2\eta] \\
&\approx \frac{1}{R}[\sin^2\alpha_0 - 2\sin\alpha_0 \cos\alpha_0 \cdot \eta]
\end{aligned} \tag{103}$$

$$\begin{aligned}
\tau &= \frac{1}{R}\cos(\alpha_0 - \eta)\sin(\alpha_0 - \eta) \\
&= \frac{1}{R}(\cos\alpha_0 \cos\eta + \sin\alpha_0 \sin\eta)(\sin\alpha_0 \cos\eta - \cos\alpha_0 \sin\eta) \\
&\approx \frac{1}{R}(\cos\alpha_0 + \sin\alpha_0 \cdot \eta)(\sin\alpha_0 - \cos\alpha_0 \cdot \eta) \\
&\approx \frac{1}{R}(\cos\alpha_0 \sin\alpha_0 - \cos^2\alpha_0 \cdot \eta + \sin^2\alpha_0 \cdot \eta) \\
&= \frac{1}{R}(\cos\alpha_0 \sin\alpha_0 + (1 - 2\cos^2\alpha_0)\eta)
\end{aligned} \tag{104}$$

The transverse curvature of a helix with constant angle is zero, but when the angle varies along the length of the wire, transverse curvature will in fact occur. In a similar way as for straight beams, the transverse curvature may be taken as the change in angle per unit length, assuming small deformations:

$$\kappa_2 = -\frac{d\eta}{dX^1} \tag{105}$$

Here, X^1 is the arc length coordinate along the wire, as defined in section 4. Using the above expressions, the *change* in twist and curvature are:

$$\Delta\kappa_2 = -\frac{d\eta}{dX^1} \tag{106}$$

$$\Delta\kappa_3 = -\frac{2\sin\alpha_0 \cos\alpha_0}{R} \cdot \eta \tag{107}$$

$$\Delta\tau = \frac{1 - 2\cos^2\alpha_0}{R} \cdot \eta \tag{108}$$

An expression for the axial strain of the wire is also needed in order to proceed. Let the actual strain in the wire be ϵ_a, which will differ slightly from ϵ due to the end restraint. The difference is found from geometric considerations as shown in figure 18:

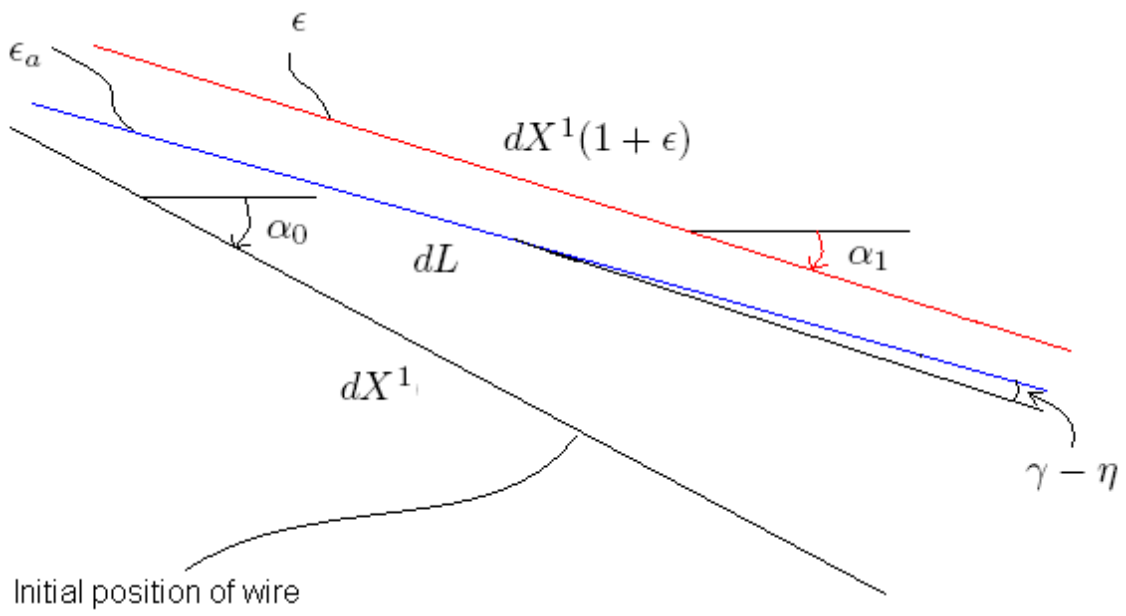

Figure 18: Axial strain along the actual path versus a uniform strained helix.

As the axial strain along the strained helix is known to be ϵ, an infinitesimal element on the strained helix has the length $dX^1(1+\epsilon)$. The actual length of the element is assigned the symbol dL. The relative angle between the two paths are $\gamma - \eta$, and therefore:

$$\cos(\gamma - \eta) = \frac{dX^1(1+\epsilon)}{dL} \tag{109}$$

The axial strain is then found to be:

$$\begin{aligned} \epsilon_a &= \frac{dL - dX^1}{dX^1} = \frac{1+\epsilon}{\cos(\gamma-\eta)} - 1 \\ &= \frac{1+\epsilon-\cos(\gamma-\eta)}{\cos(\gamma-\eta)} \approx \frac{1+\epsilon-(1-\frac{1}{2}(\gamma-\eta)^2)}{1-\frac{1}{2}(\gamma-\eta)^2} \\ &= \frac{\epsilon+\frac{1}{2}(\gamma-\eta)^2}{1-\frac{1}{2}(\gamma-\eta)^2} \approx \epsilon + \frac{1}{2}(\gamma-\eta)^2 \end{aligned} \tag{110}$$

It is noted that this expression is equivalent to the additional axial strain in a beam due to lateral deflection, as given in [18]. The only difference is that $w_{,x}$ is replaced with $\gamma - \eta$.

5.2.3 Potential energy

Now that expressions for all the curvature components and axial strain have been developed, it is possible to establish the total elastic potential energy in the wire as a *functional* of the angle $\eta(X^1)$. A functional is a function of another function (in this case η) which in

turn is a function of some other variable (in this case X^1). Functional theory is described in for example [22].

The energy is derived by integrating over the volume of the structure. For beam structures, this integrations simplifies to an integral over the length of the beam. The expression used here is found in [23], and takes both bending, torsion and warping stiffness into account. The axial strain energy per unit volume is added to the expression, which gives the total strain energy in the armor wire, Π:

$$\Pi = \frac{1}{2}\int_0^L EA\epsilon_a^2 + EI_2(\Delta\kappa_2)^2 + EI_3(\Delta\kappa_3)^2 + GI_t(\Delta\tau)^2 - E\Gamma\Delta\tau_{,11}\Delta\tau \; dX^1 \tag{111}$$

The warping term may be simplified using integration by parts. As the wire is fully fixed at the end fitting, $\Delta\tau$ is zero at $X^1 = 0$. Far away from the end restraint the wire will follow the helical path with a constant angle, and thus $\Delta\tau_{,1} = 0$ at $X^1 = L$. This means that the term including these quantites vanish:

$$\int_0^L \Delta\tau_{,11}\Delta\tau \; dX^1 = [\Delta\tau \cdot \Delta\tau_{,1}]_0^L - \int_0^L (\Delta\tau_{,1})^2 \; dX^1 = -\int_0^L (\Delta\tau_{,1})^2 \; dX^1 \tag{112}$$

Now insert this result together with the strain and curvature expressions from equations (106)-(108) into the expression for the strain energy:

$$\begin{aligned}\Pi = \frac{1}{2}\int_0^L & EA(\epsilon + \frac{1}{2}(\gamma - \eta)^2)^2 + EI_2(-\frac{d\eta}{dX^1})^2 + EI_3(-\frac{2\sin\alpha_0\cos\alpha_0}{R}\cdot\eta)^2 \\ & + GI_t(\frac{1-2\cos^2\alpha_0}{R}\cdot\eta)^2 + E\Gamma(\frac{1-2\cos^2\alpha_0}{R}\cdot\frac{d\eta}{dX^1})^2 \; dX^1\end{aligned} \tag{113}$$

5.2.4 Minimization of the potential energy

A fundamental concept in physics and structural mechanics is the principle of minimum potential energy, which states that a structure will deform into the position that minimizes the total potential energy [16]. This principle will be used here in order to find the solution for $\eta(X^1)$. Assuming there are no other types of energy but the eleastic strain energy in the wire, the problem is reduced to finding the function which minimizes the strain energy given in equation (113).

One last thing is however required, and that is a *constraint* which makes sure that the far end of the wire (away from the end fitting) is at the correct place. This is ensured by demanding that η is such that the actual wire position coincides with the strained helix at $X^1 = L$. In other words, the constraint is zero relative lateral motion between the actual curve and the strained helix at the end. The geometry is shown in figure 19.

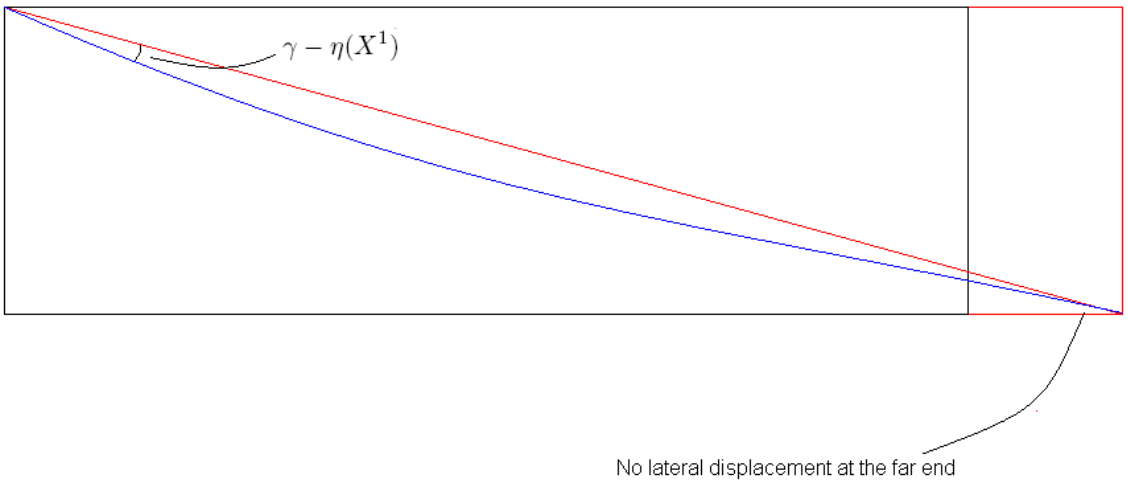

Figure 19: Constraint: the wire end should be at the correct position.

The relative lateral motion may be found by integrating the lateral component of the displacement along the X^1-axis. Assuming small strains and displacements, the constraint is expressed mathematically as:

$$\begin{aligned} \int_0^L (1+\epsilon_a)\sin(\gamma-\eta)dX^1 = 0 \\ \Rightarrow \int_0^L (\eta-\gamma)dX^1 \approx 0 \end{aligned} \tag{114}$$

The problem is now to minimize the potential energy under the constraint given above. Let the integrand in the expression for the strain energy be $F(X^1, \eta, \eta')$, and the integrand in the constraint be $G(X^1, \eta)$, i.e:

$$\begin{aligned} F(X^1,\eta,\eta') =& \frac{1}{2}EA(\epsilon + \frac{1}{2}(\gamma-\eta)^2)^2 + \frac{1}{2}EI_2(-\frac{d\eta}{dX^1})^2 + \frac{1}{2}EI_3(-\frac{2\sin\alpha_0\cos\alpha_0}{R}\cdot\eta)^2 \\ &+ \frac{1}{2}GI_t(\frac{1-2\cos^2\alpha_0}{R}\cdot\eta)^2 + \frac{1}{2}E\Gamma(\frac{1-2\cos^2\alpha_0}{R}\cdot\frac{d\eta}{dX^1})^2 \end{aligned} \tag{115}$$

and:

$$G(X^1,\eta) = \eta - \gamma \tag{116}$$

The problem of minimizing the potential energy can be solved using Lagrange multipliers as described in [24]. The solution is found by finding the minimum of a new functional, K, defined as:

$$K = \int_0^L (F + \lambda G)\, dX^1 \tag{117}$$

where λ is an unknown constant. The minimum of this new functional is found using the Euler equation [24]:

$$\frac{\partial(F+\lambda G)}{\partial\eta} - \frac{d}{dX^1}(\frac{\partial(F+\lambda G)}{\partial\eta'}) = 0 \tag{118}$$

Since the expressions are rather long, take one term at a time:

$$\begin{aligned}\frac{\partial(F+\lambda G)}{\partial\eta} &= \frac{\partial}{\partial\eta}[\frac{1}{2}EA(\epsilon+\frac{1}{2}(\gamma-\eta)^2)^2 + \frac{1}{2}EI_2(-\eta')^2 + \frac{1}{2}EI_3(-\frac{2\sin\alpha_0\cos\alpha_0}{R}\cdot\eta)^2 \\ &+ \frac{1}{2}GI_t(\frac{1-2\cos^2\alpha_0}{R}\cdot\eta)^2 + \frac{1}{2}E\Gamma(\frac{1-2\cos^2\alpha_0}{R}\cdot\eta')^2 + \lambda(\eta-\gamma)] \\ &\approx \frac{\partial}{\partial\eta}[\frac{1}{2}EA(\epsilon^2+\epsilon(\gamma-\eta)^2) + \frac{1}{2}EI_2(\eta')^2 + 2EI_3\frac{\sin^2\alpha_0\cos^2\alpha_0}{R^2}\eta^2 \\ &+ \frac{1}{2}GI_t\frac{(1-2\cos^2\alpha_0)^2}{R^2}\eta^2 + \frac{1}{2}E\Gamma\frac{(1-2\cos^2\alpha_0)^2}{R^2}(\eta')^2 + \lambda(\eta-\gamma)] \\ &= EA\epsilon(\eta-\gamma) + 4EI_2\frac{\sin^2\alpha_0\cos^2\alpha_0}{R^2}\eta + GI_t\frac{(1-2\cos^2(\alpha_0))^2}{R^2}\eta + \lambda\end{aligned} \tag{119}$$

And the last term:

$$\begin{aligned}\frac{d}{dX^1}(\frac{\partial(F+\lambda G)}{\partial\eta'}) &= \frac{d}{dX^1}(EI_2\eta' + E\Gamma\frac{(1-2\cos^2\alpha_0)^2}{R^2}\eta') \\ &= EI_2\eta'' + E\Gamma\frac{(1-2\cos^2\alpha_0)^2}{R^2}\eta''\end{aligned} \tag{120}$$

Inserting the above results into the Euler equation yields a second order differential equation:

$$(EI_2+E\Gamma\frac{(1-2\cos^2(\alpha_0))^2}{R^2})\eta'' - (EA\epsilon+4EI_3\frac{\sin^2\alpha_0\cos^2\alpha_0}{R^2}+GI_t\frac{(1-2\cos^2\alpha_0)^2}{R^2})\eta = \lambda - EA\epsilon\gamma \tag{121}$$

which can be written as:

$$B\eta'' - D\eta = \lambda - EA\epsilon\gamma \tag{122}$$

where the constants B and D are defined as:

$$B = EI_2 + E\Gamma\frac{(1-2\cos^2\alpha_0)^2}{R^2} \tag{123}$$

$$D = EA\epsilon + 4EI_3\frac{\sin^2\alpha_0\cos^2\alpha_0}{R^2} + GI_t\frac{(1-2\cos^2\alpha_0)^2}{R^2} \tag{124}$$

5.2.5 Solution of the differential equation

The next step in the analysis is of course to solve the differential equation. Assume a solution on the form:

$$\eta = Ce^{kX^1} \tag{125}$$

which gives:

$$\eta'' = Ck^2 e^{kX^1} \tag{126}$$

The total solution is the sum of the particular and the homogenous solution. Let us first find the particular solution by inserting the assumed solution into equation (122):

$$Bk^2 Ce^{kX^1} - DCe^{kX^1} = \lambda - EA\epsilon\gamma \tag{127}$$

The above equation is valid for all X^1 only if $k = 0$. Hence:

$$\begin{aligned} -DC &= \lambda - EA\epsilon\gamma \\ \Rightarrow C &= \frac{EA\epsilon\gamma - \lambda}{D} \end{aligned} \tag{128}$$

This means that the particular solution is simply:

$$\eta_p = C = \frac{EA\epsilon\gamma - \lambda}{D} \tag{129}$$

The homogenous solution is found by setting the right hand side of equation (122) equal to zero. This gives:

$$\begin{aligned} Bk^2 Ce^{kX^1} - DCe^{kX^1} &= 0 \\ \Rightarrow Bk^2 - D &= 0 \\ \Rightarrow k &= \sqrt{\frac{D}{B}} \end{aligned} \tag{130}$$

This gives the homogenous solution:

$$\eta_h = C_1 e^{-kX^1} + C_2 e^{kX^1} \tag{131}$$

Intuitively, η can not be allowed to grow without limits as X^1 increases. This implies that $C_2 = 0$. The total solution is now reduced to:

$$\eta = \eta_p + \eta_h = \frac{EA\epsilon\gamma - \lambda}{D} + C_1 e^{-kX^1} \tag{132}$$

The constant C_1 is found from the boundary condition $\eta(0) = 0$ to be:

$$C_1 = -\frac{EA\epsilon\gamma - \lambda}{D} \tag{133}$$

This produces the solution:

$$\eta = \frac{EA\epsilon\gamma - \lambda}{D}(1 - e^{-kX^1}) \tag{134}$$

The only remaining issue is to find the unknown constant λ. To find this we need to insert the expression for η into the constraint from equation (114):

$$
\begin{aligned}
&\int_0^L (\eta - \gamma) dX^1 = 0 \\
\Rightarrow &\int_0^L (\frac{EA\epsilon\gamma - \lambda}{D}(1 - e^{-kX^1}) - \gamma) dX^1 = 0 \\
&\Rightarrow \int_0^L \frac{EA\epsilon\gamma - \lambda}{D}(1 - e^{-kX^1}) dX^1 = \gamma L \\
&\Rightarrow (\frac{EA\epsilon\gamma - \lambda}{D})[X^1 + \frac{1}{k}e^{-kX^1}]_0^L = \gamma L \\
&\Rightarrow (\frac{EA\epsilon\gamma - \lambda}{D})(L - \frac{1}{k}(1 - e^{-kL})) = \gamma L \\
&\Rightarrow \frac{EA\epsilon\gamma - \lambda}{D} = \frac{\gamma L}{L - \frac{1}{k}(1 - e^{-kL})} \\
&\Rightarrow \frac{EA\epsilon\gamma - \lambda}{D} = \frac{\gamma}{1 - \frac{1}{kL}(1 - e^{-kL})} \\
&\Rightarrow \frac{EA\epsilon\gamma - \lambda}{D} \approx \gamma
\end{aligned}
\tag{135}
$$

The last step in the above derivation is correct only if L is large, something which it will surely be for a deep water flexible riser. This ends the search of the unknown perturbation of the lay angle. When the above result is inserted into equation (134), the final solution for η appears as a very simple exponential function:

$$\underline{\eta = \gamma(1 - e^{-kX^1})} \tag{136}$$

where k is (as previously found):

$$k = \sqrt{\frac{EA\epsilon + 4EI_3\frac{\sin^2\alpha_0\cos^2\alpha_0}{R^2} + GI_t\frac{(1-2\cos^2\alpha_0)^2}{R^2}}{EI_2 + E\Gamma\frac{(1-2\cos^2\alpha_0)^2}{R^2}}} \tag{137}$$

5.2.6 Comments to the solution

The solution for η seems intuitively correct, as it starts at zero and gradually increases towards γ. How fast η increases along the X^1-axis is determined by the single parameter k. If k is large, the change is rapid and if k is small the rate of change is low. k is however a function of several cross sectional parameters, as well as the initial lay angle and radius of the pipe and also the strain, ϵ. It is therefore of interest to investigate the relative importance of the different terms. This may help in determining which physical effects that dominaties.

This investigation will be done by looking at a typical flexible pipe with $R = 0.1$ m and $\alpha_0 = 35°$. The armor wire is given the dimensions 9 x 3 mm. The material is steel, with $E = 2.1 \cdot 10^{11}$ Pa and $G = 8 \cdot 10^{10}$ Pa. The cross sectional parameters of the wire are, using formulas found in [25]:

$$
\begin{aligned}
A &= ab = 0.009 \text{ m} \cdot 0.003 \text{ m} = 2.7 \cdot 10^{-5} \text{ m}^2 \\
I_2 &= \frac{1}{12}a^3 b = \frac{1}{12} \cdot (0.009 \text{ m})^3 \cdot 0.003 \text{ m} = 1.82 \cdot 10^{-10} \text{ m}^4 \\
I_3 &= \frac{1}{12}ab^3 = \frac{1}{12} \cdot 0.009 \text{ m} \cdot (0.003 \text{ m})^3 = 2.03 \cdot 10^{-11} \text{ m}^4 \\
I_t &\approx \frac{1}{3}[1 - 0.6\frac{b}{a}]ab^3 = \frac{1}{3}[1 - 0.6 \cdot \frac{3}{9}] \cdot 0.009 \text{ m} \cdot (0.003 \text{ m})^3 = 6.48 \cdot 10^{-11} \text{ m}^4 \\
\Gamma &= \int_S \varphi^2 \, dS = 6.54 \cdot 10^{-17} \text{ m}^4
\end{aligned}
\tag{138}
$$

Γ was found using numerical integration of the warping function given in equation 78. For a pipe strain of $\epsilon_p = 0.001$, the individual terms in k are:

$$
\begin{aligned}
&EA\epsilon = 2.1 \cdot 10^{11} \text{ Pa} \cdot 2.7 \cdot 10^{-5} \text{ m}^2 \cdot \cos^2 35^\circ \cdot 0.001 = 3804.6 \text{ N} \\
&4EI_3 \frac{\sin^2 \alpha_0 \cos^2 \alpha_0}{R^2} \\
&= 4 \cdot 2.1 \cdot 10^{11} \text{ Pa} \cdot 2.03 \cdot 10^{-11} \text{ m}^4 \cdot \frac{\sin^2 35^\circ \cos^2 35^\circ}{(0.1 \text{ m})^2} = 375.5 \text{ N} \\
&GI_t \frac{(1 - 2\cos^2 \alpha_0)^2}{R^2} \\
&= 8 \cdot 10^{10} \text{ Pa} \cdot 6.48 \cdot 10^{-11} \text{ m}^4 \cdot \frac{(1 - 2\cos^2 35^\circ)^2}{(0.1 \text{ m})^2} = 60.6 \text{ N} \\
&EI_2 = 2.1 \cdot 10^{11} \text{ Pa} \cdot 1.82 \cdot 10^{-10} \text{ m}^4 = 38.22 \text{ Nm}^2 \\
&E\Gamma \frac{(1 - 2\cos^2 \alpha_0)^2}{R^2} \\
&= 2.1 \cdot 10^{11} \text{ Pa} \cdot 6.54 \cdot 10^{-17} \text{ m}^4 \cdot \frac{(1 - 2\cos^2 35^\circ)^2}{(0.1 \text{ m})^2} = 1.6 \cdot 10^{-4} \text{ Nm}^2
\end{aligned}
\tag{139}
$$

The first three terms given above are those present in the numerator of k. As seen, the axial strain term represents 90 % of these three terms, and is definitively the most important one among these. The torsional stiffness term constitutes only 1.4 %, and is almost negligible.

The two last terms above are those in the denominator of k. Here, the bending stiffness term dominates completely, and the warping stiffess contribution is totally negligible. One may thus conclude that the axial strain level and the bending stiffness about the strong axis are the most important parameters which defines the behaviour of the wire close to

the end restraint. The axial strain term is however dependent on the strain level in the pipe, and will be smaller for lower strains than in this example . This means that the bending stiffness about the weak axis and also the torsional stiffness will be important at low levels of pipe strain. The warping stiffness is extremely small, and will never be important to the solution.

5.2.7 Stress components

The stress components considered are the longitudinal stresses which can be divided into pure axial stress σ_a, bending stress from bending about the X^2-axis (strong axis) σ_{b2}, bending stress from bending about the X^3-axis (weak axis) σ_{b3} and warping stress σ_w. Simple formulas from beam theory will be used to evaluate the stresses. The different components are calculated as:

$$\begin{aligned}\sigma_a &= E\epsilon_a = E(\epsilon + \frac{1}{2}(\gamma - \eta)^2) \\ &= E(\epsilon + \frac{1}{2}(\gamma - \gamma(1 - e^{-kX^1}))^2) = E(\epsilon + \frac{1}{2}\gamma^2 e^{-2kX^1})\end{aligned} \tag{140}$$

$$\sigma_{b2} = \frac{M_2}{I_2} \cdot X^3 = \frac{EI_2\Delta\kappa_2}{I_2} \cdot X^3 = -E\frac{d\eta}{dX^1} \cdot X^3 = -Ek\gamma e^{-kX^1} \cdot X^3 \tag{141}$$

$$\begin{aligned}\sigma_{b3} &= -\frac{M_3}{I_3} \cdot X^2 = -\frac{EI_3\Delta\kappa_3}{I_3} \cdot X^2 = E \cdot \frac{2\sin\alpha_0\cos\alpha_0}{R} \cdot \eta \cdot X^2 \\ &= E\gamma \cdot \frac{2\sin\alpha_0\cos\alpha_0}{R}(1 - e^{-kX^1}) \cdot X^2\end{aligned} \tag{142}$$

$$\begin{aligned}\sigma_w &= E\varphi(X^2, X^3)\Delta\tau_{,1} = E\varphi(X^2, X^3)\frac{1 - 2\cos^2\alpha_0}{R}\frac{d\eta}{dX^1} \\ &= Ek\gamma\varphi(X^2, X^3)\frac{1 - 2\cos^2\alpha_0}{R}e^{-kX^1}\end{aligned} \tag{143}$$

At the end fitting, $X^1 = 0$, and hence the stress components are:

$$\sigma_a = E(\epsilon + \frac{1}{2}\gamma^2) \approx E\epsilon \tag{144}$$

$$\sigma_{b2} = -Ek\gamma \cdot X^3 \tag{145}$$

$$\sigma_{b3} = 0 \tag{146}$$

$$\sigma_w = Ek\gamma\varphi(X^2, X^3)\frac{1 - 2\cos^2\alpha_0}{R} \tag{147}$$

The axial stress is uniform over the cross section, while the bending stress varies linearly and is largest at the edges where $X^3 = -\frac{a}{2}$. The warping stress has a more complex distribution due to the warping function, but the value of interest is the maximum value along the edge. Using the same cross section data and the same axial strain as in the previous discussion, the numerical values are:

$$\gamma = 0.6109 - \tan^{-1}\left(\frac{\tan 0.6109}{1 + 0.001}\right) = 0.00047 \tag{148}$$

$$\sigma_a = 2.1 \cdot 10^{11} \text{ Pa} \cdot \cos^2 35^\circ \cdot 0.001 = 140.9 \text{ MPa} \tag{149}$$

$$\sigma_{b2,max} = 2.1 \cdot 10^{11} \text{ Pa} \cdot 10.53 \text{ m}^{-1} \cdot 0.00047 \cdot 0.0045 \text{ m} = 4.7 \text{ MPa} \tag{150}$$

$$\sigma_w = 2.1 \cdot 10^{11} \text{ Pa} \cdot 10.53 \text{ m}^{-1} \cdot 0.00047 \cdot 2.9 \cdot 10^{-6} \cdot \frac{1 - 2\cos^2 0.6109}{0.1} = 0.01 \text{ MPa} \tag{151}$$

As seen, the warping stress is very small, and gives no significant contribution to the total stress. The warping stiffness was also found to be insignificant to the wire deformation close to the end. It is thus concluded that warping may be neglected in relation with tensile armor wires and end restraints.

The bending stress is however far more interesting, as it constitutes 3 % of the total longitudinal stress. This means that if only the axial stress is taken into account, the predicted stress is 3 % too low. For high cycle fatigue, the fatigue life of a steel component is typically proportional to $(\Delta\sigma)^{-3}$ [26], meaning that a 3 % increase in dynamic stress will give a 8.5 % decrease in fatigue life. And this is only for the particular case considered above. The next step will be to see how the bending component varies as a function of the axial stress, and also what role the dimensions of the armor wire plays.

5.2.8 Bending stress at the end fitting

To get a picture of the relative magnitude of the local bending stress at the end fitting, the stress formulas derived previously have been used to calculate numerical values for a wide range of pipe strain. The calculations have been performed in Matlab, and results are shown in figure 20, where the ratio between local bending stress and axial stress are shown for two different wire dimensions. The blue line shows results for a wire of width 9 mm and thickness 3mm, while the red line shows a larger wire of width 15 mm and thickness 6 mm. The radius of the pipe is 0.1 meters and the lay angle is 35° in both cases.

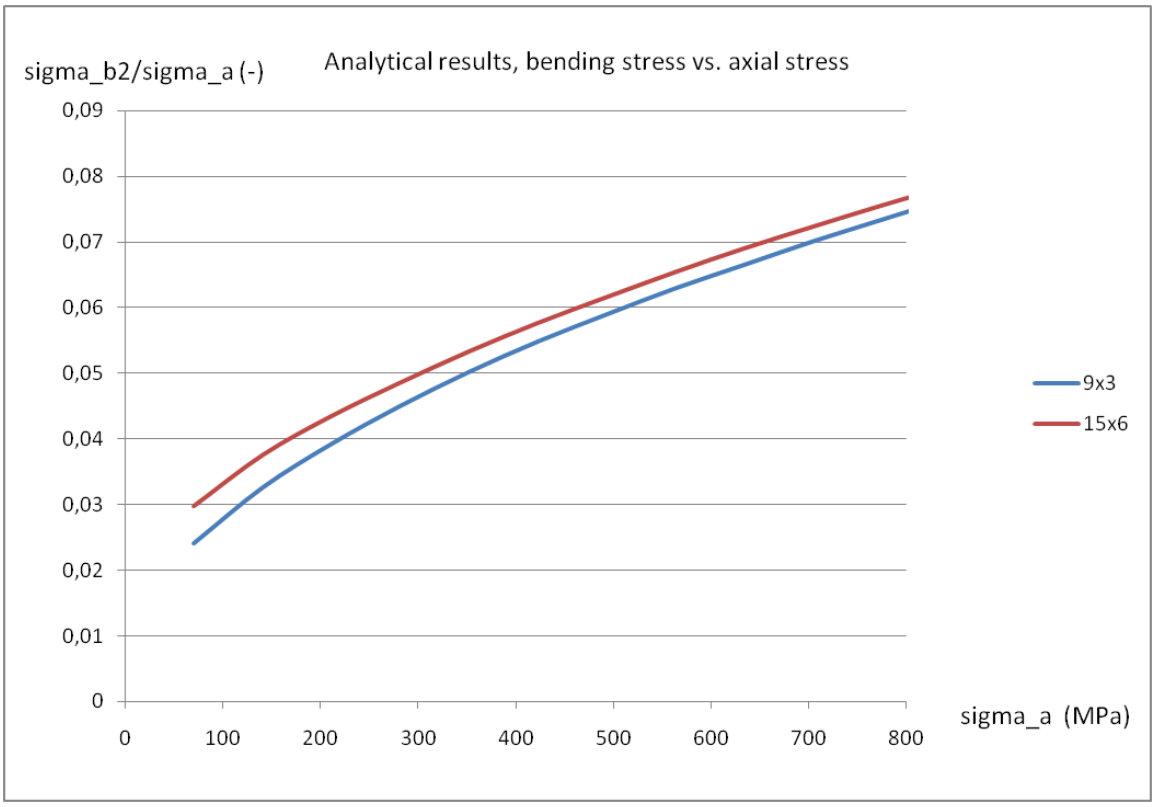

Figure 20: Analytical results for the ratio between bending and axial stress.

As seen in the figure, the bending component grows larger relative to the axial stress as the stress increases, and the bending stress exceeds 6 % of the axial stress for an axial stress above 500 MPa. The rate of increase in bending stress is relatively large at low strain levels, but it does however decay as the axial stress increase. Even so, the relative magnitude of bending stress continues to increase. It is also observed that the two curves in the figure are located very close to each other despite the relatively large differences in wire dimensions. The bending component is slightly larger for the biggest wire, even though the big wire has a lower width-to-thickness ratio than the small wire.

One could have thought that the dimensions of the wire are more important, and it is therefore of interest to look deeper into the variables which determine the bending stress. σ_{b2} was found to be proportional to k, and even though the expression for k is quite complex, the two most important terms are those containing the axial strain and the bending stiffness about the strong axis. This was seen in the previous discussion of the solution. Using an approximate expression containing only these two dominating terms, k reduces to:

$$k \approx \sqrt{\frac{EA\epsilon}{EI_2}} = \sqrt{\frac{ab}{\frac{1}{12}ba^3}}\epsilon^{0.5} = \sqrt{\frac{12}{a^2}}\epsilon^{0.5} \approx 3.46\frac{\epsilon^{0.5}}{a} \tag{152}$$

Inserting this approximate result into equation (145) yields:

$$\sigma_{b2,max} \approx 3.46E\gamma\frac{\epsilon^{0.5}}{a}\frac{a}{2} = 1.73E\gamma\epsilon^{0.5} \tag{153}$$

This verifies the fact that the magnitude of the localized bending stress at a given pipe strain is virtually independent of the size of the cross section. Since γ is a linear

function of the pipe strain ϵ_p, and hence also ϵ, the above result indicates that the bending stress is approximately proportional to $\epsilon^{\frac{3}{2}}$. The ratio between σ_{b2} and σ_a should then be proportional to $\epsilon^{0.5}$, which is in aggreement with the shape of the curve in figure 20.

5.3 End fitting stresses - Aflex/Bflex

A major shortcoming of the analytical results presented in the previous section is the lack of friction. The tensile armor layers will contract under tension, and thus high contact pressures between layers will occur near the end fitting. The high contact pressure makes it possible to get large friction forces, and these forces will seek to pull the wire along with the surrounding layers as the pipe elongates. Looking back at figure 17, this means that the friction forces will try to fix the wire to the curve defined by γ, and this again means that the bending stress at the end fitting will become even larger than what was found before.

In this section, a finite element model of a single tensile armor wire will be established using the new curved beam element described in section 4.6. Analyses will be done for the same cases as was done analytically, with varying friction coefficient. This is to test the agreement between the analytical and the numerical method and also to investigate the importance of friction.

5.3.1 Description of FEM model

The model is based on the new curved beam element described in section 4.6 and the Bflex2010 program system is used for the analyses. The aim is to simulate the same scenario as previously done analytically, i.e. a single tensile armor wire on a supporting circular layer subjected to axial straining. The model is quite simple and consists of three different types of elements:

- Curved beam elements (hshear353) for the tensile armor wire.
- Pipe elements (pipe31) for the supporting layer. The element is a beam element with 6 degrees of freedom at each end.
- Specialized contact elements (hcont453) to represent normal and frictional contact between the two above elements.

The length of the model is set to 8 pitches, and for a lay angle of 35° and a radius of 0.1 meters this gives a model length of 7.179 meters. 400 elements are used to model the wire, and each wire element has a pipe element and a contact element connected to it. Boundary conditions are applied both to the wire elements and the pipe elements. Those applied to the pipe elements are:

- End 1 fixed in all 6 degrees of freedom.
- End 2 free to move in the longitudinal direction and fixed in the remaining 5 degrees of freedom.

It is important to note that for the curved beam element, the degrees of freedom are not the actual displacements, but the displacements *relative* to the supporting surface. This means that if one fixes *all* the nodal displacements for the wire, it is not fixed in space, but it is "glued" to the supporting surface. The boundary conditions applied to the wire elements are:

- Wire fixed in longitudinal and lateral direction at both ends of the model.

The loading is applied through gradually increasing prescribed displacements. This is done through two individual degrees of freedom. The node belonging to the pipe element at end 2 of the model (away from the end fitting) is pulled in the longitudinal direction a distance corresponding to the pipe strain, ϵ_p. At the same time, the node belonging to the wire element at the end fitting is rotated an angle corresponding to the change in lay angle when the pipe is axially strained, γ. This simulates the rotational restraint due to the anchoring. For any level of pipe strain, this angle is calculated according to equation (98).

The entire model is shown in figure 21 and an enlarged view of the wire close to the end fitting is shown in figure 22. In the last of the two figures, the magnitude of bending stress is indicated by the color.

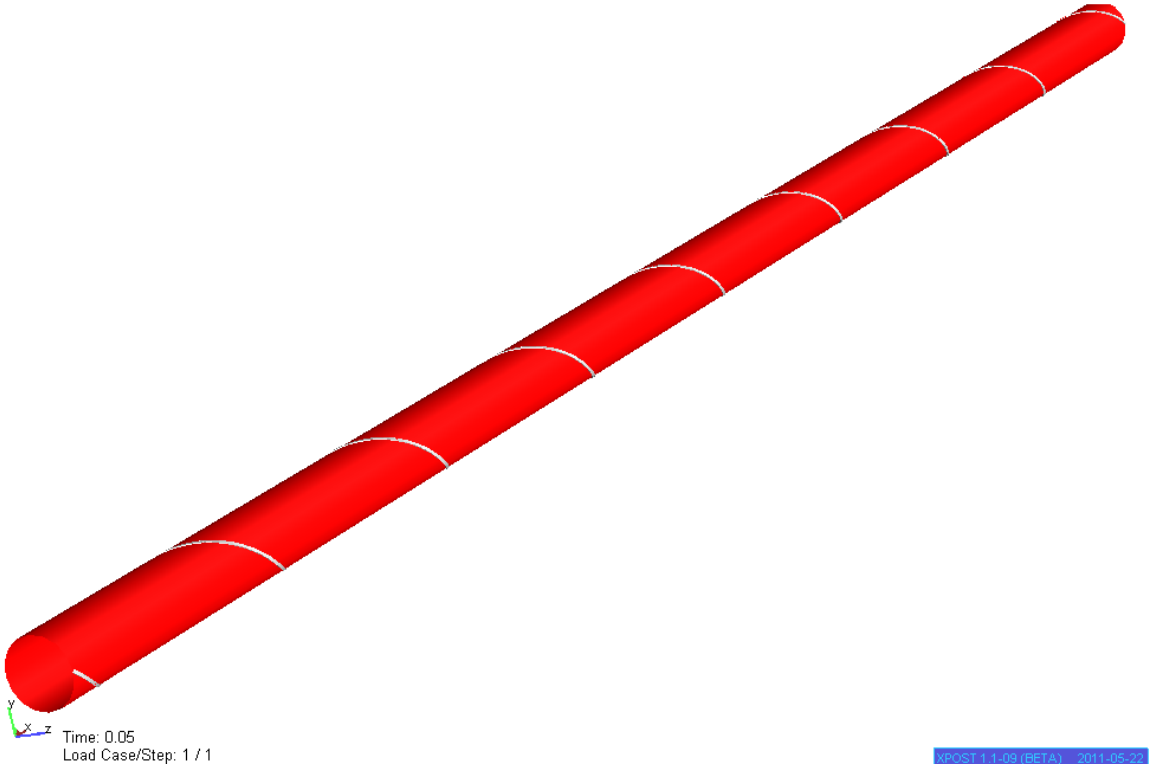

Figure 21: The Aflex/Bflex finite element model used to calculate end fitting stresses.

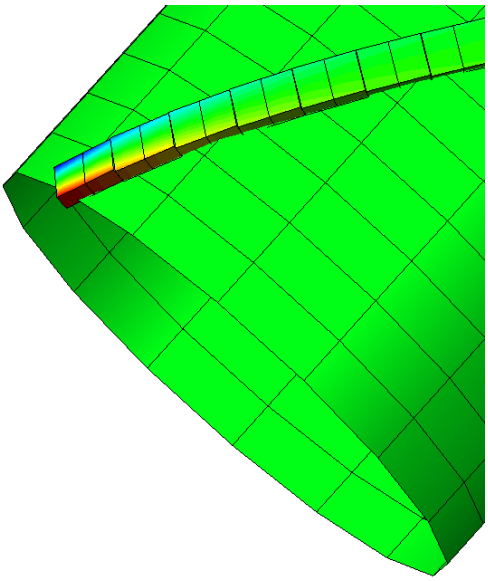

Figure 22: Close up view of the armor wire at the end restraint.

5.3.2 Results

Analyses have been performed with the finite element model described above. Two different sets of analyses have been done. The first one with a 9 x 3 mm wire and the second one with a 15 x 6 mm wire. It is of interest to compare the results from the frictionless analyses with the analytical results presented earlier. In order to do so, the Aflex/Bflex results have been plotted together with the analytical results:

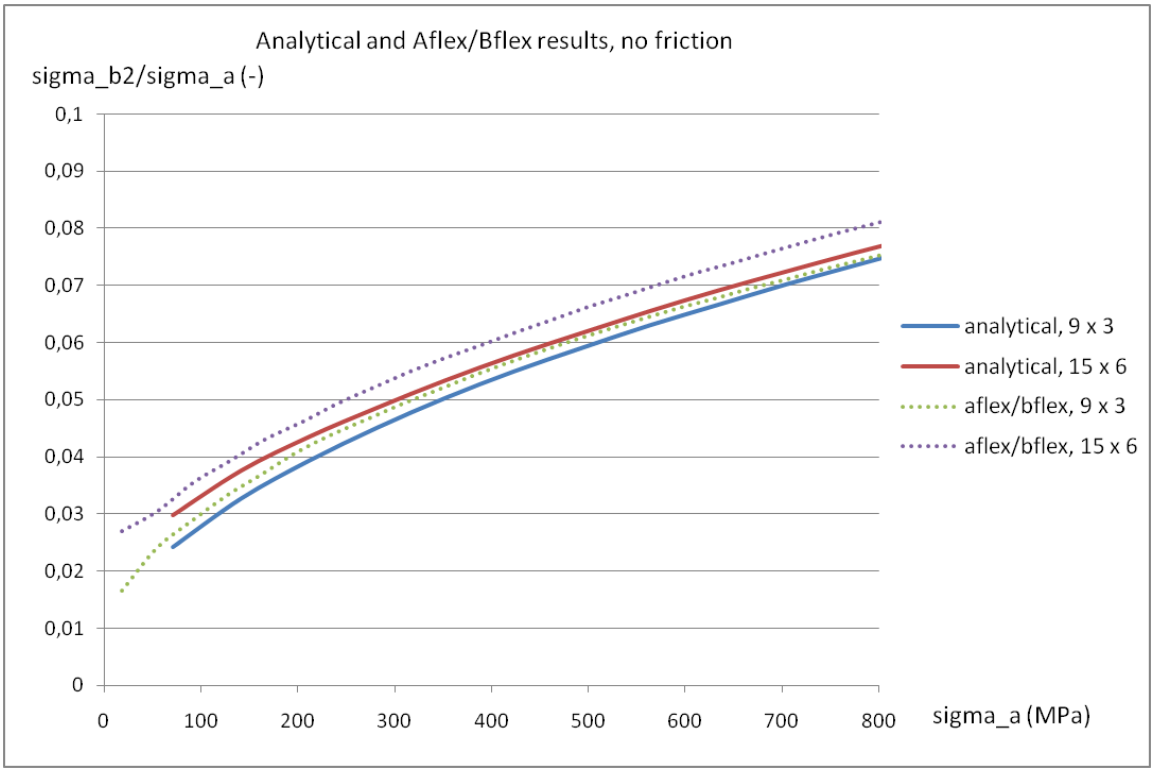

Figure 23: Comparison of analytical and numerical results, no friction.

The results are very similar, and especially for the 9 x 3 mm wire, the analytical and numerical analyses agree very well. This is encouraging, although the numerical results report a slightly larger ratio between the bending stress and the axial stress than what was found analytically for the 15 x 6 mm wire. The difference is however small, which indicates that the analytical model provides good results.

Next, the results from the Aflex/Bflex analyses with friction are presented. The friction coefficient between the layers are varied, and results are shown in figures 24 and 25 below.

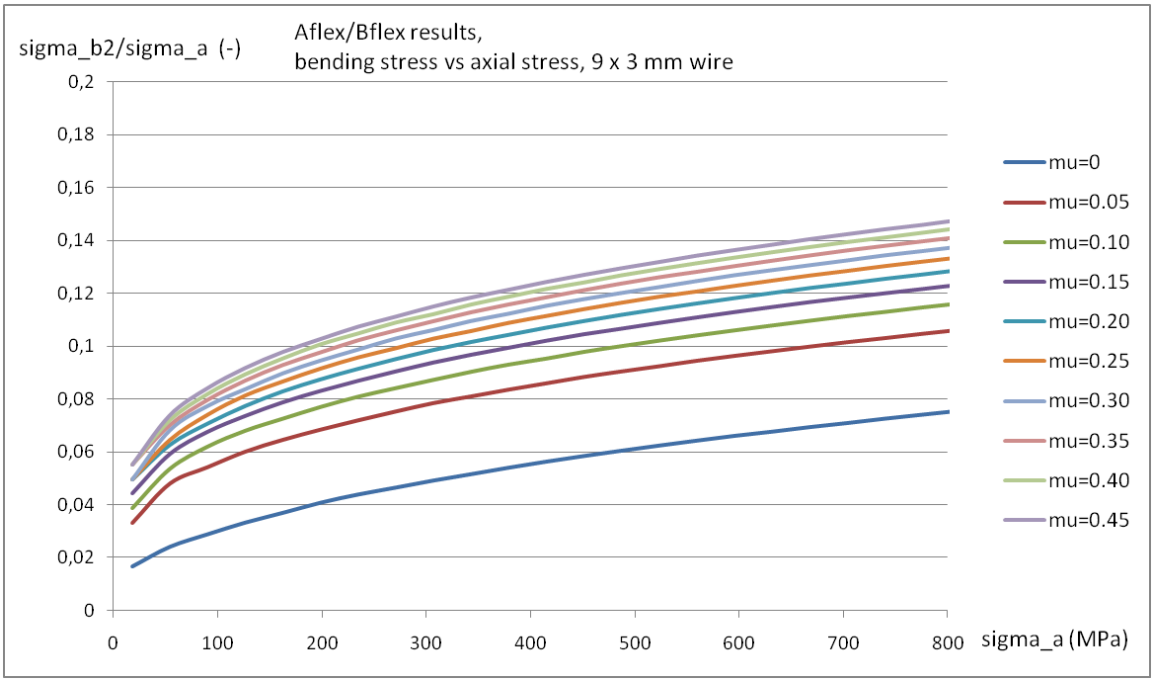

Figure 24: Aflex/Bflex results for end fitting bending stress, 9 x 3 mm wire.

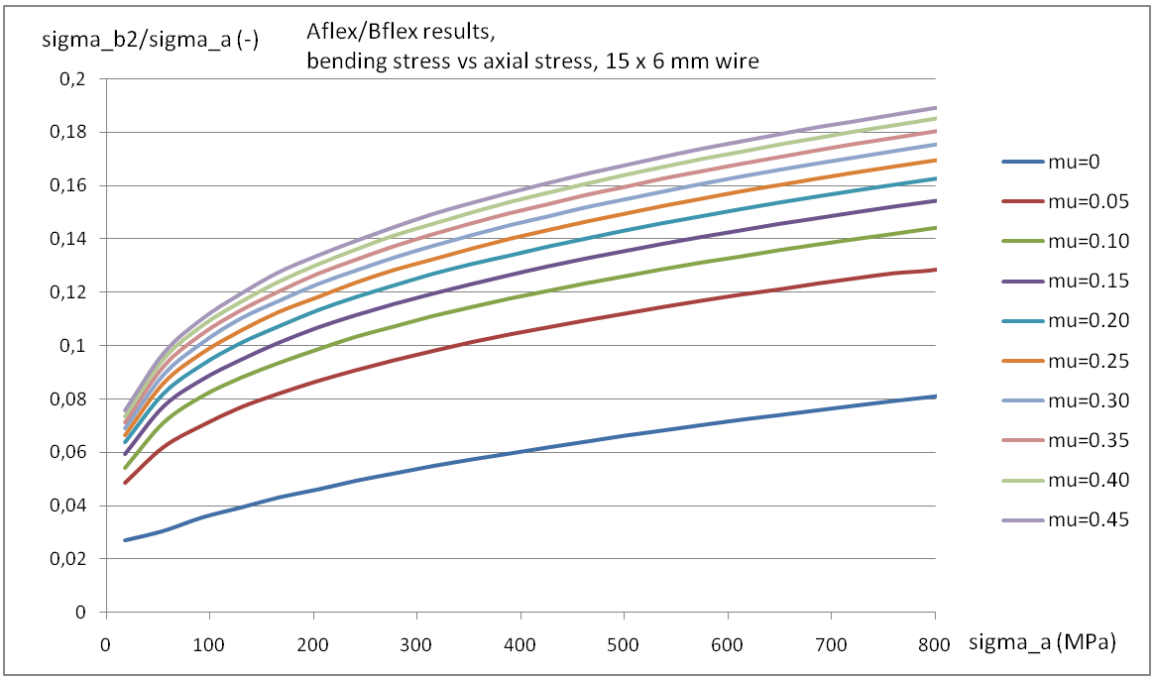

Figure 25: Aflex/Bflex results for end fitting bending stress, 15 x 6 mm wire.

As seen, the friction greatly increases the bending stress at the end fitting. There is a major increase from $\mu = 0$ to $\mu = 0.05$, but the increase is not as large when the friction coefficient is increased further. The bending stress does however continue to grow for increasing friction coefficient. An interesting detail is the different effect the friction has on the small and the big wire. For zero friction, the results are very close to each other. However, when friction is included, the difference between the two wires becomes much larger. Take the point where $\sigma_a = 500\ MPa$ as an example. For a friction coefficient of 0.15, the ratio between bending and axial stress is close to 0.14 for the big wire, but for the small wire it is below 0.11. The difference continues to increase for even larger friction coefficients. It is therefore of interest to investigate if this is reasonable or not.

The reason why friction increases the local bending stress is that the friction forces will try to fix the wire to the supporting layer. This layer will elongate as the pipe is stretched, and due to the lay angle of the wire, a longitudinal displacement of the supporting layer will have a transverse component relative to the wire. It is this transverse displacement which leads to the change in lay angle called γ in the previous discussions. In the vicinity of the end restraint, the lay angle is not allowed to change and hence relative slip between the supporting layer and the armor wire must occur. One may intuitively understand that if the friction forces are large, they will "quickly" force the lay angle to change, meaning that the transverse curvature of the wire will be large close to the end fitting. This will be associated with large bending stress. To illustrate this, the transverse curvature is plotted as a function of the arc length coordinate X^1 in figure 26 below. The plot goes from $X^1 = 0$ to $X^1 = 300$ mm, i.e. it is the part near the end fitting that is shown. The curve with the largest value at $X^1 = 0$ is for $\mu = 0.45$ and the other is for no friction.

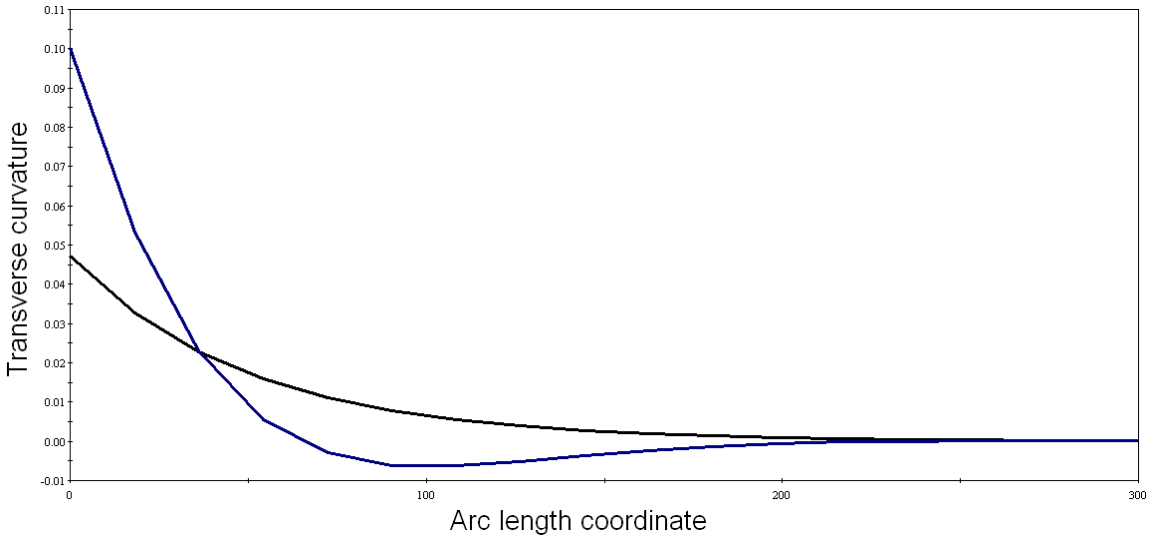

Figure 26: Transverse curvature close to the end fitting with and without friction.

So why is this effect larger for the big wire than the small one? It can of course be multiple reasons to this, but an important point is that the maximum friction force is related to the contact pressure, and the contact pressure depends on the axial *force* in the wire, not only the stress. The axial force in the big wire is of course larger than in the small wire if the axial stress in the two is the same. This means that the contact pressure at a given axial stress will be larger for the big wire. This in turn means that the maximum lateral friction force is larger, which results in larger localized bending stress.

The analyses did only include a single armor wire, which means that the contact pressure from a second armor layer is not directly accounted for. Even so, the results may be used for a flexible riser with *two* tensile armor layers, if one uses a friction coefficient 3 times larger than what it really is. This is illustrated in figure 27 below:

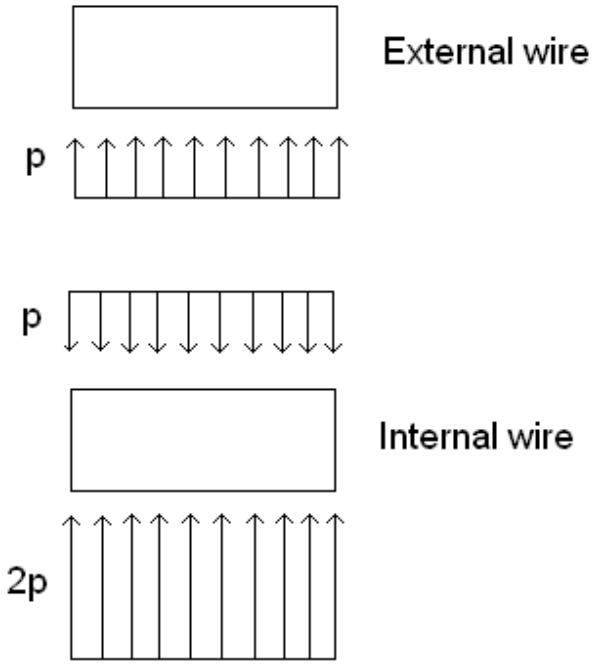

Figure 27: Contact pressure if two armor layers are applied.

Imagine that there is only one armor layer, and the contact pressure on the inside is p. If a second armor layer is added, a contact pressure of magnitude p must also act on the inside of the new layer, which means that the contact pressure beneath the inner layer must increase to $2p$ to maintain equilibrium. Thus, the total contact force on the inner wire is $2p$ on the inside and p on the outside. There will be friction on both sides of the inner wire, and the available lateral friction force (or stress) is now $\mu p + \mu 2p = 3\mu p$. This indicates that the effect of the additional external tensile armor layer is achieved by using a 3 times larger friction coefficient. For example, if the actual friction coefficient is 0.15, the 0.45-curves in the above results should be used for a flexible pipe with two tensile armor layers.

This means that for a flexible pipe with two tensile armor layers with wires of dimension 15 x 6 mm and a friction coefficient of 0.15 between the steel material and the supporting layer, one may experience a localized bending stress of approximately 16 % of the axial stress if the pure axial stress is 400 MPa. This is significant, and should be included in fatigue analyses of the armor wires. It is however noted that all the above calculations rests on the assumption that the armor wires are fully fixed at the end fitting. The accuracy of this assumption depends on the end fitting construction, and more detailed analyses taking the end fitting behaviour into the calculations should be performed.

6 External pressure buckling

6.1 Introduction

Tensile armor wires in flexible risers are designed primarily to withstand large axial tensile loads due to weight and environmental actions. To maintain the flexibility of the pipe, the individual wires are made slender. This may be an issue in cases where the pipe is subjected to a compressive axial force, because the slender cross section makes the wires susceptible to elastic buckling. A compressive axial force may occur when the pipe is loaded by external pressure. As discussed in a number of textbooks, for example [27], both internal and external pressure will give rise to so called *end cap forces*. This means that in a scenario where the internal pressure is low and the external pressure is high, the wires may be subjected to compression. An example of such a scenario is the installation phase. If a riser is being installed in deep water while it is empty inside, the part of the riser close to the touch down point may be in danger. There will be very little tension from riser weight, and the high external pressure combined with large pipe curvature may be critical.

It must of course be taken into account that the armor wires are part of a larger structure, and that the surrounding layers will provide support. This means that compressive failure may happen as a result of failure of the supporting layers, or slip between layers. Hence, compressive failure is not necessarily a true buckling phenomenon.

There are basically two directions in which the wires may deflect when they fail. They may move outwards or sideways. The associated failure modes are *radial* and *lateral* buckling. The two modes are very different because of interaction with the surrounding layers of the pipe, and the critical load for each mode will be determined from different parameters. For radial failure, the strength and stiffness of the layers outside the tensile armor will be important. These layers are typically the external plastic sheath and a tape layer used specifically to prevent radial failure of the armor wires. When it comes to lateral failure, the friction coefficient and pipe curvature are important, as lateral friction forces will restrain the wires from buckling.

In this section, both analytical and numerical analyses will be done in order to investigate the buckling behaviour of armor wires. As there is little previous work done in this area, emphasis will be put on determining the governing effects and important parameters. In order to compare the different buckling modes and decide which one is critical, a single measure of the buckling load is needed. Here, the *axial stress* in the tensile armor wires is used to identify the buckling load. As an example, a flexible riser with a mean tensile armor layer radius of 0.1 meter, a lay angle of 35°, wire dimensions equal to 9 x 3 mm and a total of 100 tensile armor wires will be used. The wires are assumed to be of steel with a modulus of elasticity equal to 200 GPa. Other parameters are varied in order to investigate how the capacity changes.

6.2 Analytical buckling calculations

6.2.1 Radial buckling

The radial failure mode is also known as *bird-caging*, and was first observed in 1989 [4]. This failure mode may in theory occur in two different ways:

- Failure of supporting layer (anti buckling tape)

- Elastic buckling without tape failure

The first mode above is not really a buckling failure, it is simply triggered by the loss of support. When the ultimate strength of the anti buckling tape is exceeded, a sudden radial expansion of the tensile armor layers will take place. The second mode is a true buckling phenomenon which is quite similar to buckling of a straigth beam on an elastic foundation.

Before any strength calculations are performed it is of interest to summarize some important physical effects. The external pressure, which is the driving force for buckling, is of course also acting in the radial direction, pushing the external sheath *inwards* (given that the external sheath is intact). This will directly counteract the radial expansion. In order to get radial buckling, the net force in the radial direction must be directed *outwards*. Thus one may ask if radial buckling due to hydrostatic pressure is at all possible? A simple consideration of the radial forces on the external sheath is enough to answer this question. Say that a flexible riser is empty, and the external hydrostatic pressure is p_e. For a pipe with external radius R_e, the compressive force due to the pressure will be:

$$T_w = p_e \pi R_e^2 \tag{154}$$

As given in equation (2), the contact pressure felt by the anti buckling tape/external sheath is approximately:

$$p_T \approx \frac{T_w \tan^2 \alpha}{2\pi R^2} \tag{155}$$

where α as usual is the lay angle, and R is the mean radius of the armor wires. Inserting for T_w gives:

$$p_T \approx \frac{p_e \pi R_e^2 \tan^2 \alpha}{2\pi R} = p_e \frac{R_e^2 \tan^2 \alpha}{2R^2} \tag{156}$$

As p_T acts outwards and p_e inwards, radial displacement can only take place if $p_T > p_e$. From the above expression it is seen that this is only the case if:

$$\frac{R_e^2 \tan^2 \alpha}{2R^2} > 1 \tag{157}$$

Now, if $\alpha = 35°$, this means that the ratio between the external radius and the radius of the tensile armor must be:

$$\frac{R_e}{R} > \sqrt{\frac{2}{\tan^2 \alpha}} \approx 2 \tag{158}$$

This is unlikely for most flexible risers, as the external radius and mean radius of the tensile armor layers are normally quite close. It may possibly happen for small diameter pipes. The above result indicates that investigation of radial buckling when the annulus is assumed to be *flooded* is far more interesting. When seawater has penetrated the external sheath, the hydrostatic pressure acts on both sides, meaning that the net radial pressure from seawater is zero. This allows for radial expansion and buckling, and this was in fact the case when the radial failure mode was observed in 1989. The assumption of a flooded annulus is therefore used in the succeeding analyses.

Radial failure mode 1, anti buckling tape failure

When the annulus is flooded, there is nothing but the layers on the outside of the tensile armor to restrain radial expansion. There is little support provided by any plastic layers, and therefore they will be totally neglected in this context. Thereby, it is the anti buckling tape alone that must carry the radial pressure due to expansion of the tensile armor, and it is the ultimate strength of the anti buckling tape which will determine the critical external pressure.

The external pressure leads to a compressive load which further will give a contact pressure acting on the anti buckling tape as given by equation (2). The tape is thin, and hence the circumferential stress which arises may be found as [25]:

$$\sigma_{tape} = \frac{R_t}{t} p_T \approx \frac{R_t}{t} \frac{T_w \tan^2 \alpha}{2\pi R^2} \tag{159}$$

where R_t is the mean radius of the tape layer and t is the thickness of the tape. Failure will occur when this stress reaches the ultimate tensile strength of the tape, $\sigma_{u,tape}$. As seen, the stress in the tape does not depend on the cross sectional dimensions of the tensile armor wires, or any material parameters at all. For a given flexible pipe where lay angle and radii are given, the only way to increase the capacity with respect to this failure mode is to increase the tape thickness, or use a stronger tape.

It is further assumed that $R_t \approx R$, i.e. that the mean radius of the tensile armor layers and anti buckling tape are approximately the same. Inserting for the axial force using equation (1), an expression is found which relates the stress in the anti buckling tape to the axial stress in the tensile armor wires:

$$\sigma_{tape} \approx \frac{n\sigma_a A}{t} \frac{\cos\alpha \tan^2 \alpha}{2\pi R} \tag{160}$$

Here, n is the total number of tensile armor wires, σ_a is the axial stress in the armor wires and A is the cross section area of a single wire. By rearranging the above expression, the critical axial stress in the armor wires is given by the ultimate strength of the tape:

$$\sigma_{a,max} \approx \frac{\sigma_{u,tape} t}{nA} \frac{2\pi R}{\cos\alpha \tan^2 \alpha} \tag{161}$$

The critical axial stress in the armor wires as given by the above equation is shown in figure 28 for varying $\sigma_{u,tape}$ and different tape thicknesses. All other parameters are defined from the example riser described in this sections introduction.

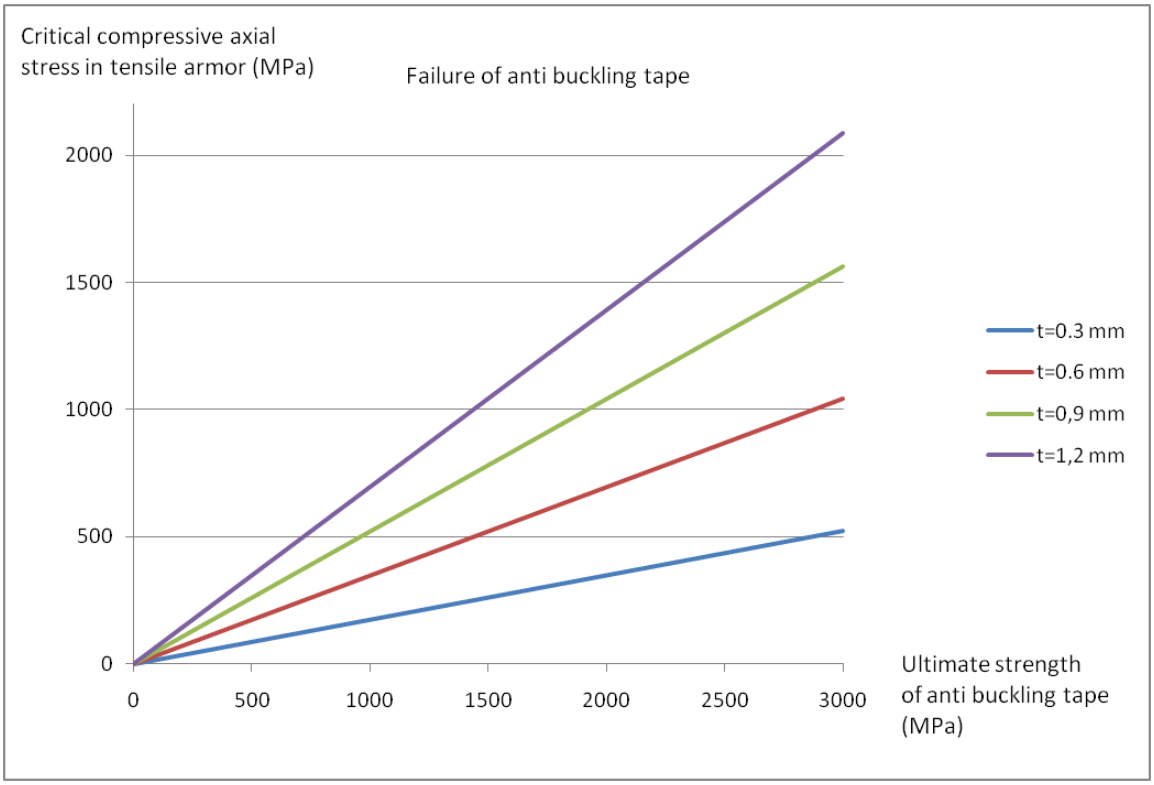

Figure 28: Critical compressive stress in tensile armor wires as a function of anti buckling tape strength.

It is seen how the critical compressive stress in the tensile armor wires increases proportionally with both the strength and thickness of the anti buckling tape. If a tape material with an ultimate tensile strength of 1500 MPa and a thickness of 0.6 mm is used, the maximum compressive stress in the armor wires will be approximately 500 MPa. The capacity may however be doubled by doubling the tape thickness.

Radial failure mode 2, elastic buckling

The second radial failure mode is an elastic buckling mode, where the armor wires deflect radially in a sinusoidal pattern. The solution to a similar problem, which is buckling of a straight beam on a uniform elastic support, is given in [28]. Here, the critical load is found using energy principles and an assumed buckling shape. The internal potential energy contains contributions from bending of the wire and the straining of the elastic foundation. In this case, the foundation is the anti buckling tape, and its stiffness will be important to the critical load. In the analyses performed here, it is assumed that each wire behaves as an individual structural member, meaning that there is no interaction between wires. The total number of wires are taken into account by scaling the stiffness of the supporting tape. Hence, the buckling load may be determined by looking at a single wire.

Beacuse bending energy and the elastic energy in the foundation/tape will dominate, it seems likely that the straight beam solution as given in [28] will provide reasonable results for a curved armor wire as well. Whether or not this is correct will be seen when the results are compared to the finite element analyses.

As the tensile armor wire is restrained from deflecting inwards due to the large stiffness of the underlying layers, it is assumed that it only deflects outwards. A possible buckling

shape is shown in figure 29:

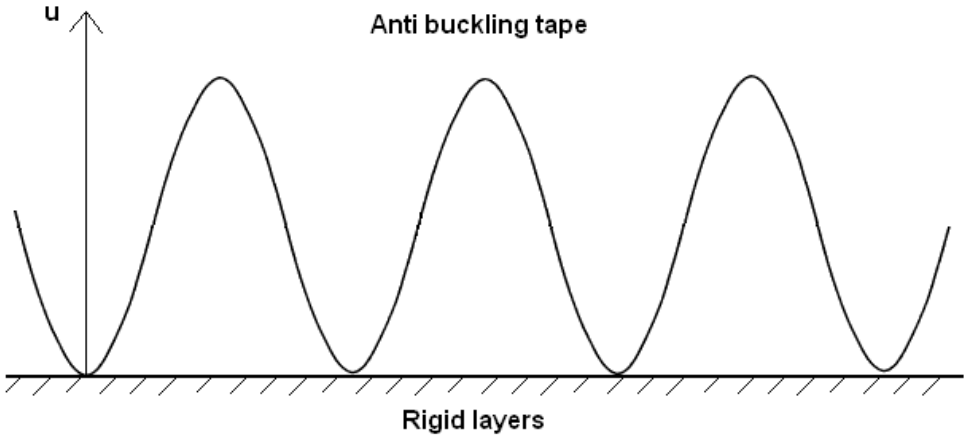

Figure 29: Assumed radial buckling shape.

Using the symbol u for the radial deflection, the assumed buckling shape is:

$$u = u_0 \sin \frac{m\pi X^1}{l} \tag{162}$$

The anti buckling tape is represented by radial springs with a stiffness per unit length, k. The internal elastic bending and spring energy over an arbitrarily length l is then:

$$\begin{aligned} W_i &= \frac{1}{2}\int_0^l EI_3 u_{,11}^2 dX^1 + \frac{1}{2}\int_0^l ku^2 dX^1 \\ &= \frac{1}{2}EI_3 \int_0^l \frac{m^4\pi^4}{l^4} u_o^2 \sin^2 \frac{m\pi X^1}{l} dX^1 + \frac{k}{2}\int_0^l u_0^2 \sin^2 \frac{m\pi X^1}{l} dX^1 \\ &= \frac{1}{4}EI_3 \frac{m^4\pi^4}{l^3} u_0^2 + \frac{1}{4}klu_0^2 \end{aligned} \tag{163}$$

The work done by the axial compressive load, Q_1, is given by the axial shortening as the wire buckles:

$$\begin{aligned} W_e &= -Q_1 \int_0^l \frac{1}{2} u_{,1}^2 dX^1 = -\frac{Q_1}{2}\int_0^l \frac{m^2\pi^2}{l^2} u_0^2 \cos^2 \frac{m\pi X^1}{l} dX^1 \\ &= -\frac{Q_1 m^2\pi^2}{4l} u_0^2 \end{aligned} \tag{164}$$

The principle of minimum potential energy gives the critical compressive load:

$$\begin{aligned} &\frac{d\Pi}{du_0} = \frac{dW_i}{du_0} + \frac{dW_e}{du_0} = 0 \\ &\Rightarrow \frac{1}{2}EI_3 \frac{m^4\pi^4}{l^3} u_0 + \frac{kl}{2}u_0 - \frac{Q_1 m^2\pi^2}{2l} u_0 = 0 \\ &\Rightarrow Q_1 = \pi^2 EI_3 (\frac{m}{l})^2 + \frac{k}{\pi^2}(\frac{l}{m})^2 \end{aligned} \tag{165}$$

It is seen that the elastic buckling load depends strongly upon $\frac{m}{l}$, the number of half waves per unit length. The critical load will be the lowest possible, and may be found graphically by plotting the solution for different $\frac{m}{l}$. In order to relate the results to an actual flexible pipe, it is necessary to find the spring stiffness k from known pipe parameters. This may be done in the following way.

As previously stated, the external layers feel a pressure, p_T, as given in equation (2). This pressure is equivalent to a line load on each tendon, and the magnitude of this line load is:

$$q_2 = p_T \frac{2\pi R}{n} \cos\alpha \tag{166}$$

where n is the total number of tensile armor wires in the pipe. The factor $\frac{2\pi R}{n}$ comes from projecting the total pressure around the circumference onto the individual wires. The factor $\cos\alpha$ takes into account that the length along the armor wire is longer than along the pipe's longitudinal axis, thus the lay angle reduces the line load. Now the strain in the anti buckling tape when subjected to a radial displacement, u_2, is:

$$\epsilon = \frac{u_2}{R} \tag{167}$$

The stress in the anti buckling tape when subjected to internal pressure was given in equation (159), and by combining this expression with $\sigma = E\epsilon$ gives the radial displacement of the tape for a given internal pressure:

$$u_2 = p_T \frac{R^2}{Et} \tag{168}$$

In the above result it has also been assumed that $R_t \approx R$. Inserting for p_T using the relationship given in equation (166) results in:

$$\frac{q_2}{u_2} = \frac{2\pi}{n} \frac{Et}{R} \cos\alpha \tag{169}$$

This is the radial stiffness of the anti buckling tape per unit length along the wire, i.e. the parameter k in equations (163) - (165). Not surprisingly, the stiffness depends on both the thickness and modulus of elasticity of the tape. The necessary equations for calculating the elastic radial buckling load for a given pipe geometry, tape strength and thickness have now been established. Results for the example riser with varying modulus of elasticity and different thicknesses for the tape are shown in figure 30.

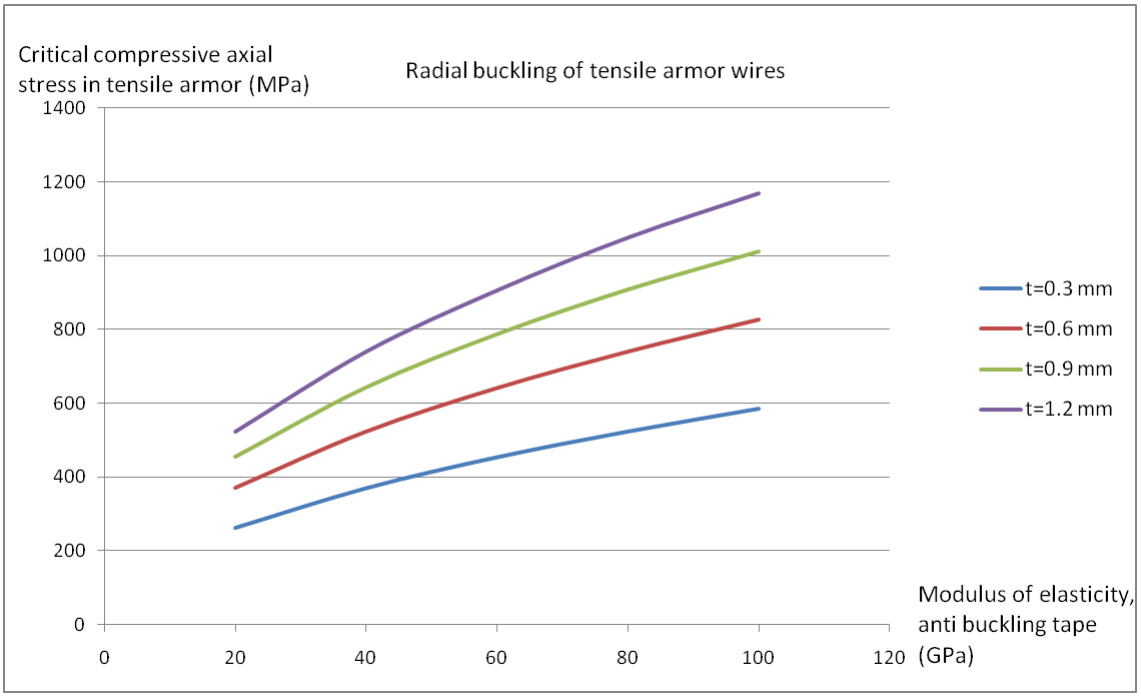

Figure 30: Elastic buckling stress for armor wires as a function of tape stiffness.

The figure shows that the critical stress is not proportional to the tape stiffness in this case. This is because the bending stiffness of the armor wire also gives a significant contribution to the buckling strength of the wire. If this failure mode is to occur, the critical compressive stress must be lower than the one for the tape failure mode given previously. This will then depend on the ratio between the elastic modulus and the ultimate strength of the tape. For example, for a tape thickness of 0.6 mm and an ultimate strength of 2000 MPa, the elastic modulus of the tape must be less than approximately 80 GPa for elastic buckling to occur. If the elastic modulus is higher than 80 GPa, the tape will fail before the elastic buckling load is reached. This is seen by comparing figures 28 and 30.

6.2.2 Lateral buckling

If the anti buckling tape is sufficiently strong to prevent radial buckling, the wire has only one way to go, and that is sideways. However, if the wire is to slide in the lateral direction, it must overcome the friction forces from the surrounding layers. If hydrostatic pressure is acting on the external plastic sheath, there will be very high contact pressures, thus making it hard to overcome the friction. Therefore, the assumption of a flooded annulus will be used here as well. This should make the results presented here "worst case" scenarios.

As previously discussed, the wires will try to deflect outwards in the radial direction when compressed axially. This is due to the initial normal curvature of the wire, κ_3. The wires need to be restrained by an external layer, and from the equilibrium equation in radial direction which was given in section 4.3, the restraining line load in the radial direction is:

$$q_2 = \kappa_3 Q_1 \tag{170}$$

where Q_1 is the axial compressive force in the wire. This line load is the equivalent opposing reaction to the pressure excerted on the external layer, as given by equation (2). The friction force may also be considered as a line load acting along the wire, and its magnitude is determined by the contact force per unit length, q_2, and the friction coefficient between the external layer and the wire, μ. There may in principle be friction forces acting in both the longitudinal and the lateral direction of the wire, but it is only the *lateral* friction that restrains lateral movement. For simplicity it will be assumed in the analytical calculations that the longitudinal friction force is zero, meaning that the full magnitude of the friction force may be utilized in the lateral direction. From this assumption it follows that the lateral friction force per unit length is:

$$q_3 = \mu q_2 = \mu \kappa_3 Q_1 \tag{171}$$

It is evident from the above equation that axial compression will actually increase the available friction force and in this way help prevent buckling. However, the lateral friction force in equation (171) is based on full utilization of friction in the lateral direction. In reality, longitudinal friction forces will be present when a flexible pipe is bent, meaning that the available lateral friction force will be reduced. Therefore it is possible that equation (171) severely overestimates the lateral friction force when the pipe is subjected to bending. If this is true there will be a significant difference in the analytical results presented in this section, and the finite element results presented next.

The starting point for the analytical calculations will be to consider an armor wire with an initial transverse curvature due to bending. Imagine that a portion of the flexible riser has been bent to a constant radius of curvature ρ. As discussed in [3], the lateral sliding of the wires will be restrained even for small friction coefficients. One may therfore argue that a good approximation for the tendon curvature is given by the *loxodromic* curve curvature [3]:

$$\kappa_2 = -\frac{\cos\alpha}{\rho}(1+\sin^2\alpha)\sin\theta \tag{172}$$

Here, θ the angle in a polar coordinate system with origo in the pipe center, i.e. $\theta = \frac{2\pi Z^1}{L_p}$ where Z^1 is going in the longitudinal direction of the pipe and L_p is the pitch length. Thus the transverse curvature along the wire will vary sinusoidally with a period equal to the pitch length of the wire. It is likely that the wire will follow this curvature pattern during buckling, meaning that the buckling curvature will be as illustrated in the figure below:

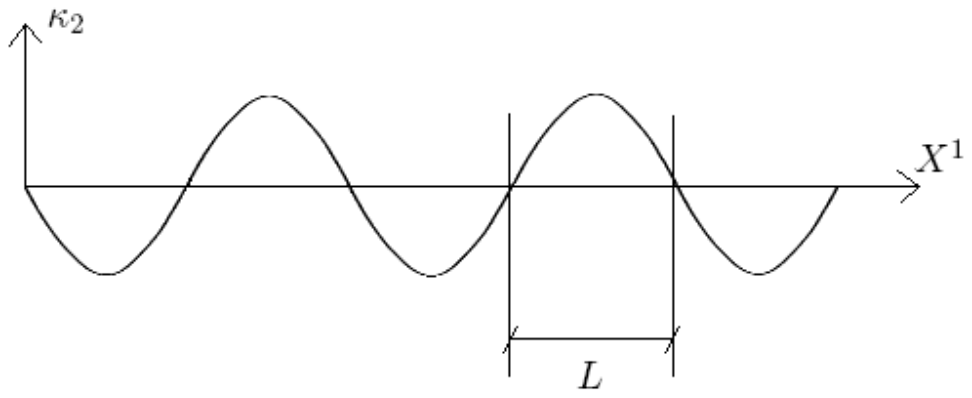

Figure 31: Lateral buckling curvature given by the initial curvature from bending.

Depending on the amplitude of the initial transverse curvature, there will be some parts of the wire that may slide, while other parts will be fully restrained by the friction. Assuming that the only forces acting on the wire are the axial compressive force, Q_1, and the lateral friction q_3 as given in equation (171), a criterion for lateral sliding is found directly from the equilibrium equation in the lateral direction:

$$\begin{aligned} \kappa_2 Q_1 = q_3 = \mu\kappa_3 Q_1 \\ \Rightarrow \kappa_2 = \mu\kappa_3 \end{aligned} \tag{173}$$

This means that for a given pipe curvature, the section along an armor wire where κ_2 is larger than $\mu\kappa_3$ may be subjected to lateral sliding and buckling. At the remaining sections, where κ_2 is smaller than $\mu\kappa_3$, no lateral slip is possible, and buckling cannot take place here. In this way, the initial curvature defines a slip zone of a certain length within each $\frac{1}{2}$-pitch of wire. This is shown in figure 32

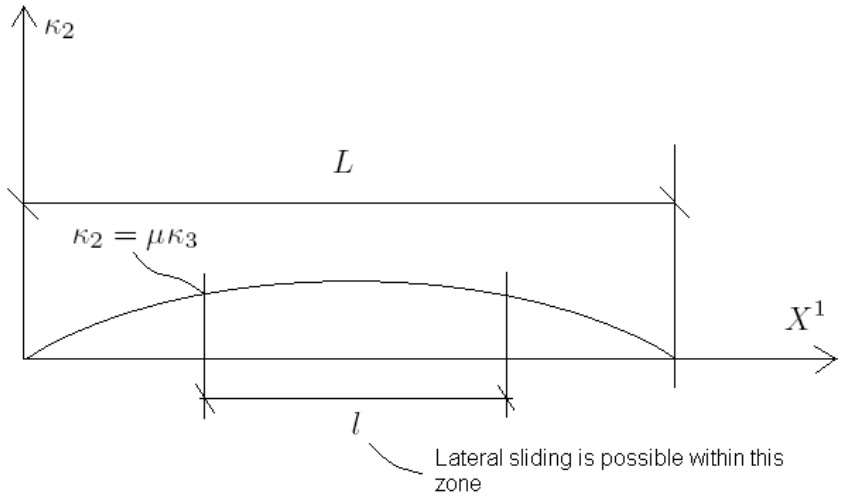

Figure 32: Lateral sliding is possible only in a zone defined by the initial transverse curvature.

The length of this zone can be approximated by combining the above sliding criterion with the loxodromic expression for transverse curvature. The point of transition between possible slip and no slip is given as:

$$\begin{aligned} \rho^{-1}\cos\alpha(1+\sin^2\alpha)\sin\left(\frac{\pi X^1}{L}\right) = \mu\kappa_3 \\ \Rightarrow X^1 = \frac{L}{\pi}\sin^{-1}\left(\mu\frac{\kappa_3}{\rho^{-1}\cos\alpha(1+\sin^2\alpha)}\right) \end{aligned} \tag{174}$$

Thus the length of the slip sone is:

$$l = L - 2X^1 = L\left(1 - \frac{2}{\pi}\sin^{-1}\left(\mu\frac{\kappa_3}{\rho^{-1}\cos\alpha(1+\sin^2\alpha)}\right)\right) \tag{175}$$

The length of this slip zone will be used to calculate the critical stress in an approximate way. For straight beams, the elastic buckling load, or Euler buckling load, is given by [28]:

$$\sigma_E = \frac{\pi^2 E I_2}{A l_k^2} \tag{176}$$

The buckling length l_k depends on the boundary conditions. For a straigh beam of length l which has ends that are free to rotate, $l_k = l$, while for a beam clamped at both ends, $l_k = 0.5l$ [28]. Inspired by this fact, it will in the following be assumed that within each $\frac{1}{2}$-pitch length of wire, the part which buckles may be modelled as a straight beam of a length given by equation (175). The boundary conditions are more complicated. Will the part which is free to slide behave as pinned or clamped? The truth is probably somewhere in between. To keep it simple, one may argue that if only a small portion of the wire is able to slip, the remaining parts will provide sufficient support for the beam to behave as clamped. If, however, the entire wire can slide, then there is no support and the beam will behave as pinned. Following this idea, a simple interpolation formula for the buckling length is suggested:

$$l_k = 0.5l(1 + \frac{l}{L}) \tag{177}$$

where l is the length of wire able to slide within each $\frac{1}{2}$-pitch length of wire, and L is the full $\frac{1}{2}$-pitch length along the wire. Equations (175) - (177) have been used to plot the elastic buckling stress as a function of initial pipe curvature for different friction coefficients. The results are shown below:

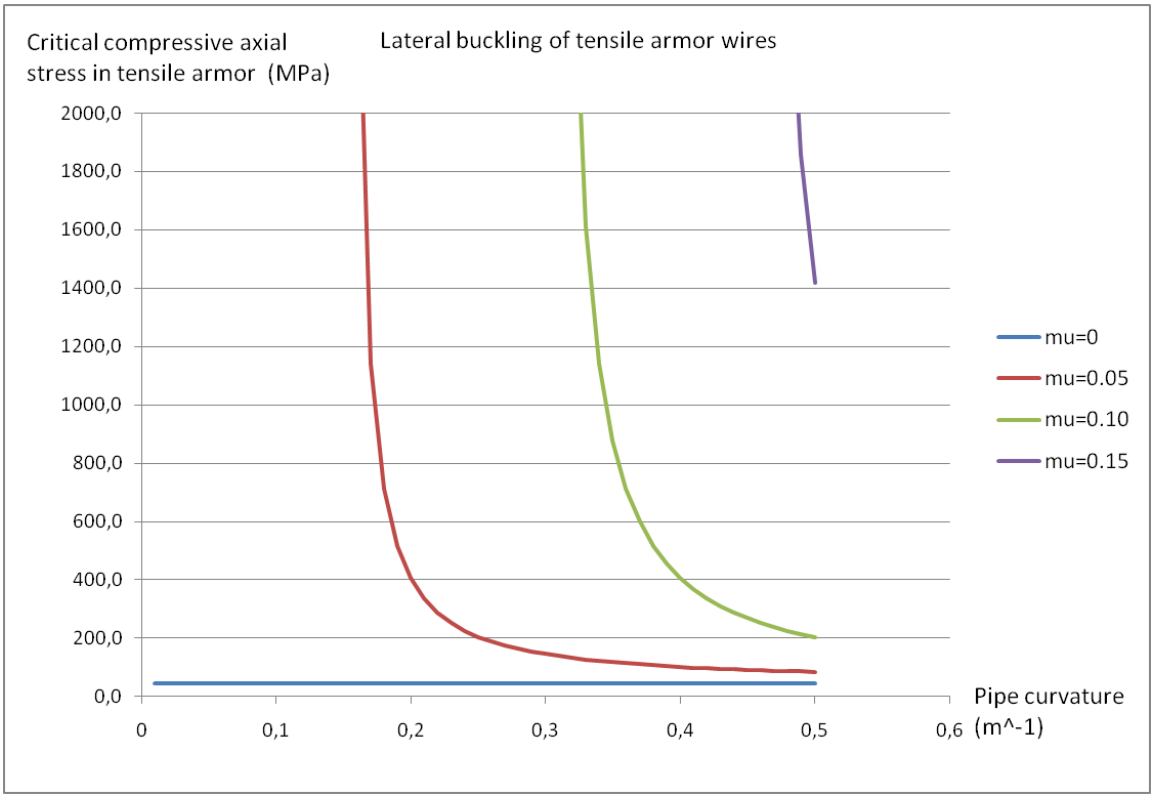

Figure 33: Analytical results for lateral buckling stress.

As seen, there is a very strong dependence upon both friction coefficient and pipe curvature. This is as expected from this simple analytic model, as the friction coefficient and transverse curvature defines the length of wire which is able to slide. For zero friction

there is no dependency upon curvature, as the entire wire is able to slide at any curvature, but once friction is included, the critical stress increases. Lateral buckling is not possible when the curvature is such that $\kappa_2 < \mu\kappa_3$ along the entire wire, and therefore the critical stress is infinite. Once the curvature is large enough to allow sliding, the critical stress drops, and approaches the same value as for zero friction if the curvature is large enough.

The effect of friction is large, and even for the lowest friction coefficients, a high pipe curvature is needed for buckling to occur. When comparing to the critical stress for radial buckling given in figures 28 and 30, it seems unlikely that lateral failure will occur unless the friction is low and the curvature is very high.

Because the friction is so important, it may be that a more accurate model taking the longitudinal friction and sliding into account is needed. There is also of interest to see if cyclic bending may reduce the buckling load. This will be investigated in the next section.

6.3 Buckling analyses - Aflex/Bflex

The purpose of this section is essentially to repeat the buckling analyses in the previous section using the finite element method and the new curved beam element which has been developed as part of this thesis. Both radial and lateral buckling analyses will be performed, and the results compared to the analytical results previously obtained. In addition, lateral buckling analyses will be done using cyclic curvature. Whether or not this reduces the lateral buckling load will be investigated.

In order to focus on the fundamental effects, the finite element model will only include a single armor wire. In reality there may be interaction between the different armor wires, both internally in a layer and also between one layer and another. The aim of this study is to gain knowledge about the basic mechanism of tensile armor buckling, and including all armor wires would only make it harder to interpret the results and explain the physics behind what is happening. Performing analyses including interaction between armor wires remains to be done in the future.

6.3.1 The model

The model is mainly the same as the one described in section 5.3, which was used in assessing the local stress at the end fitting. The geometry and structural elements remain the same, and the dimensions of the armor wire is 9 x 3 mm in all the analyses.

New contact elements are however added in order to represent the anti buckling tape. A spring element type called spring137 is used to represent radial contact as well as longitudinal and lateral friction between the tensile armor wire and the external layer. Spring137 is a point spring, and every node along the armor wire is attached to one of these point springs. The point springs are given a radial stiffness which corresponds to the radial stiffness of the anti buckling tape. This stiffness is defined by equation (169), but because the spring in the Aflex/Bflex model is a point spring, the stiffness is multiplied with the lengh of the armor wire element. The reason for using a point spring is that it has the possibility for nonlinear stiffness characteristics. This is necessary in order to simulate rupture of the anti buckling tape.

To simulate friction, the longitudinal and lateral degrees of freedom of the springs are coupled to the radial degree of freedom such that the maximum friction force is μ times the contact force. If this force is exceeded, the stiffness drops to approximately zero, simulating sliding under friction. The stiffness characteristics of the friction spring and

their effect on the results are discussed in section 6.3.4.

The boundary conditions are:

- The pipe node at the middle of the pipe fixed in all 6 degrees of freedom.
- Armor wire fixed in the longitudinal and lateral direction at both ends.

The compressive load is modelled as a negative internal pressure.This gives no physical meaning, and is merely a practical way of obtaining a compressive axial force in the armor wire, as the program automatically accounts for the end cap force. Because the goal is to simulate the pipe with a flooded annulus, the pressure load is given as internal and negative instead of external. If the load had been applied as external pressure, the extra contact pressure would have been included in the analysis, and this is undesireable.

6.3.2 Radial buckling analyses

Radial failure mode 1, anti buckling tape failure

The springs representing the anti buckling tape is given a high initial stiffness, but as the force reaches a critical value, the stiffness drops to zero. This simulates failure of the anti buckling tape. The thickness and modulus of elasticity is fixed at $t = 0.6\ mm$ and $E = 100GPa$, and the ultimate tensile strength is varied in the different analyses. The spring characteristics are entered as a force/displacement relationship, and the radial displacement when the tape fails is found from the ultimate strain:

$$u_{2,u} = R\epsilon_u = R\frac{\sigma_u}{E} \tag{178}$$

The force associated with this displacement is entered as:

$$F_{2,u} = k_{spring}u_{2,u} \tag{179}$$

where k_{spring} is the radial point spring stiffness, which is determined by multiplying the expression in equation (169) with the length of the armor wire element. This is the maximum force in the tape, which corresponds to the ultimate tensile strength.

A number of analyses have been run using different tape strength. Friction combined with zero pipe curvature ensures that no lateral buckling occurs. The results clearly shows that the wire suddenly pops out when the tape fails. The results are visualized in the computer program Xpost, and a picture showing the wire just after the tape has failed is shown in figure 34.

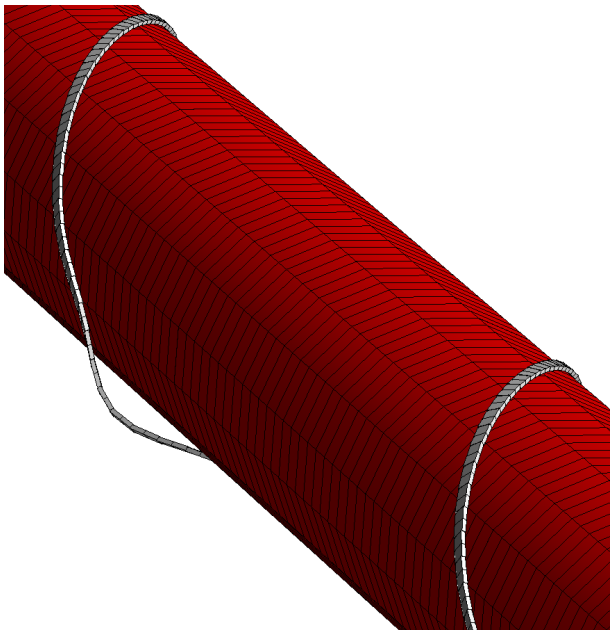

Figure 34: Visualization of Aflex/Bflex results after failure of the anti buckling tape.

Results in terms of maximum compressive stress in the armor wire is presented in the next figure, together with the equivalent analytical results found previously:

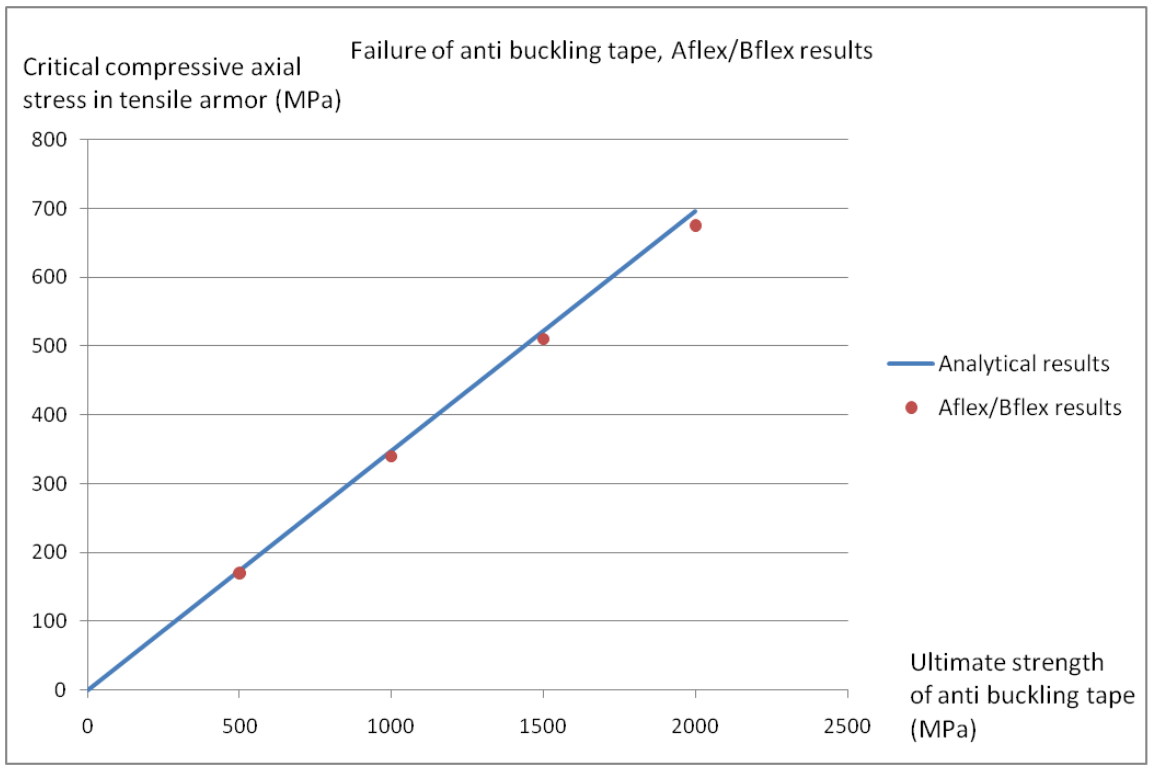

Figure 35: Aflex/Bflex results and analytical results for maximum compressive stress in armor wire, anti buckling tape failure.

The finite element results are almost exactly the same as the analytical. This is as expected, because of the simple failure mechanism. It is only the stress in the anti buckling tape that matters, and this is found accurately by analytic formulas. It seems unnecessary

to perform numerical analyses with different tape stiffnesses and thicknesses as there are strong indications that the results would match the analytical results here as well.

Radial failure mode 2, elastic buckling

The only change in the model compared to the one used in the analyses of radial failure mode 1 is that the radial springs now has a linear force/displacement relationship. This means that the springs still simulate the stiffness of the anti buckling tape in the same way, but the stiffness is constant, i.e. the tape never fails. This forces the wire to buckle in mode 2. The buckling mode appears as shown in figure 36.

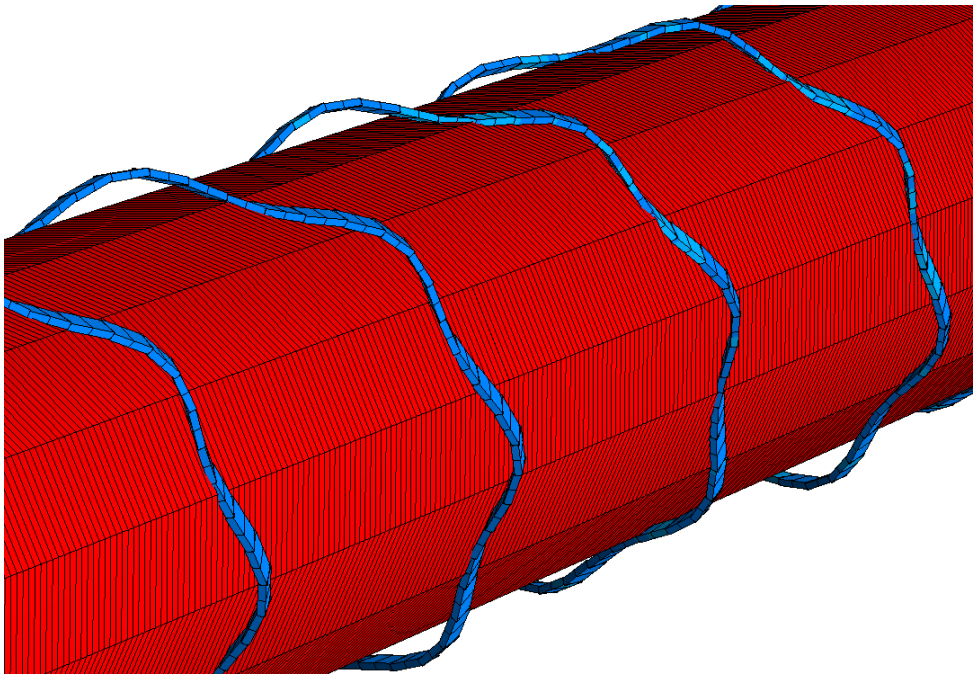

Figure 36: Visualization of Aflex/Bflex results, radial elastic buckling.

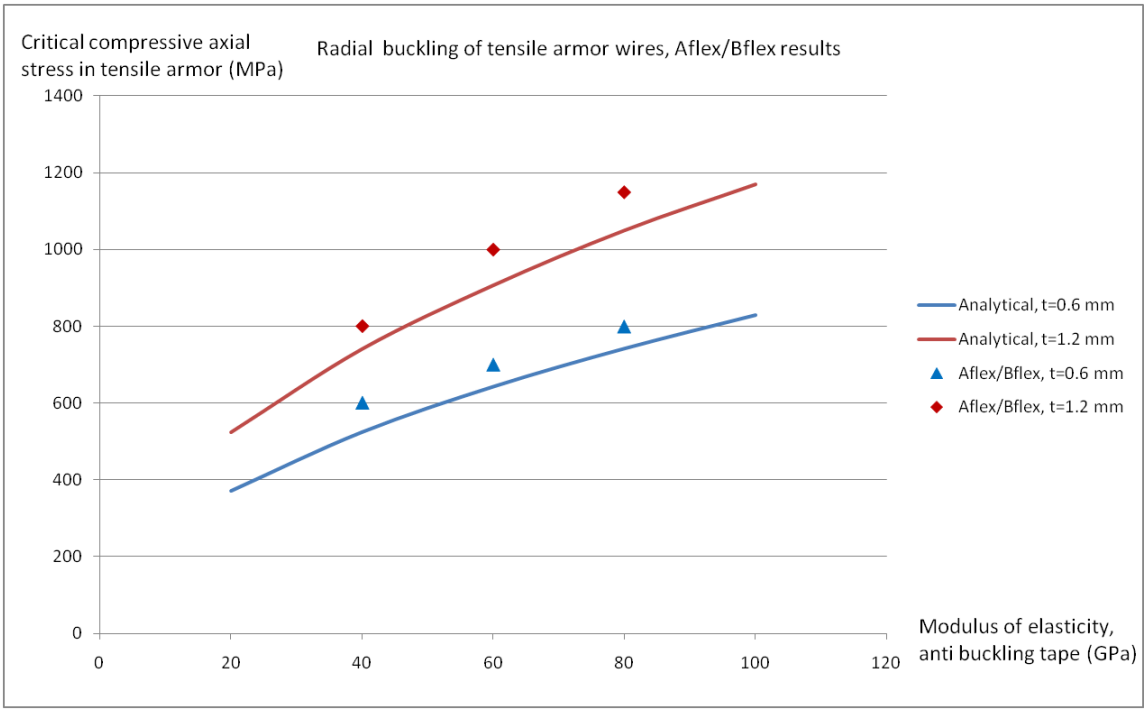

Figure 37: Aflex/Bflex results and analytical results for maximum compressive stress in armor wire, radial elastic buckling.

This sinusoidal buckling shape is clearly seen in the visualization, and it matches the assumed shape of the analytical solution well. The Aflex/Bflex results are shown in figure 37 together with the analytical results. A small discrepancy between the two types of analysis is seen, but the overall agreement is good. From the above results it seems like the finite element model predicts a capacity approximately 8 - 14 % larger than what was found analytically, but the numbers are in fact not accurate enough to say this with certainty. The uncertainty in the Aflex/Bflex results is due to the finite size of the load increments. One can only say whether or not buckling has occured at any given load increment. So if the wire actually buckles in the middle of two load increments, it would seem like it buckles in the last. This error may be reduced by using very small load increments close to the point where failure is expected.

When the above Aflex/Bflex results were obtained, results were only printed at approximately every 50 MPa of axial stress in the wire, meaning that the uncertainty is almost of the same magnitude as the discrepancy between the analytical and numerical results. This means that a better agreement could have been found if a better resolution in results had been used.

With this in mind, the results shown in figure 37 is rather convincing, and it seems like both the analytical and numerical model is capable of predicting the radial elastic buckling load.

6.3.3 Lateral buckling analyses

Gradually increasing pipe curvature

Analyses for a selection of friction coefficients have been performed. The analyses were done by first applying the pressure load. Next, gradually increasing prescribed curvature is given to the pipe elements to simulate bending of the pipe. The magnitude of the

pipe curvature increases linearly towards the middle of the pipe, such that the point of maximum curvature is at the center of the model. The prescribed curvature is increased until the armor wire buckles sideways. At this point, the static anlysis diverges, and the last few steps are run dynamic in order to get past the point of buckling. Figures 38 and 39 shows the center part of the model before and after lateral buckling has occured.

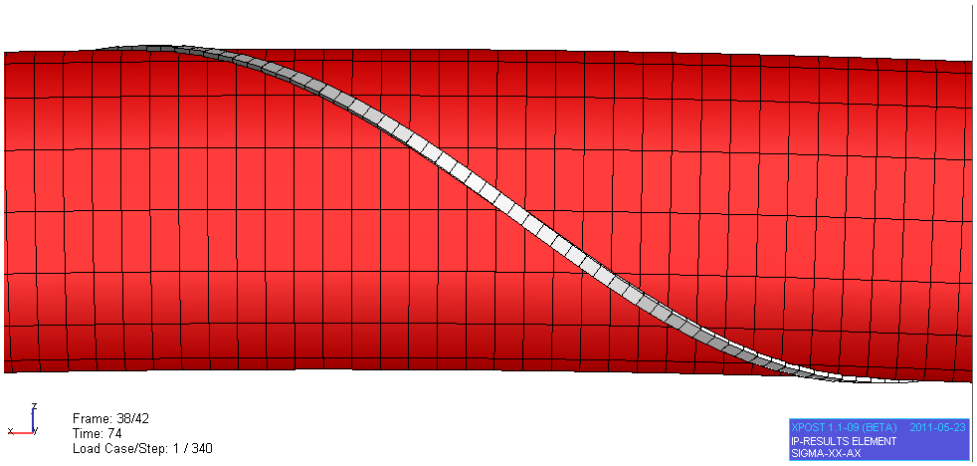

Figure 38: Aflex/Bflex model prior to lateral buckling.

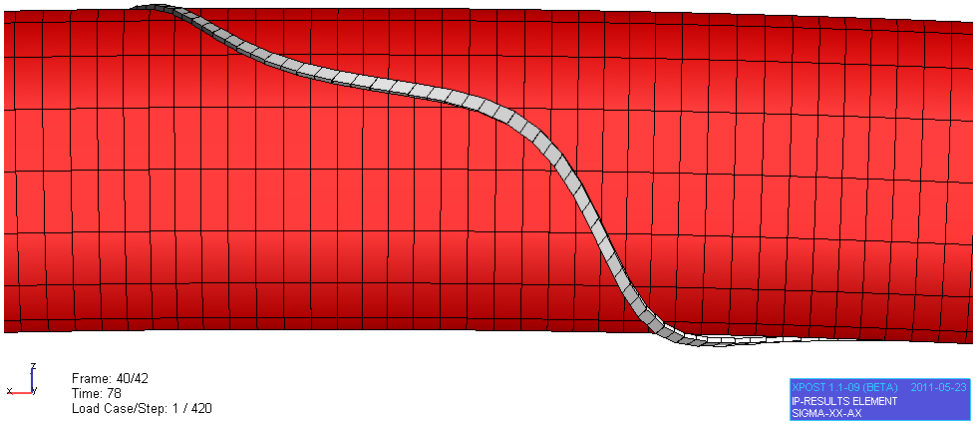

Figure 39: Aflex/Bflex model after lateral buckling.

The springs simulating the anti buckling tape has been given a high stiffness to ensure that buckling can take place in the lateral direction only. Analysis results are presented in figure 40 below, together with the analytical results given previously. The reported axial stress is taken at the neutral axis of the pipe, i.e. the axial stress as a result of bending is not included.

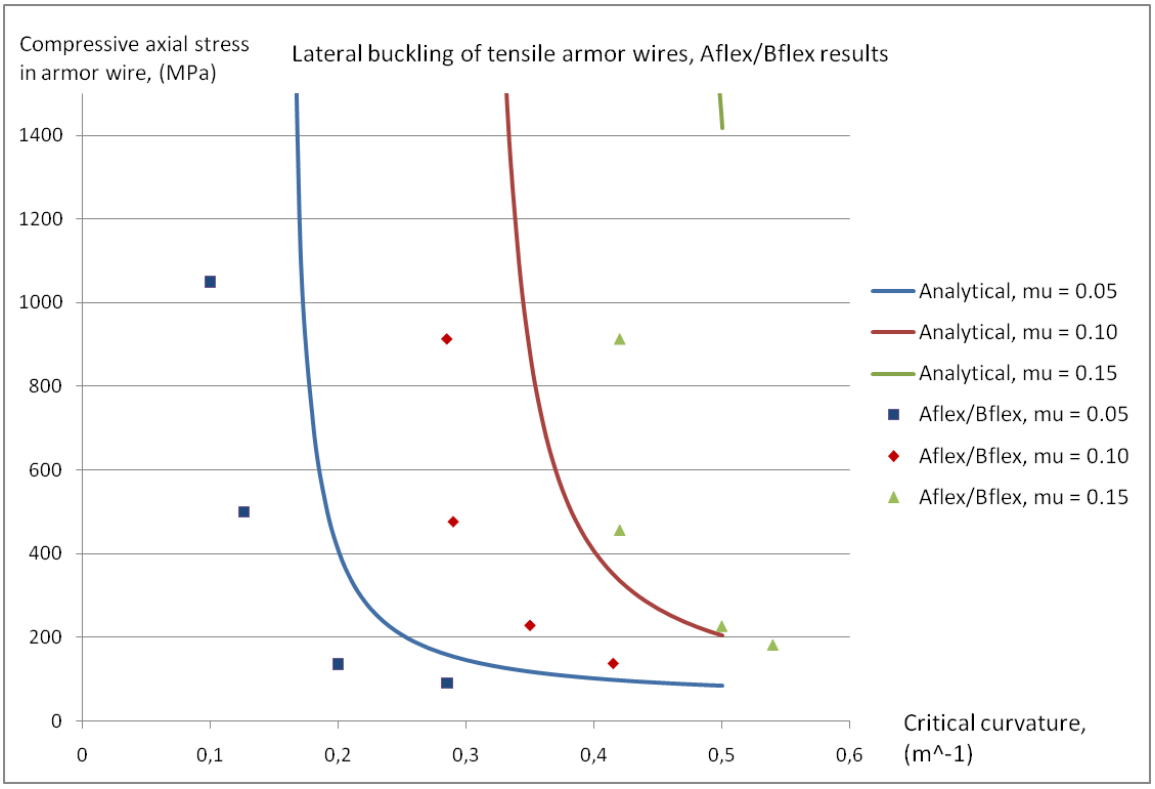

Figure 40: Aflex/Bflex results and analytical results for lateral buckling stress, gradually increasing curvature.

The numerical results are marked with solid dots and the analytical results with lines. The number of numerical results are somewhat limited, but it is clear that the trend is very much the same as in the analytical results. Also here, the strong dependence upon the friction coefficient is seen, and increasing the friction coefficient means that the wire can withstand a much higher compressive force or curvature before buckling. There is however a significant discrepancy between the analytic results and those obtained with the Aflex/Bflex model. The main difference seems to be that failure occurs at a lower curvature than what was found analytically. This is probably due to the assumption used in the anaytical calculations that the friction forces may be fully utilized in the lateral direction. What happens in the finite element model is that longitudinal friction forces contributes to the total magnitude of friction, meaning that slip occurs over a larger zone than predicted by the analytical formulas presented previously.

Cyclic pipe curvature

Due to the dynamic behaviour of a flexible riser, it is of interest to check if the lateral buckling strength may be reduced by applying cyclic curvature. Even if the maximum curvature is smaller than the critical curvature for buckling, one may imagine that the wire slides laterally a very small distance (without buckling) for each cycle. In this way the maximum tranverse curvature of the wire may gradually increase for each global curvature cycle. If this is the case, the wire will at some point obtain a transverse curvature so large that it buckles.

The same Aflex/Bflex model as before is used to investigate this. A combination of compressive stress and curvature is selected such that buckling should *not* occur if the curvature is static. Now the prescribed curvature is varied from zero to the maximum

value repeatedly, simulating an exaggerated state of cyclic curvature. Ideally, a large number of analyses with different curvatures, stress and friction coefficients should be done. It is impossible to say in advance how many cycles are required, and in some cases a large number of cycles may be necessary.

It is not within the scope of this thesis to do such an extensive study, but a smaller number of analyses will be done in order to provide some information about how cyclic curvature affects the capacity. Because of limited computer resources, the number of cycles in each analysis will be kept below 25. This might be too few cycles to induce buckling in some cases, but the results will in any case show if the wire accumulates more transvere curvature for each cycle. If it is so, it seems likely that buckling will occur after a larger number of cycles.

Analyses with a friction coefficient of 0.10 and 0.15 has been performed, and the results are summarized in the tables below:

Table 2: Analysis results for cyclic curvature, $\mu = 0.10$

Axial stress in armor wire (MPa)	**Maximum pipe curvature** (m^{-1})	**Number of cycles to failure**
300	0.29	2
300	0.25	5
300	0.2	21
300	0.15	No increasing lateral displacement

Table 3: Analysis results for cyclic curvature, $\mu = 0.15$

Axial stress in armor wire (MPa)	**Maximum pipe curvature** (m^{-1})	**Number of cycles to failure**
300	0.4	3
300	0.35	5
300	0.29	11
300	0.25	22
300	0.2	>25
300	0.15	No increasing lateral displacement

The results show that in some cases the armor wire gradually slides sideways, and suddenly buckles. This happens only in the cases where the pipe curvature is above a critical level. For example, in the case of $\mu = 0.10$, there is no sign of increasing lateral sliding for a maximum curvature of 0.15 m^{-1}. Only in the cases with a maximum curvature of 0.2 m^{-1} or higher are an increasing lateral deflection observed. In practical matters it is not that interesting just how many cycles which give failure, but it is important to know if failure will occur or not for a given combination of curvature variation and stress. The results presented here indicate that there exists a critical curvature limit, meaning that if the curvature is kept below this limit there will be no buckling, but if this limit is exceeded, failure may occur after some number of cycles. From the above results

it appears that this curvature limit is somewhere between 0.15 m^{-1} and 0.2 m^{-1} for a friction coefficent of both 0.10 and 0.15, given a compressive stress of 300 MPa,.

To illustrate how the wire gradually slides sideways, snapshots of the lateral wire displacement is shown in figure 41 below. The figure shows the lateral displacement relative to the supporting pipe structure as a function of the wire arc-length at different time steps. All the snapshots are taken at maximum curvature, so the difference between one curve and the next corresponds to the lateral sliding in a single cycle. As seen in the figure, the lateral displacement increases dramatically when a critical curvature has been accumulated.

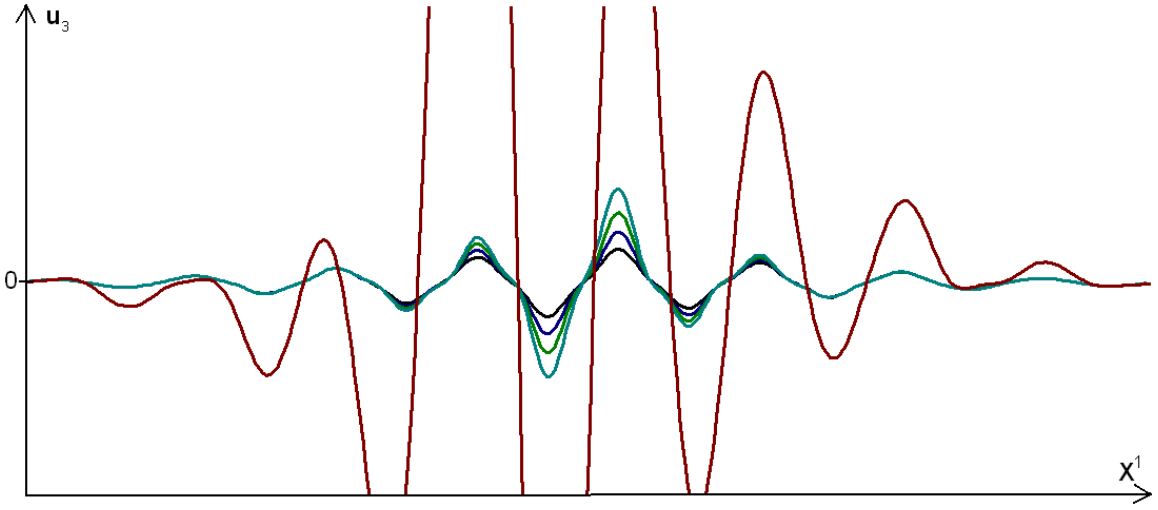

Figure 41: Lateral displacement of armor wire subjected to cyclic curvature.

Comparing the results using cyclic curvature to the results obtained by monotonically increasing the curvature, it is seen that cyclic curvature clearly has a negative effect on the capacity. Taking the case with a friction coefficient of 0.15 as an example, it was found that the curvature had to reach values as large as 0.42 m^{-1} to get buckling using static curvature, and this was for a compressive stress of 900 MPa. Here we have seen that by varying the curvature, lateral buckling may occur at a maximum curvature of 0.2 m^{-1} and a compressive stress of 300 MPa. This is still a large curvature, but significantly lower than before.

The finite element model used in the analyses consists of a single armor wire and a pipe core. It was initially believed that the characteristics of the core was unimportant to the results for wire buckling, and therefore there has been no focus on the value of the axial stiffness of the pipe elements. It was however noticed during the analysis work that the axial strength of the supporting pipe elements actually had some effect on the results. This is probably related to the fact that a stiff core will carry more axial force than a soft core. In the results presented here, an axial stiffness (EA) of $1 \cdot 10^6$ N was used. The bending stiffness of the pipe core was found to have no significant impact on the results.

6.3.4 Lateral buckling and friction modelling

As friction between the tensile armor wires and the external layer is highly important for the lateral buckling strength, it seems in place to investigate and discuss the modelling of this phenomenon. The finite element model simulates *dry friction*, or *Coulomb friction* using springs. The maximum force in such a spring is determined as μ times the

contact force, and as long as the force is below this value the stiffness is very high. This simulates full stick between the wire and the external layer. To ensure absolutely zero displacement under stick conditions, the stiffness of the spring would have to be infinitely large. However, to avoid numerical problems, the spring stiffness cannot be extremely large relative to the other terms in the system stiffness matrix. In the numerical analyses done previously in this thesis work, an elastic displacement of the friction springs of 1 mm has been allowed. The force-displacement characteristics of the friction springs are illustrated in figure 42.

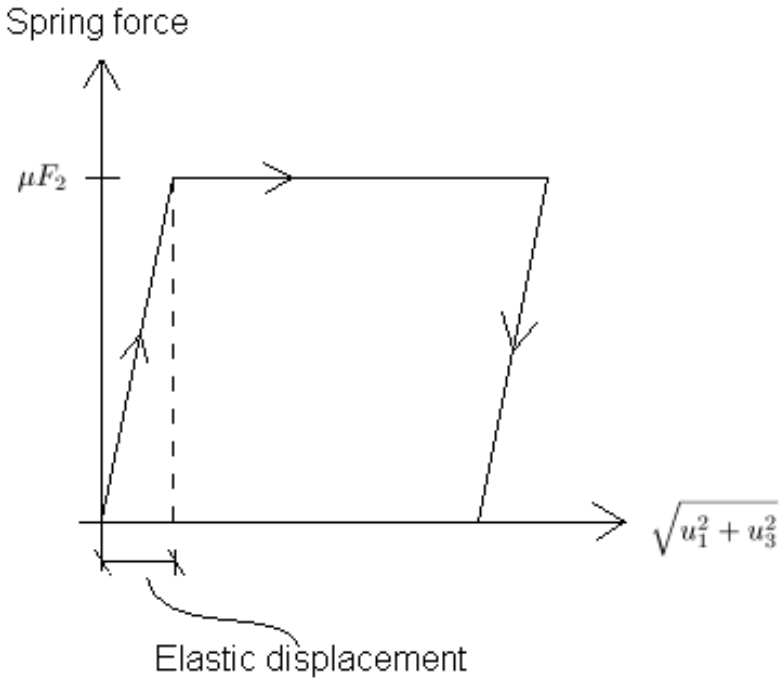

Figure 42: Force-displacement diagram for the friction springs.

Lateral buckling under cyclic curvature was triggered by very small lateral displacements for each cycle. Because this failure mode is sensitive to small displacements, it seems likely that the results may be affected by changing the allowed elastic friction spring displacement. Whether or not this influences the results will now be investigated.

Analyses with $\mu = 0.15$ has been repeated, using 0.1 mm as the new elastic friction spring displacement. The compressive stress in the wire is the same as before, and the new results are shown in the table below:

Table 4: New results, using an elastic friction springs displacement of 0.1 mm. $\mu = 0.15$

Axial stress in armor wire (MPa)	**Maximum pipe curvature** (m^{-1})	**Number of cycles to failure**
300	0.29	4
300	0.2	9
300	0.15	15
300	0.1	>25

As suspected, the elastic friction spring displacement has an effect on the results. When this value is reduced from 1 mm to 0.1 mm, it is evident that a lower number of cycles are required to obtain the buckled configuration. A possible explaination to this may be that the elastic friction zone along the wire is shorter when the elastic displacement is reduced, meaning that sliding takes place over a larger portion of the wire.

Another effect which may be important is that when the curvature has reached maximum and the process is reversed towards zero curvature, an elastic springback occurs due to the elasticity of the springs. This means that the wire will be "pushed" back towards its initial position by the friction springs. This is *not* a real physical effect, but it is a result of the way the friction force is modelled. If the spring pushes the wire back, it will slow down the buckling process, as the lateral displacement per cycle will be diminished.

The case with a smaller elastic displacement should give a better representation of the reality, as the elasticity in the friction springs is unphysical.

In the initial cyclic curvature analyses, no increasing lateral displacement was found for a maximum pipe curvature of 0.15 m^{-1}, but with the elastic spring displacment reduced to 0.1 mm, the wire actually buckles after 15 curvature cycles. A gradually increasing lateral displacement is observed for a maximum curvature as low as 0.1 m^{-1}. When it comes to practical use of the results, it means that one may expect lateral buckling to occur at even lower curvatures, because real life friction will have no elastic displacement at all.

Because the modelling of friction is important to the results, further studies should be performed. A more comprehensive study of how the friction spring characteristics affects the results may provide valuable information. Perhaps it is possible to tune the friction spring such that the results is as close to reality as possible. It may also be considered to use alternative methods for friction modelling, which does not involve the spurious elastic deformation.

7 Conclusions

This thesis has focused on problems relevant for deep water applications of flexible risers. Two different issues have been investigated, namely local stresses in tensile armor wires at the end fitting when the riser is subjected to large axial loads, and buckling of tensile armor wires under compression due to external pressure.

Both analytical and numerical calculations have been performed, and a central part of the numerical analysis has been the development of a new curved beam element for the finite element code Aflex. The new element includes rotational degrees of freedom around the weak axis of the wire cross section, which enables the simulation of radial buckling phenomena. The new element has been used extensively in analyses of both stresses at the end fitting and armor wire buckling, and the element performs well. The new element has also been implemented in a special version of the Bflex2010 program.

The investigation of local stresses at the end fitting are based on the assumption that tensile armor wires are fully fixed at the point of termination. It is uncertain how good this approximation is, but in any case the assumption is conservative. Any flexibility in the end fitting structure will reduce the local stresses.

In the investigation of local stresses at the end fitting, analytical calculations were performed in order to get an understanding of the problem. Terms due to warping of the cross section were included, and the longitudinal warping stress was calculated and compared to other stress components. The warping stiffness was found to give no significant contribution to the solution, and the warping stress was totally negligible. Thus it has been established that there is no need to include warping stiffness terms, or take warping stress into account when doing analyses of tensile armor wires close to end terminations.

The localized bending stress is however more interesting. In the analytical calculations it was found that the magnitude of bending stress relative to the pure axial stress increases for increasing axial stress, and the ratio is approximately proportional to the square root of the pipe strain. This means that the bending component is more important when the riser is subjected to large tensile loads, and may thus be important for deep water risers. It was also found that the ratio between bending and axial stress is virtually independent of the wire cross section dimensions as long as friction forces are disregarded.

There were no friction forces included in the analytical model, and because large contact pressure will build up as a result of the tensile force in the armor wires, friction will be important. The analytical expressions presented in section 5 is therefore perhaps more of academic than practical interest. Friction was however included in the finite element analyses with the new curved beam element. The finite element analyses agreed very well with the analytical results when friction was set to zero, thus verifying that the analytical model is correct within its limits. As expected, the results change significantly when friction between the wire and supporing layer is included. With friction, the ratio between bending and axial stress is no longer independent of the cross section dimensions, as a larger cross section area will give a larger axial force and contact pressure. Analysis results show that for an armor wire of dimensions 15 x 6 mm, the bending stress exceeds 16% of the axial stress at an axial stress of 400 MPa for a riser with two tensile armor layers and a friction coefficient of 0.15. The percentage is even larger if the axial stress is increased further. This indicates that the localized bending stress will constitute a significant part of the total longitudinal stress in the tensile armor wire, given that the wire is fully fixed at the end termination.

When it comes to buckling of tensile armor wires, two different modes has been in-

vestigated, namely *radial* and *lateral* buckling. The importance of annulus conditions has been discussed, and it was shown that outwards radial motion of the armor wires is unlikely if the annulus is dry. Therefore, the analyses in this thesis have been performed with the assumption of a flooded annulus.

Both analytical and numerical studies of the different buckling modes have been performed, and the new curved beam element has been used for the numerical studies. One of the objectives has been to find out under which circumstances the armor wire buckles radially or laterally. There is however no simple formula for this, as there are many parameters influencing the capacity. In the analyses, an example riser with a given radius, lay angle, wire dimensions and number of wires is used, but other parameters are varied to investigate how the capacity changes. It is found that the capacity to the first radial failure mode, which is anti buckling tape failure, is determined by the ultimate tensile strength of the tape along with the tape thickness. The second radial failure mode is elastic buckling of the armor wire, where the anti buckling tape acts as an elastic foundation. The capacity with respect to this failure mode is given by the bending stiffness of the wire, the anti buckling tape thickness and the modulus of elasticity of the tape. This means that the capacity with respect to both radial failure modes may effectively be increased by applying a thicker tape layer.

Comparison between the analytical and finite element results agree very well for both radial failure modes. The small differences between the two methods found for radial failure mode 2 is most likely due to the size of the intervals used for storing results. It is therefore believed that both the analytical and finite element results are correct, and that both methods may be used to predict the capacity with respect to radial buckling.

The lateral buckling strength is however somewhat more difficult to predict than the radial, and the mechanism is quite different. The armor wires will be restrained from lateral displacement by friction forces, but at some point the friction will be overcome, and lateral sliding can take place. This nonlinear process is captured by the finite element model, and an attempt to describe it analytically has also been done. There is however a significant discrepancy between the analytical and numerical results, even though both methods show that the critical wire stress is strongly related to pipe curvature and friction coefficient.

The analytical model is based on calculating the Euler buckling load for a straight beam, using the length of the "slip zone" as an important input parameter. The length of the slip zone is determined by the friction coefficient and pipe curvature, hence the large correlation between critical stress and these two quantities. Compared to the finite element results, the analytical method overpredicts the capacity. This is because the analytical model assumes that all available friction force can be utilized in the lateral direction. This is not the case, because longitudinal friction forces are present when a flexible pipe is subjected to bending. Thus the lateral friction force is reduced. This effect is included in the finite element model, and the results from the finite element analyses are therfore regarded as most correct.

Through finite element analyses it has also been observed that cyclic curvature will effectively decrease the buckling capacity. By alternating the pipe curvature between zero and a given value, the armor wire may gradually slide sideways. After a number of cycles, the accumulated transverse curvature become so large that the wire buckles. This happens even if the maximum curvature is significantly lower than the critical value observed when the curvature was monotonically increased. This may be important to the design of deepwater risers, because dynamic curvature always will be present due to the

environmental forces.

It was however found that the behaviour during cyclic bending was affected by the numerical characteristics of the spring elements simulating friction. The validity of the results is therefore somewhat uncertain, but they indicate that lateral buckling may be an issue for pipe curvatures in the vicinity of 0.1 m^{-1} combined with a compressive stress of 300 MPa, even if the friction coefficient is as large as 0.15.

7.1 Recommendations for further work

The accuracy of the predicted bending stress at the end fitting depends on the validity of the assumption that the armor wires are fully fixed at the end. In order to be truly confident in the results, further studies taking the actual geometry and material properties of the end fitting into account should be performed. The localized bending stress calculated in this thesis arises due to the rotational restraint, and if the armor wires are able to rotate only slightly inside the end fitting, this will affect the results.

There is undoubtfully more work to do when it comes to buckling of armor wires. To start with, this thesis has focused on a single armor wire in contact with an external tape layer. In reality, there is a large number of wires, separated in different layers. Forces may be transferred from one layer to the neighbouring as both normal and frictional force, and interaction effects may alter the behaviour. The Aflex/Bflex model may be used to analyse a riser cross section including all armor wires through proper use of contact elements. In addition, contact between wires in the same layer will probably occur during lateral buckling, and contact elements can possibly also be utilized to capture this effect.

Further, the armor wire material has been assumed to behave linearly elastic at all times. As large bending stresses may occur when the wire buckles, the material behaviour may in reality be elastoplastic. The true material behaviour might be included in a future finite element analysis of the problem.

It was observed that lateral buckling as a result of cyclic curvature may occur at relatively low stresses for certain combinations of curvature and friction coefficient. A more extensive study of this phenomenon is necessary in order to provide a complete understanding of it. However, the issue of results depending on the elastic stiffness of the contact friction springs (as discussed in section 6.3.4) needs to be solved. New analyses with smaller allowable elastic deformation may be performed, and possibly, the results will converge when a sufficiently small value is used. If this is unsuccessful, some alternative way of friction modelling may be necessary.

References

[1] C. Pettenati-Auziere, "Flexible dynamic risers: State of the art," 1985.

[2] J. A. Witz, "A case study in the cross-section analysis of flexible risers," tech. rep., Department of Mechanical Engineering, University College London, 1994.

[3] S. Sævik, *On Stesses and Fatigue in Flexible Pipes.* PhD thesis, The Norwegian Institute of Technology, 1992.

[4] F. Bectarte and A. Coutarel, "Instability of tensile armour layers of flexible pipes under external pressure," in *OMAE 2004: 23rd International Conference on Offshore Mechanics and Arctic Engineering*, 2004.

[5] S. Sævik, "Simplified models for predicting stress ranges due to dynamic bending," 2005.

[6] S. Timoshenko and J. N. Goodier, *Theory of Elasticity.* McGraw-Hill, 1951.

[7] M. W. Bræstrup and J. B. Andersen, *Design and Installation of Marine Pipelines.* Blackwell Science, 2005.

[8] Y. Shen, F. Ma, Z. Tan, and T. Sheldrake, "Developement of the end fitting tensile wires fatigue analyis model: Sample tests and validation in an unbonded flexible pipe," in *Offshore Technology Conference*, 2008.

[9] Z. Tan, T. Sheldrake, C. Lopers, and G. Karabelas, "Behaviour of tensile wires in unbonded flexible pipe under compression and design optimization for prevention," in *OMAE 2006: 25th International Conference on Offshore Mechanics and Arctic Engineering*, 2006.

[10] S. Berge, A. Engseth, I. Fylling, C. Larsen, B. Leira, I. Nygaard, and A. Olufsen, "Handbook on design and operation of flexible pipes," tech. rep., Sintef, 1992.

[11] ANSI/API, "Recommended practice for flexible pipe," tech. rep., American Petroleum Institute, 2008.

[12] I. Kraincanic and E. Kebadze, "Slip initiation and progression in helical armouring layers of unbonded flexible pipes and its effect on pipe bending behaviour," *The Journal of Strain Analysis for Engineering Design, Vol. 36*, 2001.

[13] S. Sævik, "Stresses due to pressure, tension and torsion," 2010.

[14] C. H. Edwards and D. E. Penney, *Calculus, Sixth Edition.* Prentice Hall, 2002.

[15] I. Langen and R. Sigbjørnsson, *Dynamisk analyse av konstruksjoner.* Tapir Forlag, 1979.

[16] A. E. H. Love, *A Treatise on the Mathematical Theory of Elasticity.* Dover Publications, 1944.

[17] W. D. Pilkey, *Analysis and Design of Elastic Beams: Computational Methods.* Wileys, 2002.

[18] T. Moan, *Finite Element Modelling and Analysis of Marine Strucures*. Department of Marine Technology, NTNU, 2003.

[19] S. Sævik, "Aflex, a computer program for stress analysis of flexible pipes exposed to high bending gradients," 1992.

[20] S. Sævik, *BFLEX2010 - Theory Manual*. Sintef - Marintek.

[21] T. Hill, Y. Zhang, and T. Kolanski, "The future for flexible pipe riser technology in deep water: Case study," in *Offshore Technology Conference*, 2006.

[22] K. Bell, "Forelesningsnotater i fag 37930, energimetoder," 1988.

[23] J. Amdahl, "Buckling and ultimate strength of marine structures, lecture notes in tmr4205," 2005.

[24] D. A. McQuarrie, *Mathematical Methods for Scientists and Engineers*. University Science Books, 2003.

[25] F. Irgens, *Formelsamling Mekanikk*. Tapir Forlag, 1999.

[26] S. Berge, *Fatigue Design of Welded Structures*. Department of Marine Technology, NTNU, 2004.

[27] F. G. Nielsen, *Lecture Notes in Marine Operations*. Department of Marine Technology, NTNU, 2007.

[28] T. H. Søreide, *Ultimate Load Analysis of Marine Structures*. Tapir Forlag, 1985.

Appendix: Implementation of the new curved beam element

The following is a list of all changes done in the Aflex code when implementing the new curved beam element described in section 4.6. For an explaination of the function of the different subroutines, see [19]. The subroutines are listed in the order which they are called, and the changes are listed in the order which they appear in the code.

- aflex.f:
  - Changed NDOF to 5NNOD and NBW (bandwidth) to 10.
  - Changed matrix indicators L16-L19 and L38-L40.
- insp.f:
  - Changed array dimensions.
  - Changed I3 to 5 under read boundary conditions, read point spring properties and read prescribed deflections.
  - Changed counters and added new terms under calculate initial conditions for spring force/stiffness/displacement, internal forces and element end forces.
  - Changed I1 to 5I-3 under radial spring properties.
  - Changed read statements under restart condition.
- init.f:
  - Changed the counters I1 and I2.
- anal.f:
  - Changed array dimensions.
  - Changed I1 under point spring.
  - Changed loop range from 8 to 10 under set zero global stiffness matrix.
  - Changed loop range from 10 to 12 under form element stiffness matrix.
  - Changed I1 and I2 used to add into global stiffness.
  - Changed 4NNOD to 5NNOD under residual tension forces at ends.
  - Changed I1 and I2 under contact pressure forces.
  - Changed I2 under implement spring stiffness.
  - Changed I3 under point spring stiffness.
  - Changed I1 under boundary conditions and prescribed deflections.
  - Changed 4I-1 to 5I-2 and 4I-3 to 5I-4 under update coordinates and angle.
  - Changed 4I-3 to 5I-4, 9 to 11 and 10 to 12 under adjust internal forces to take friction into account.
  - Changed 4I-2 to 5I-3 under update contact spring strains and stresses.
  - Changed 4I-3 to 5I-4 and 4I-1 to 5I-2 under calculate directional cosines.

  - Changed 4 to 5 in I3 under update fixed spring strains and stresses.
  - Changed 4I-3 to 5I-4, 4I-2 to 5I-3 and 4I-1 to 5I-2 under internal load vector for contact springs.
  - Changed 4I-1 to 5I-2 under find moment contribution from contact forces. Added internal forces for the new rotational degree of freedom due to distributed contact forces.
  - Changed I3 under support reactions.
  - Changed write statements used for writing element forces to file.
  - Changed 4 to 5 under update plastic spring values.

- stlo1.f:
  - Changed array dimensions.
  - Changed loop range from 10 to 12.
  - Changed interpolation polynomials.

- adfo.f:
  - Changed array dimensions.
  - Changed I1 from 10I-10 to 12I-12.
  - Added terms 11 and 12 for element end forces.

- mat2.f:
  - Changed array dimensions.
  - Changed loop range from 10 to 12.
  - Changed interpolation polynomials.

- adfo1.f:
  - Same changes as for adfo.f.

- geom1.f:
  - Changed array dimensions.
  - Changed loop range from 10 to 12.
  - Changed E1 to be the sum of the axial strain and the prescribed axial strain.
  - Changed interpolation polynomials.

- keik.f:
  - Changed array dimensions.
  - Changed 9 to 11 and 10 to 12 under invert Kii and correct load vector.
  - Changed 8 to 10, 9 to 11 and 10 to 12 under determine H1-matrix, calculate effective element stiffness.

- glfo.f:

  - Changed array dimensions.
  - Changed 4IEL-3 to 5IEL-4.
  - Added two internal force terms (one at each element end) and changed element degree of freedom numbers.

- adst.f:
  - Changed array dimensions.
  - Changed 4 to 5 in loop range and matrix operations.

- spst.f:
  - Changed array dimensions.
  - Changed I1, I2, I3 and I4.
  - Added 5 terms, SK(i,5).

- adsp.f:
  - Changed array dimensions.
  - Changed 4 to 5 in loop range.

- gstr.f:
  - Changed array dimensions.
  - Changed I1 and I2.
  - Added term 9 and 10 in the local vector.

- stra.f:
  - Changed array dimensions.
  - Changed I2.
  - Changed old terms and added terms 5 and 10 in the local displacement vector.

- upda1.f:
  - Changed array dimensions.
  - Changed 8 to 10 in loop range.
  - Changed 9 to 11 and 10 to 12 in determine internal u.
  - Changed interpolation polynomials.

- stre1.f:
  - Changed array dimensions.
  - Changed 10 to 12 in loop range.
  - Changed interpolation polynomials.

- adfo2.f:
  - Same changes as for adfo.f and adfo1.f.

- zspr.f:
  - Changed I2.
- xfric.f:
  - Changed I2 and I3.
- hysp.f:
  - Changed I1 and I3.
- prel.f:
  - Changed array dimensions.
  - Changed 4I-3 to 5I-4 in element axial stress.
- prne.f:
  - Changed 4I-1 to 5I-2 and 4I-3 to 5I-4 under write element stresses.
  - Changed 4I-1 to 5I-2, 4I-2 to 5I-3 and 4I-3 to 5I-4 under deflection and spring status.
- prdi.f:
  - Changed array dimensions.
  - Changed 4 to 5 under nodal displacement.